Dissertation

submitted to the

combined Faculties for the Natural Sciences and for Mathematics

of the

Ruperto-Carola University of Heidelberg

for the degree of

Doctor of Natural Sciences

presented by

Diplom-Chemiker Andreas Schleifenbaum

born in Munich, Germany

Oral-examination: 27.01.06

Title:

Novel Fluorescent Sensors for Dynamic Intracellular Signalling

Referees:

Prof. Dr. Nils Metzler-Nolte, University of Heidelberg

PD Dr. Carsten Schultz, University of Dortmund/EMBL Heidelberg

Inaugural-Dissertation

zur

Erlangung der Doktorwürde

der Naturwissenschaftlich-Mathematischen Gesamtfakultät der

Ruprecht-Karls-Universität Heidelberg

vorgelegt von

Diplom-Chemiker Andreas Schleifenbaum

aus München

Tag der mündlichen Prüfung: 27.01.06

Titel der Arbeit:

Neue Fluoreszenzsonden für intrazelluläre Signalwege

Gutachter:

Prof. Dr. Nils Metzler-Nolte, Universität Heidelberg

PD Dr. Carsten Schultz, Universität Dortmund/EMBL Heidelberg

Hiermit bestätige ich, dass ich die Arbeit selbständig verfasst und keine anderen als die angegebenen Quellen und Hilfsmittel benutzt habe.

Heidelberg, im September 2005

_____

Andreas Schleifenbaum

Wenn man's nur probiert so geht's,
das heißt mitunter – doch nicht steht's.
Wilhelm Busch

Table of contents

Abstract

Protein kinase C (PKC), comprised of ten isozymes, is an abundant regulator of cellular function. PKC activity in living cells is commonly assayed in *in vitro* experiments with cell lysate. Monitoring PKC activity in single living cells is not possible with such experiments. This thesis presents a novel fluorescent reporter for PKC activity in living cells. The kinase C probe (KCP-1) consists of a PKC specific substrate sequence that is flanked by two fluorescent proteins, which are capable of fluorescence resonance energy transfer (FRET). The substrate sequence is truncated pleckstrin, which is specifically phoshorylated by PKC between a pleckstrin homology and DEP domain. Green fluorescent protein square (GFP^2) and enhanced yellow fluorescent protein (EYFP) were chosen as FRET partners, because of their perfect overlap of donor emission and acceptor excitation.

The probe reported PKC activity after stimulation of cells with drugs and mitogens, including phorbol ester, diacylglycerol, histamine, and bradykinin. The KCP-1 signal was reversed after cell treatment with the PKC specific inhibitor Gö6983. Stable cell lines and transgenic fly embryos which expressed KCP-1 demonstrated that the probe was not toxic to cells. Live cell or *in vitro* tests demonstrated KCP-1 specificity for PKC over protein kinase A (PKA), calcium/calmodulin dependent kinase (CaMKII), protein kinase B, and aurora kinases. These experiments demonstrated that KCP-1 can be used in living cells to specifically monitor PKC activity.

KCP-1 was simultaneously observed in single cells with other fluorescent probes, including indicators for the PKC activators calcium and diacylglycerol. These tests demonstrated feasibility and limitations of such experiments. Furthermore, these, as well as *in vitro* experiments suggested that KCP-1 primarily reported activities of calcium independent PKC isozymes.

One application of KCP-1 is drug-screening assays. Initial experiments with the stable cell line demonstrated that the probe can be used in such assays after further optimization of experimental parameters.

Optimization of the probe involved modification of several features: KCP-1 mutants were altered in the membrane targeting PH domain. These constructs lacked residual translocation activity of this domain. The probe's PKC substrate loop harboured three phosphate acceptor amino acids. These were mutated systematically to alanines or glutamates. Comparison of responses from the different mutants showed a) that one specific serine in KCP-1 was necessary and sufficient to

produce a maximal response and b) that these three amino acids contributed differently to the FRET change. Potentially, these results can be conferred to pleckstrin, a protein of unknown function.

Furthermore, KCP-1's substrate loop was altered to extend specificity to other kinases. One of the engineered constructs responded to PKA activation.

In summary, a novel FRET reporter for PKC activity was developed and its applications and limitations were tested. The probes specificity could be extended to PKA and therefore, the reporter may serve as a platform for further probe development.

Zusammenfassung

Protein Kinase C (PKC) umfasst zehn Isoenzyme und reguliert eine Vielzahl an zellulären Funktionen. PKC-Aktivität in Zellen wird üblicherweise durch *in vitro* Experimente mit Zelllysaten untersucht. Der Nachteil solcher Methode ist, dass sie keinen Aufschluss über PKC-Aktivität in einzelnen, lebenden Zellen geben kann. Die vorliegende Arbeit stellt eine neue Fluoreszenzprobe für PKC-Aktivität vor. Die Kinase C Probe (KCP-1) besteht aus einer PKC-spezifischen Substratsequenz, die von zwei fluoreszenten Proteinen flankiert wird. Fluoreszenz Resonanzenergie Transfer (FRET) zwischen den gewählten Fluorophoren ist möglich. Die Substratsequenz ist ein verkürztes Pleckstrin, ein Protein das spezifisch von PKC zwischen einer Pleckstrin-Homologie (PH) und einer DEP Domäne phosphoryliert wird. Grün-fluoreszierendes Protein (GFP^2) und gelb-fluorezierendes Protein (EYFP) waren die FRET-Partner der Wahl, da bei diesen Donoremissions- und Akzeptoranregungsspektren perfekt überlappen.

Die Probe zeigte PKC-Aktivität in lebenden Zellen an. Zellen wurden unter anderem mit Phorbolester, Diacylglycerol, Histamin und Bradykinin stimuliert. Das Signal wurde durch Gabe von Gö6983, einem PKC-spezifischen Inhibitor, aufgehoben. Zelllinien, die stabil mit KCP-1 transfiziert waren, und KCP-1 transgene Fliegenembryonen zeigten, dass das Protein nicht zelltoxisch war. Experimente in lebenden Zellen oder *in vitro* zeigten, dass KCP-1 von PKC phosphoryliert wurde, aber nicht von Protein kinase A (PKA), Kalzium/Calmodulin abhängiger Kinase (CaMKII), Protein Kinase B und Aurora Kinasen. Diese Experimente demonstrieren, dass KCP-1 in lebenden Zellen verwendet werden kann um spezifisch PKC-Aktivität zu verfolgen.

KCP-1 wurde parallel mit anderen Fluorezenzproben, darunter welche für die PKC-Aktivatoren Kalzium und Diacylglycerol, beobachtet. Diese Experimente zeigten Möglichkeiten und Einschränkungen solcher Untersuchungen. Außerdem legten diese, als auch *in vitro* Experimente nahe, dass KCP-1 vornehmlich Aktivität von kalziumunabhängigen PKC Isoformen anzeigt.

Eine mögliche Anwendung von KCP-1 sind Screening-Verfahren für PKC-Inhibitoren. Vorläufige Experimente mit KCP-1-stabilen Zelllinien zeigten, dass solche Methoden prinzipiell möglich sind, aber noch weiterer Optimierung bedürfen.

KCP-1 kann durch verschiedene Änderungen verbessert werden: KCP-1 wurde in der PH Domäne mutiert, welche aktiviertes Pleckstrin mit der Zellmembran assoziiert. Solche Konstrukte zeigten keine Aktivität dieser Domäne.

Die Substratsequenz von KCP-1 beinhaltete drei Aminosäuren, die phosphoryliert werden können. Diese wurden systematisch zu Alaninen oder Glutamaten permutiert. Vergleiche der Signale dieser Proben zeigte, dass a) ein spezifisches Serin für eine maximalen FRET-Änderung hinreichend und notwendig war und, dass b) die drei Aminosäuren unterschiedlich stark zur FRET-Änderung beitrugen. Möglicherweise sind diese Ergebnisse auf Pleckstrin übertragbar, einem Protein mit unbekannter Funktion.

Des Weiteren wurde die Substratsequenz von KCP-1 mutiert, so dass die Kinasespezifität entweder geändert oder erweitert wurde. Eines dieser Konstrukte zeigte Signale nach Aktivierung von PKA.

Zusammengefasst, wurde mit KCP-1 eine neue FRET-Probe für PKC-Aktivität entwickelt und deren Möglichkeiten und Limitationen getestet. Die Spezifität der Probe konnte von PKC auf PKA ausgedehnt werden und lässt damit hoffen, dass KCP-1 eine allgemeine Plattform für weitere Probenentwicklung darstellen könnte.

Abbreviations

aa	Amino acid
ATP	Adenosine triphosphate
BSA	Bovine serum albumin
CaMKII	Calcium/calmodulin dependent kinase II
cAMP	Cyclic adenosine monophosphate
CCD	Charge coupled device
cDNA	Complementary DNA
cGMP	Cyclic guanosinemonophosphate
DAG	Diacylglycerol
DEP	Dishevelled, Egl-10, Pleckstrin
DiOG	1,2-Di-*O*-octanoyl glycerol
DMSO	Dimethylsulfoxid
dNTP	Deoxynucleotide triphosphate
EBFP	Enhanced blue fluorescent protein
ECFP	Enhanced cyan fluorescent protein
EDTA	Ethylendiamintetraacetic acid
EGF	Epidermal growth factor
EGFP	Enhanced green fluorescent protein
EYFP	Enhanced yellow fluorescent protein
FP	Fluorescent protein
FRET	Fluorescence resonance energy transfer
GFP	Green fluorescent protein
GFP^2	Green fluorescent protein square
GPCR	G-protein coupled receptor
GTP	Guanosine triphosphate
Hepes	4-(2-Hydroxyethyl)-1-piperazineethanesulfonic acid
HTS	High throughput screen
IP_3	Inositol 1,4,5-trisphosphate
KCP-1	Kinase C probe 1
KCP-1/AAA	Kinase C probe with the mutations S113A, T114A, S117A
KCP-1/EEE	Kinase C probe with the mutations S113E, T114E, S117E
$KCP\text{-}1/X^1X^2X^3$	Kinase C probe with the mutations $S113X^1$, $T114X^2$, $S117X^3$
mGFP	Monomeric GFP
min	Minutes
mRFP	Monomeric red fluorescent protein
MOPS	Morpholinepropanesulfonic acid
NaN	Not a number (= null)
nm	Nanometer
NMR	Nuclear magnetic resonance
PAGE	Polyacrylamide gel electrophoresis
PC	Phosphatidylcholine
pCiCF	FRET vector: Citrine-dummy-ECFP
pCiG2	FRET vector: Citrine-dummy-GFP^2
pCiRF	FRET vector: Citrine-dummy-mRFP
pYG	FRET vector: EYFP-dummy-GFP^2
PCR	Polymerase chain reaction
PDK-1	Phosphoinositol dependent kinase 1
PH	Pleckstrin homology
PIP_2	Phosphatidylinositol 4,5-bisphosphate
PKA	Protein kinase A

PKB	Protein kinase B
PKC	Protein kinase C
PKD	Protein kinase D
PKG	Protein kinase G
PKM	Catalytic subunit of protein kinase C
PLC	Phospholipase C
PMA	4β-12-*O*-Tetradecanoylphorbol 13-acetate
PMT	Photo multiplier tube
PTP1B	Phosphotyrosinephosphatase 1B
RACK	Receptor for activated C kinase
ROI	Region of interest
S/N	Signal to noise
SD	Standard deviation
SDS	Sodium dodecyl sulfate
STICK	Substrates that interact with C kinase
T4-PNK	T4-polynucleotide kinase
TBE	Tris, borate, EDTA
TPA	4β-12-*O*-Tetradecanoylphorbol 13-acetate
YFP	Yellow fluorescent protein

1 Introduction

1.1 Phosphate esters regulate cells

Life is fundamentally coupled to tight control of cell fate and function. In turn, cellular function is dependent on a complicated and densely interwoven network of signal transduction. Many mechanisms that control proteins' activities are known. One of the most common systems is phosphorylation and dephosphorylation of hydroxyl amino acids, which gained prominence in the early 1930s.[1, 2] A small chemical moiety, a phosphate group, is coupled to or cleaved from a protein, thereby rendering it active, inactive or making it a substrate for other cellular processes. The use of phosphates is an elegant mechanism by which nature reversibly marks proteins.[3] The phosphate group is derived directly from the most abundant energy source in the cell, adenosinetriphosphate (ATP). The phosphoric acid ester bond formed is stable, but can be cleaved easily by phosphatases, which ensures the reversibility of signals. Several enzyme classes, called kinases, are known to transfer phosphate groups from ATP to proteins and thereby activate or deactivate targets directly or indirectly.

1.2 Protein kinase C

One of the most scrutinized kinases is protein kinase C (PKC; reviewed in [4-9]). More than 40000 articles illuminate different aspects of this serine/threonine kinase. PKC, discovered in 1977 by Yasutomi Nishizuka and colleagues,[10-13] is now recognized to be a central actor on the stage of cellular signalling and plays a multitude of key roles.[14] PKC is involved in the regulation of a plethora of cellular events, ranging from gene transcription[15] and cell cycle control,[16, 17] to cytoskeletal function[18] and cell migration,[19] as well as senescence[20] and apoptosis.[21] This variety in function implicates deregulation of PKC activity in a multitude of diseases,[22] like diabetes,[23] alcohol related diseases,[24] dysfunctions of the central nervous system,[25] and, most prominent: cancer.[26-34]

Due to the vast number of PKC's cellular functions it is not surprising that PKC stimulation can occur via a multitude of signals. A classical example is initiation by binding of agonists to cell surface receptors, generation of second messengers like diacylglycerol (DAG) and *myo*-inositol 1,4,5-trisphosphate (IP_3) and subsequent release of calcium from internal stores.[35] DAG and Ca^{2+} are direct activators of PKC (Figure 1.1A).[36-39]

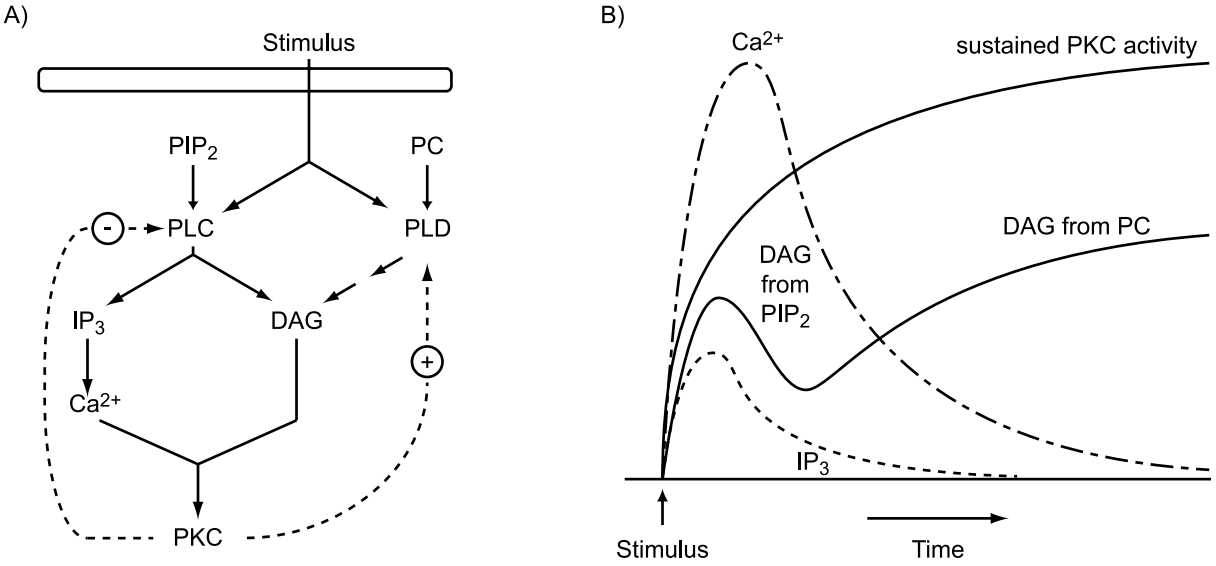

Figure 1.1: A) Cell stimulation activates signaling cascades. For example, phospholipases C (PLC) and D (PLD) are activated and hydrolyze membrane lipids to second messengers (diacylglycerol, DAG, and *myo*-inositol 1,4,5-trisphosphate, IP_3, which in turn activate protein kinase C (PKC). PKC regulates the lipases via negative and positive feedback loops. B) This mechanism leads to an early response parallel to phosphatidyl 4,5-bisphosphate (PIP_2) degradation (transient DAG increase, paralleled by calcium levels), and late responses due to sustained DAG concentrations from phosphatidylcholine hydrolysis (graphics are adapted from reference [40]).

A fast DAG signal is generated by phospholipase C (PLC)-mediated hydrolysis of phosphatidylinositol 4,5-bisphosphate (PIP_2) to DAG and IP_3. Such a short pulse of DAG from PIP_2 hydrolysis transiently activates PKC and results in early cell responses. However, the DAG level does not persist due to metabolism in cells and is not sufficient for cell activation. Sustained DAG levels and subsequent PKC activity are required for long lasting effects, like proliferation or differentiation. Prolonged increased DAG concentrations are attributed to hydrolysis of phosphatidylcholine (PC). PC is degraded by phospholipase D (PLD) to phosphatidic acid (PA), which subsequently is dephosphorylated by a phosphomonoesterase. This cascade occurs later in cell activation than PIP_2 breakdown (Figure 1.1B).[40-44]

PKC can be artificially activated by soluble and membrane-permeant DAG analogues, like 1,2-di-*O*-octanoylglycerol (DiOG, Figure 1.2A), which is metabolised in cells. In contrast, phorbol esters, like 4β-12-*O*-tetradecanoylphorbol 13-acetate (TPA or PMA, Figure 1.2B), permit a (relatively) specific and long-lasting activation of PKC.[45, 46] These molecules mimic DAGs, but they are not degraded in living cells.

PKC activity can be inhibited with various bisindolyl maleimides. These compounds attach to the ATP binding cavity of kinases and therefore, are often unspecific and inhibit several kinases.[47] For example, the natural compound

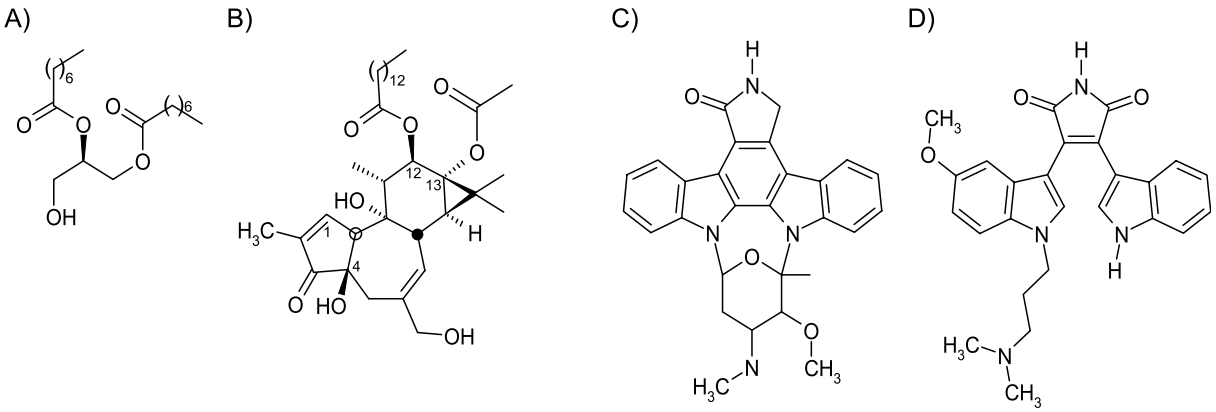

Figure 1.2: PKC is activated by diacylglycerol (A: 1,2-di-*O*-octanoyl glycerol) or phorbol esters (B: TPA). Bisindolyl maleimides (C: staurosporine, D: Gö6983) inhibit PKC by blocking the ATP binding site.

staurosporine (Figure 1.2C) is a potent inhibitor of PKC and several other members of the AGC [cAMP-dependent protein kinase (PKA)/ cGMP-dependent protein kinase (PKG)/ protein kinase C (PKC)] kinase family.[48] A relatively specific PKC inhibitor is Gö6983 (Figure 1.2D), a derivative of staurosporine.[49, 50]

The cloning and sequencing of mammalian PKC in the mid-1980s[51, 52] revealed that the kinase consists of 10 isoenzymes, which are classified into three sets: conventional (α, splicing variants βI and βII, and γ), novel (two pairs of closely related kinases: ε and η, and δ and θ), and atypical (ζ, ι) PKCs. Apart from these, two other, distantly related protein kinases were classified as PKCμ and PKCν, but now comprise a different kinase family, called protein kinase D (PKD).

The three PKC groups are closely related in terms of sequence and structure and differ primarily in regulation (Figure 1.3). They have a conserved, catalytic, C-terminal kinase domain next to a regulatory moiety. These are connected via a proteolytically labile linker. When the linker is cleaved, the regulatory domain

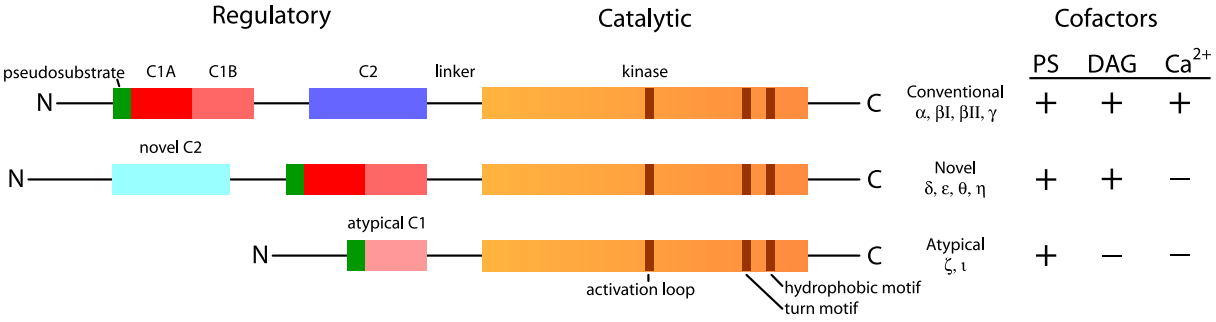

Figure 1.3: PKC is comprised of 10 isozymes that can be classified into three categories. Conventional and novel PKCs are activated by binding of tandemly repeated C1 domains to DAG. In addition, conventional PKCs are regulated by calcium that binds to the classical, but not novel C2 domain. Activity of atypical PKCs is thought to be controlled by phosphorylation. All PKC isoforms need phosphatidylserine (PS) as cofactor. Maturation of the PKC isozymes depends on proper phosphorylation of several amino acids in the catalytic subunit.

no longer controls the activity of the catalytic domain. The free catalytic domain is therefore constitutively active. It is named protein kinase M (PKM), since the only required cofactor is Mg^{2+}.[10]

Physiological activity of all PKC (holo-)isozymes depends on the presence of phosphatidyl serine (PS).[53] In fact, PKC activity was originally defined as lipid dependent kinase activity in tissue preparations.[54] The regulatory units of all isoforms harbor one or two cystein rich C1-domains that can bind to diacylglycerol or phorbol esters and thereby, localize the protein to membranes and activate it.[55-58] However, this module is mutated in atypical PKCs, rendering them insensitive to DAG or TPA. Therefore, conventional and novel, but not atypical PKCs are regulated by DAG levels. In addition, activity of conventional PKCs is controlled by a C2 domain, which, after coordinating Ca^{2+} ions, directs the protein to membranes and enhances DAG binding.[59-63] Such a motif is absent in atypical PKCs and is mutated to an inactive form in novel PKCs.[62] Recent results support suggestions[7] that the novel C2 domain (at least of PKCδ) may serve as protein-protein interaction platform, by demonstrating that this domain can bind to phosphotyrosines.[64]

An autoinhibitory pseudosubstrate sequence is located adjacent to the C1 domain in all isoforms.[65] This sequence binds to but is not phosphorylated by the catalytic cavity of the kinase domain and therefore, renders the PKC inactive. Activation of PKC leads to structural rearrangements, especially following membrane localization, and the pseudosubstrate is released from the catalytic core, making it accessible to PKC substrates.[53, 66, 67]

Phosphorylation of PKC is another prerequisite for kinase activity.[68, 69] The first step is phosphorylation of the activation loop either by autophosphorylation[70] or by the upstream phosphoinositide dependent kinase 1 (PDK-1).[71-74] This might be the activating signal in atypical PKC isoforms, which are not regulated by Ca^{2+} or DAG. The phosphorylation invokes a structural change that positions residues for catalysis and opens the substrate binding cavity of PKC to accept the pseudosubstrate or other substrates. Subsequently, PKC is autophosphorylated in the turn motif, making the kinase catalytically competent, thermally stable and phosphatase-resistant.[75, 76] Inhibition of this step abolishes any further maturation and kinase activity. In addition, the phosphorylated turn motif might serve as a docking site in protein-protein interactions.[77] The next step leads to intramolecular

autophosphorylation in the hydrophobic motif, which stabilizes protein structure.[78-81]

The biological activity of PKC is tightly regulated by lipids and cofactors, cellular localization of enzyme and substrate, and by binding partners that serve as PKC anchors. RACKs (receptor for activated C kinase)[82-84] and STICKs (substrates that interact with C kinase)[6, 85] are the most prominent examples of such proteins. Such binding partners appear to be specific for PKC isozymes, and peptide antagonists can be used to inhibit activity of particular PKC isoforms.[86, 87]

Tight control of PKC activity ensures discrimination between the different isozymes, but invokes a multitude of challenges for the researcher. Measurement of PKC activity *in vitro* or *in vivo* is difficult and prone to errors.[54]

PKC activity *in vitro* is commonly determined by performing phosphorylation reactions with radioactive γ-^{32}P-ATP or by binding assays with radioactively marked phorbol ester.[88, 89] The reactivity difference between reactions with and without lipid vesicles is attributed to PKC activity. Crucial for PKC reactivity is the molar ratio of lipid components, cofactors and protein. The assays must be adjusted to reach a linear correlation of enzyme concentration and activity by optimizing for the PKC isozyme, lipids, and substrate. Experiments are further complicated by the lability of the enzyme (especially proteolytic cleavage and generation of constitutively active PKM), self-aggregation, and association of PKC, a hydrophobic protein, with surfaces.[54] However, such experiments do not reflect PKC activity in live cells.

Testing PKC activity in living cells is also problematic. To associate PKC activity with a cellular response, it must be shown that an agonist activates PKC, a PKC specific activator replicates the effect, and a specific PKC inhibitor blocks the effect. Specific activators and inhibitors for kinases are often limiting. Although PKC was characterized as specific phorbol ester receptor, now several other proteins are known to bind to or to be activated by phorbol esters.[90-92] Also, inhibitors, which most often target the ATP binding site of kinases, show concentration dependent cross activity.[47]

Analyzing PKC isozyme activity, whether using crude cell lysate or purified enzymes is difficult since PKC activity is dependent on lipids and lipid composition. This is certainly altered during cell extract preparation. Furthermore, subcellular localization of PKC and binding partners dictate substrate specificity.

Translocation of PKC from the cytosol to membranes is an accepted hallmark for PKC activation, although this is not true for all isozymes, e. g. PKCη.[93] In cell extracts, a redistribution of PKC activity from the cytosol to the membrane fraction, was associated with PKC activity in live cells.[93] PKC can be analyzed in cell fractions by protein separation, Western blotting, and subsequent detection with isozyme specific antibodies. This method discriminates between intact enzymes and degradation products. A faster method would be immunohistology with fluorescently labeled antibodies, which yields a better spatial resolution, but cannot differentiate between intact and compromised enzyme.[54]

Fusion of PKC to fluorescent proteins (FP, see below), allow for isozyme specific and, in particular, time resolved observation of PKC activity in living cells. Similar experiments can be performed with extracellular labeled PKC isozymes that are microinjected into cells.[94] PKC activity is correlated to cellular redistribution of the fusion protein.[95] Caveats to this approach are that the observed PKC isoform is overexpressed and might thereby disturb the cellular signaling equilibrium. Also, some fusion proteins do not behave as wild type analogs. For example, FP tagged PKCs appear to be resistant to phorbol ester induced degradation, while non-tagged proteins are susceptible.[95] A further limitation is the need for single cell imaging for the detection of the fusion protein's redistribution from cytosol to plasma membrane.

A more elegant way to detect PKC activity is identification of the phosphorylation state of a PKC specific substrate. From the advent of PKC research, phosphorylation of protein p47, later called pleckstrin (for platelet and leukocyte C kinase substrate protein and KFARKSTRRSIR, its phosphorylation site),[96] has been used as an endogenous marker for PKC activity in platelets and leukocytes.[35] The phosphorylation state of the protein is detected by transfer of radioactive phosphate *in vitro* or *in vivo*. This method avoids problems of the assays described above, but is not able to monitor time resolved PKC activity in single cells.

This thesis presents a new fluorescent reporter for PKC activity, which combines the advantages of endogenous PKC substrates with that of fluorescent reporters. The reporter consists of a pleckstrin moiety, flanked by two fluorescent proteins that are capable of fluorescence resonance energy transfer (FRET). The single components and details of FRET are introduced below.

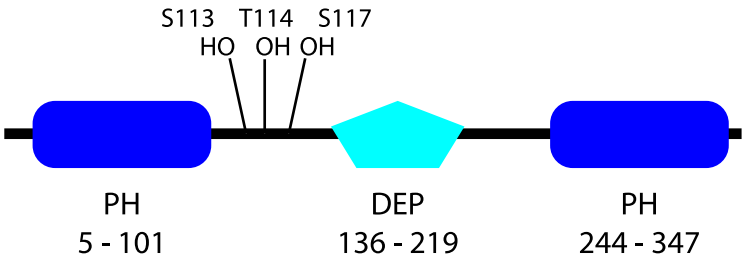

Figure 1.4: Schematic structure of pleckstrin: two terminal pleckstrin homology (PH) domains flank a DEP domain. Three amino acids, located between the N-terminal PH and the DEP domain, are phosphorylated by PKC. The DEP domain is separated from the C-terminal PH domain by a linker of 21 amino acids.

1.3 Pleckstrin

Pleckstrin (Figure 1.4), also called p47,[96-99] is the major substrate for PKC in platelets and leukocytes[100] where it is abundantly expressed (approximately 0.5% of the total protein).[101] Pleckstrin consists of two pleckstrin homology (PH) domains at the N- and C- termini that flank a DEP domain (for Dishevelled, Egl–10, Pleckstrin). PH domains are common motifs that facilitate protein-protein interactions and often bind to phospholipids.[102, 103] The DEP domain is putatively involved in protein interactions, although its exact role is not yet fully understood.[104]

PKC phosphorylates pleckstrin at three sites on a short sequence between the N-terminal PH and the DEP domain (108-KFARK$S^{113}T^{114}$RRS^{117}IRL-120; underline indicates phosphorylation sites).[105-107] Pleckstrin is specifically phosphorylated by PKC, but no isoform specificity could be detected.[107, 108] After phosphorylation, approximately 50% of pleckstrin molecules relocate from the cytosol to the plasma membrane.[109] However, phosphorylation is necessary but not sufficient for translocation, which seems to depend on guanosinetriphosphate (GTP) binding proteins in platelets.[109]

Pleckstrin appears to associate with $G_{\beta\gamma}$ and phosphatidylinositol kinases after phosphorylation.[110, 111] Pleckstrin's activation correlates with secretion of platelet granule contents.[97] Although, a clear function has not yet been assigned to pleckstrin, high abundance in platelets and phosphorylation after platelet activation suggest that it plays an important role in PKC-mediated platelet function.

To avoid confusion, it should be mentioned that another protein, named pleckstrin2, exists. This protein is 65% homologue to pleckstrin and has a similar domain organization. In contrast to pleckstrin, pleckstrin2 is expressed in a variety of tissues and lacks a PKC phosphorylation sequence.[112-114]

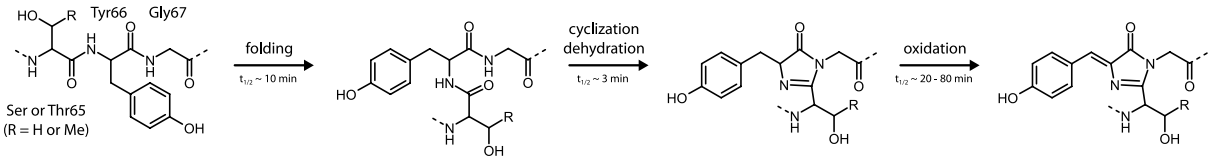

Figure 1.5: The fluorescent core in green fluorescent proteins is formed spontaneously from three amino acids in an aerobic process. Mutation of Tyr66 to His or Trp shifts excitation and emission spectra to shorter wavelengths. π-π-stacking with aromatic amino acids occurs in yellow fluorescent proteins.

1.4 Fluorescent proteins

Green fluorescent protein (GFP)[115, 116] was discovered in the early 1960s[117-119] in the jelly fish *Aequorea victoria*, but only in the last 15 years has its potential as valuable tool in life sciences been recognized.[120, 121] Fluorescent proteins and subsequent fusions with proteins of interests, have become standard tools for the investigation of biological problems.[121-123]

Common to all fluorescent proteins (FPs) is a fluorophore, produced by covalent bond formation between amino acids (Figure 1.5),[124-127] which is enclosed in a β-sheet barrel (called β-can, Figure 1.6). This shields the fluorescent core from the environment, reduces collisional quenching[128, 129] and stabilizes the protein: denaturation is only achieved with 6 M guanidinium chloride at 90°C or a pH outside

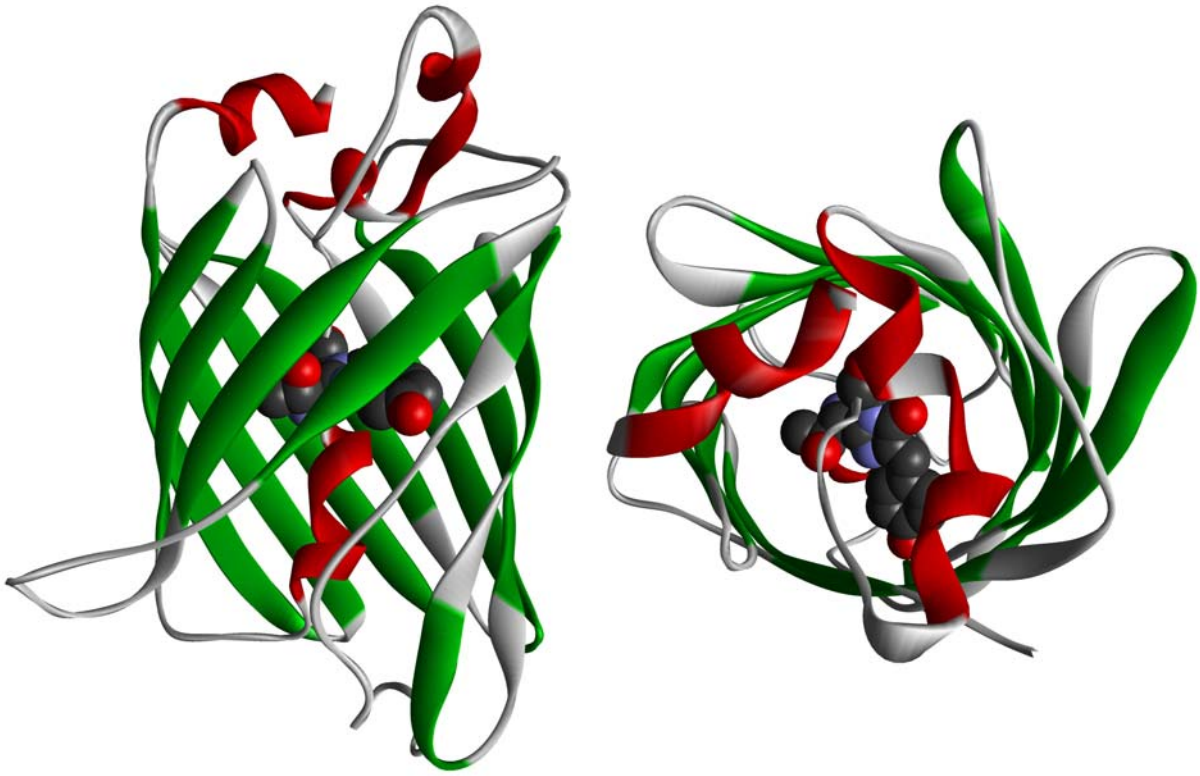

Figure 1.6: The common structure of fluorescent proteins (side and top view): a barrel of eleven β-strands (green) protects a central fluorophore (space filling model).

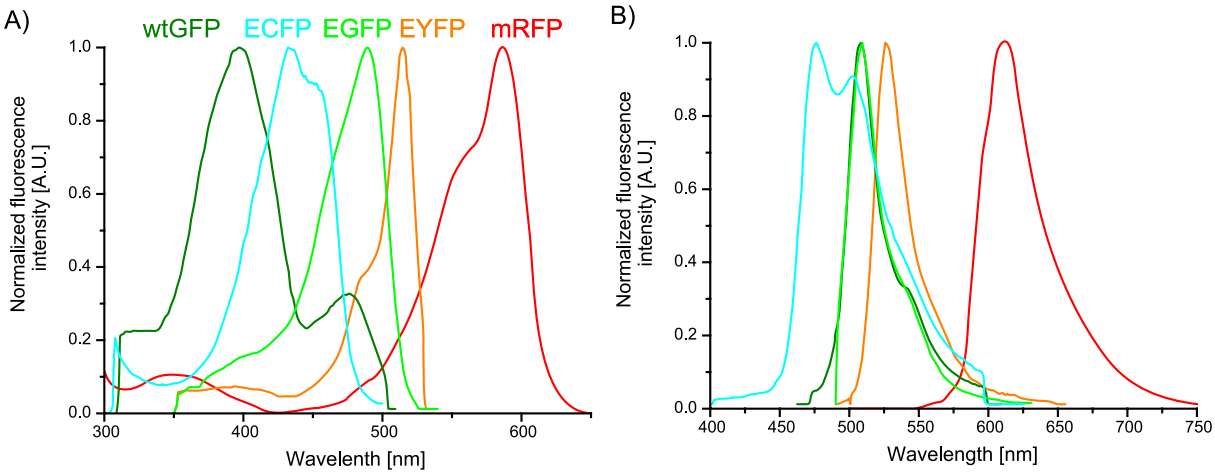

Figure 1.7: Excitation (left) and emission (right) spectra of some commonly used GFPs.

the range of 4 to 12. Renaturation occurs within minutes after dialysis or neutralization.[130, 131] Since the N- and C-terminal amino acids of GFP are in close proximity on a flat side of the β-can, they can be bridged with a short amino acid sequence and new, artificial termini can be generated in loops that connect the outer β-strands (circular permutation).[132]

Since the 1990s a multitude of variants, such as blue (BFP),[133] cyan (CFP),[125] and yellow (YFP)[128] emitting fluorescent proteins (Figure 1.7), was generated, and new green and red fluorescent proteins were discovered and isolated from marine animals.[134-142] In particular DsRed, a red fluorescent protein from the coral *Discosoma sp*, was heavily investigated and is now the precursor for more than 10 new fluorescent proteins with novel optical properties.[137, 143]

A mutation scheme for GFP is shown in Figure 1.8. Valine 1a was inserted to generate an optimized mammalian translation initiation sequence (Kozak sequence).[144] Mutations E80R and H231L were introduced with the first published GFP sequences and are probably due to PCR errors.[120] Replacing S65 by threonine causes ionization of the phenol in the chromophore, and thereby, shifts the excitation maximum from 395 nm to 490 nm.[145, 146] Substitutions of chromophore forming amino acids, such as Y66H or Y66W have a major impact on the excitation and emission spectra.[125] Proteins carrying these mutations have blue and cyan fluorescence, respectively. A yellow fluorescent variant (YFP) was created by replacing T203 with tyrosine.[128] This substitution permits π-π-stacking of the tyrosine with the chromophore and concomitant bathochromatic shift. The mutations F64L, S72A and others improve the protein's folding at 37°C.[146, 147] Additional mutations

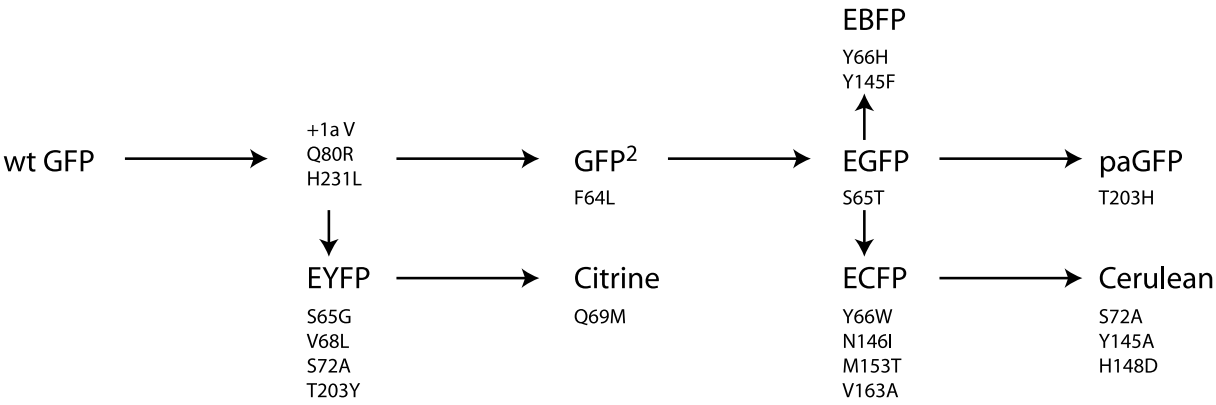

Figure 1.8: The different GFPs are obtained by mutation of single amino acids. The common ancestor is the wild type GFP derived from the jellyfish *Aequorea victoria* (EYFP: enhanced YFP; EGFP: enhanced GFP; ECFP: enhanced CFP; paGFP: photoactivatable GFP).

enhance the properties of the fluorescent proteins. For example, in the YFP-relative Citrine, the mutation Q69M closes a cavity near the chromophore and thereby reduces pH and ion concentration dependency.[148, 149] Another mutation, A206K, reduces the dimerization tendency and generates strictly monomeric GFPs (mGFP).[150]

Recently, new functionalities were incorporated into FPs. Important are photoswitchable species, whose optical properties change after UV irradiation. Most prominent are: photoactivatable (pa) FPs,[151-154] of which the main excitation band can be “switched on” by UV radiation and Kaede[155] and Kindling,[156] FPs that change their emission colour after activation. Only recently, KillerRed, an FP that induces cell death after activation with light, was presented.[157] These examples demonstrate that novel features can be added to fluorescent proteins and that the scope of applications will constantly expand, also far beyond ‘simple’ fluorescent functions.

1.5 FRET

Förster or fluorescence resonance energy transfer (FRET) was first described in 1948.[158] It is only in the last ten years that FRET became a standard tool in the life sciences.

FRET[159] is the radiationless energy transfer from a donor to an acceptor fluorophore via long-range dipole-dipole coupling. After donor excitation, relaxation does not occur via emission of a photon, which would result in fluorescence. Instead, the energy is transferred to an acceptor moiety. The acceptor may, but need not, emit a photon in response. This process reduces the excited state life-time and

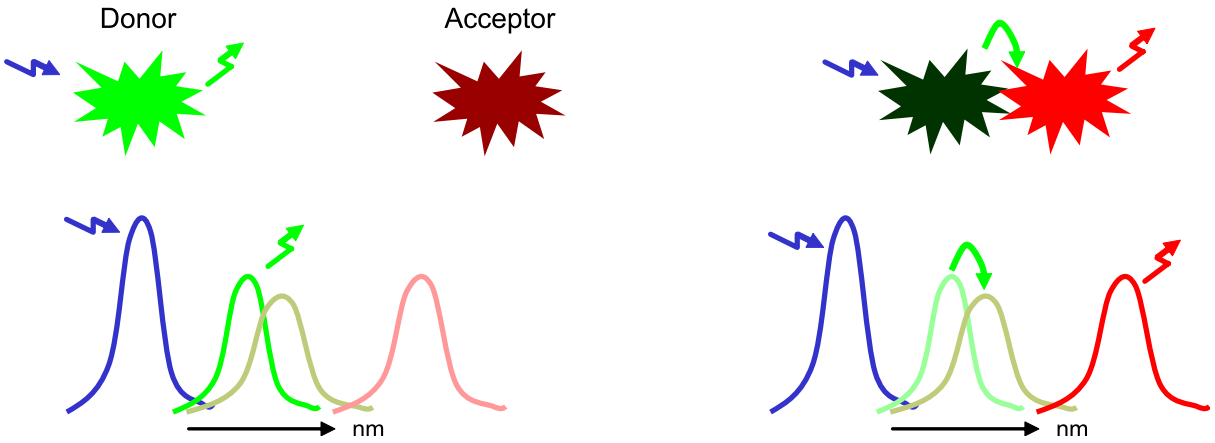

Figure 1.9: FRET is the radiationless energy transfer between a fluorescent donor (green) and an acceptor (red) moiety. Donor and acceptor must have overlapping emission and absorbance spectra: only then the donor energy can be transferred to the acceptor. The acceptor can be, but needs not to be fluorescent. The process is distance dependent: low FRET efficiency indicates separation of donor and acceptor (left), whereas close proximity of the partners results in high FRET efficiency (right). When both donor and acceptor are fluorophores, then the emission ratio represents FRET.

quantum yield of the donor. The efficiency E of the process can be calculated as $E = \frac{1}{1+(r/R_0)^6}$ with R_0, the Förster distance, being the distance with 50% FRET efficiency. R_0 can be calculated as $R_0 = c_0\ \kappa^2\ J\ n^{-4}\ Q_0$ with $c_0 = 8.8\text{x}10^{-28}$ for r in [nm], J being the overlap integral of donor emission and acceptor excitation, n the refractive index of the fluorophore separating medium, Q_0 the quantum yield of the donor, and κ is a dipole orientation factor [$\kappa = \vec{e}_1 \cdot \vec{e}_2 - 3(\vec{e}_1 \cdot \vec{e}_{12})(\vec{e}_{12} \cdot \vec{e}_2)$; $\vec{e}_1, \vec{e}_2, \vec{e}_{12}$ are the unit vectors of donor and acceptor transition dipoles and distance between their centers].

Hence, the efficiency of FRET depends on fixed parameters for a given donor/acceptor pair, like spectral overlap of donor emission and acceptor excitation, and dynamic variables, like the distance between donor and acceptor or their dipole-dipole orientation.[160] As such, a change of the relative geometry of a donor/acceptor pair can be detected by a change of FRET efficiency (Figure 1.9).

Several techniques for measuring FRET are commonly used.[159] When both donor and acceptor are fluorescent moieties, FRET can be directly evaluated by recording fluorescence values for each fluorophore and calculating a ratio of the two. A change in this ratio reflects a change in fluorescence of donor and acceptor moieties. If this is attributed to FRET, then a change of this emission ratio is directly related to a geometrical change of the dyes.

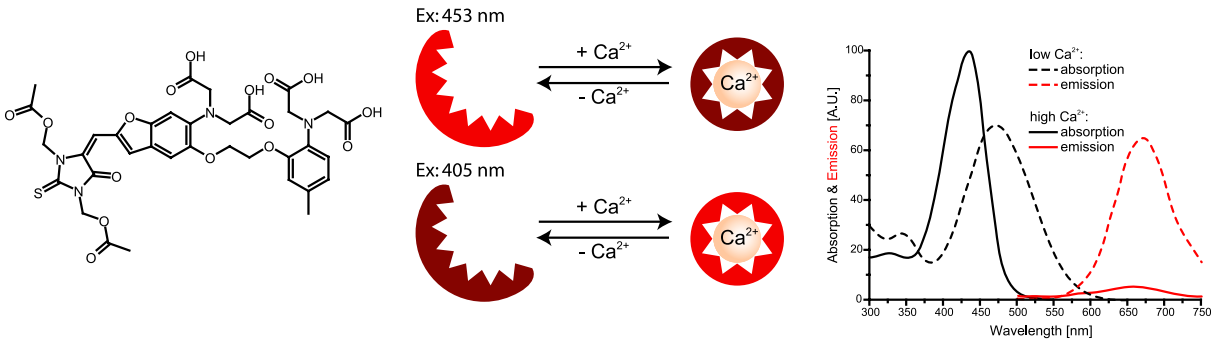

Figure 1.10: Fura red (left) coordinates Ca^{2+} and thereby changes its spectral properties (middle and right). Depending on the fluorophore's excitation, either an increase or decrease of fluorescence correlates to calcium levels (middle).

1.6 Fluorescent probes in live cell imaging

Of the innumerable and diverse fluorescent reporters used in live cell imaging,[161, 162] three different classes important for this work are introduced here. The probes are classified according signal type.

1.6.1 Probes that change fluorescence

Probes that change their fluorescence intensities are modified by or bind to a substrate. This causes their excitation and/or emission spectra change, resulting in a recordable signal. Often, such probes are small molecules, like the calcium sensitive fura dyes, which are used to measure calcium concentrations in live cells.[163] These dyes bind calcium and a concomitant change of the electron system alters fluorescent properties (Figure 1.10).[164] Another example would be the recently developed probes for *in vitro* kinase activities.[165, 166] These probes (Figure 1.11)

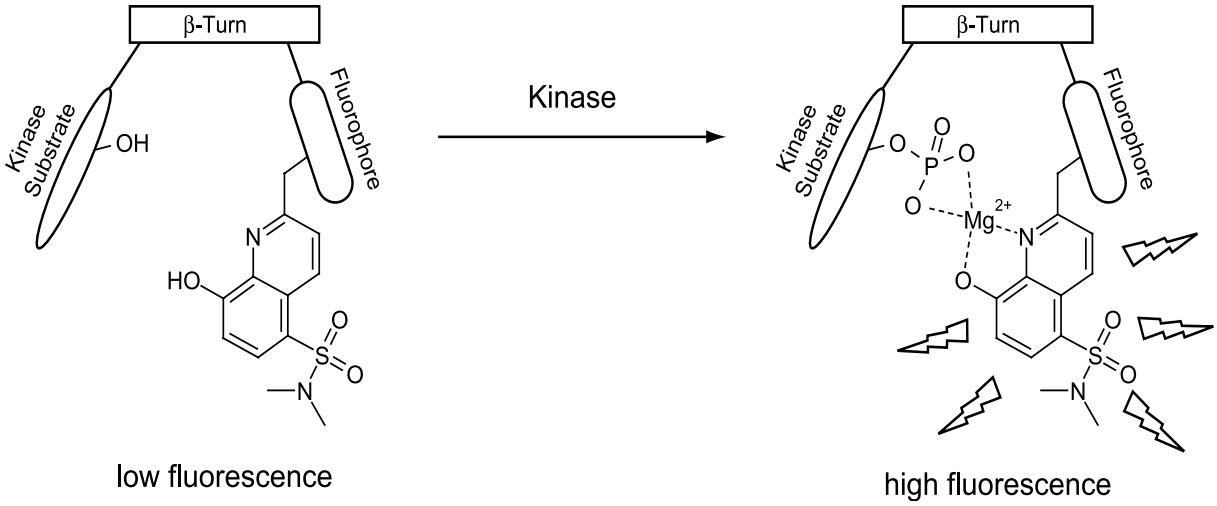

Figure 1.11: A magnesium sensitive dye recognizes the phosphorylation state of an adjacent kinase substrate sequence. The phosphate and the fluorophore coordinate magnesium and thereby change the spectral properties of the fluorophore.

consist of a kinase substrate sequence in proximity to an Mg^{2+} sensitive dye. The molecule coordinates magnesium after phosphorylation. Mg^{2+} is complexed by the phosphate group and the dye, which thereby changes its fluorescence.

Environment sensitive yellow fluorescent proteins were used to report pH or chloride concentration in living cells.[167-170] This FP has a cavity close to the chromophore, which can host protons or halides.[148, 149] The advantage of genetically encoded probes is that they are easily targeted to subcellular compartments via an attached signal sequence.[115] In another approach, a substrate sensitive moiety is inserted into the β can of an FP.[171] Binding of substrate invokes a structural rearrangement, which affects the fluorescence of the chromophore. Such an approach was chosen to generate a Ca^{2+} sensor by inserting calcium sensitive calmodulin between the amino acids 145 and 146 of YFP or Citrine.[132, 149] In another approach new termini were generated in GFPs by circular permutation. The new ends were equipped with a kinase substrate sequence and a phosphorylation recognition domain. The recognition domain binds to the substrate sequence after phosphorylation. This invokes a structural change of a fluorescent protein and subsequently, a change in fluorescence.[172, 173]

1.6.2 Probes based on translocation

Probes that report a cellular event by redistribution from one subcellular compartment to another (Figure 1.12) are most often fusion proteins of a reporter domain and a fluorescent protein.[174-177]

Such probes are targeted to a membrane either because their binding partners are located at the membrane or their affinities to membrane components are enhanced after target binding. Prominent examples are GFP fusion proteins of PH,[178-185] C1,[186] and C2[187] domains, which report phospholipid, DAG, and Ca^{2+} concentrations, respectively. In these cases, localization of the probe at the plasma membrane indicates the presence of the corresponding binding partner.

Another approach is to label a protein of interest that redistributes in a cell after its activation, for example GFP tagged PKC isozymes.[94, 188-190]

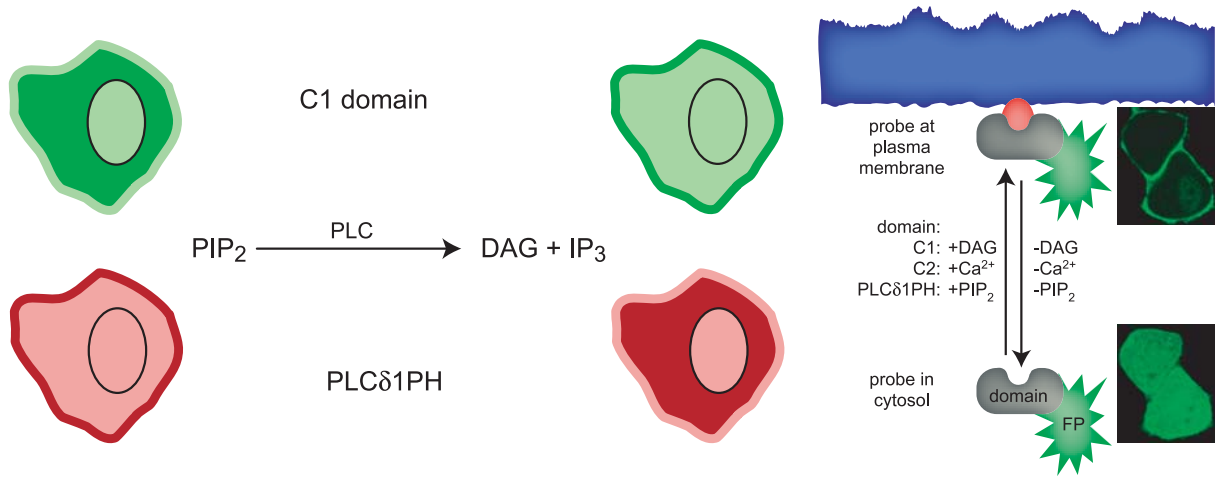

Figure 1.12: Translocation probes report target concentration by redistribution from the cytosol to the plasma membrane, or *vice versa*. For example, the PH domain of PLCδ1 recognizes PIP_2 at the plasma membrane. After PLC activation, PIP_2 is hydrolyzed to DAG and IP_3 and the PLCδ1PH relocates to the cytosol (lower panel). In parallel, DAG recruits a C1 domain to the plasma membrane (upper panel). Domain fusions with a GFP can be used to monitor such events (right part).

1.6.3 FRET probes

Probe systems based on FRET report a cellular event by changing FRET efficiency.[122] FRET partners can be small molecule dyes or GFP variants. Synthetic dyes include the whole range of chemical accessible fluorophores and optimal FRET pairs can be selected.[161, 191-194] Such probes often require elaborate chemical synthesis and must be cell-permeant or microinjected into single cells. In contrast, genetically encoded FRET reporters can be readily expressed in living cells by cDNA transfection. Additional localization sequences can be used to direct the probes to specific cellular compartments. However, dyes of such probes are restricted to the limited pool of fluorescent proteins. Up to now, predominantly CFP and YFP variants are used as FRET partners.[191]

FRET probes can be divided into inter- and intramolecular systems. The first kind of system generates a FRET signal upon association of fluorescently labelled interaction partners (Figure 1.13A).[195] The signal is lost when the components dissociate. For example, this approach was employed to monitor activation and multimerization of G protein coupled receptors (GPCR), by coexpressing ECFP and EYFP fusions of GPCR components in the same cell.[196] FRET between a small, fluorescently labelled peptide and a GFP tagged protein domain was used to measure phosphotyrosine phosphatase 1B (PTP1B) activity. When PTP1B is active, the peptide can bind and a FRET change is detected.[197]

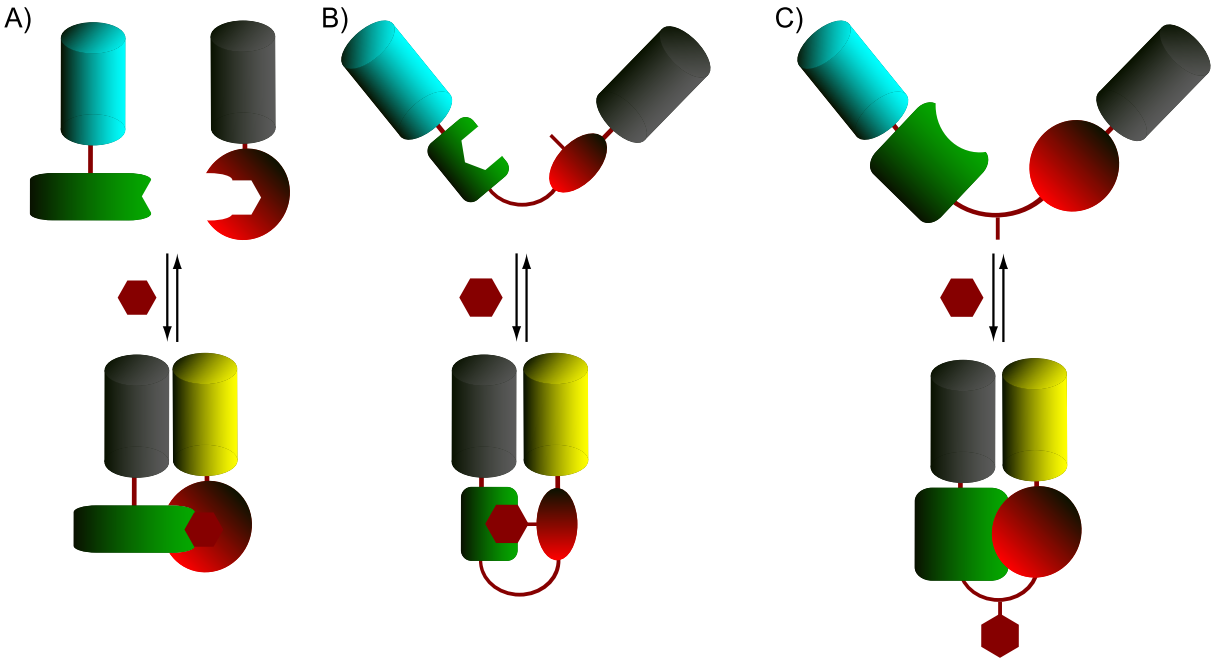

Figure 1.13: Different designs of FRET systems. A) Two labelled proteins associate and FRET partners are brought together. B) After modification, a substrate sequence binds to an intramolecular recognition domain. This changes the probe's geometry and thereby the FRET efficiency. C) Two domains alter their interaction when the intervening sequence is modified. FRET efficiency between two attached fluorophores reports the concomitant structural change.

Probes measuring intramolecular FRET can be small molecule probes or genetically encoded reporters. Small molecule probes are chemically synthesized compounds which are modified or cleaved by target enzymes. Peptide sequences that are substrates for kinases were labelled with two, FRET capable fluorophores. Phosphorylation invokes a structural change of the peptide that can be measured through FRET change.[198] Probes that are cleaved due to enzyme activity have the disadvantage of being irreversible. However, the detected FRET change can be enormous since the distance of the dyes changes from close proximity in the intact probe to virtual infinity after the probe is cleaved. For example, this approach was chosen to report lactamase,[199, 200] phospholipase,[201] and caspase activity.[202]

An early genetically encoded FRET probe was a calcium sensor, named cameleon.[149, 203-206] The probe is constructed of CFP and YFP, which sandwich the calcium binding protein calmodulin, and an M13 peptide. The affinity of M13 for calmodulin is increased when the latter binds calcium. This invokes a structural and concomitant FRET change. As a general scheme, two fluorescent proteins flank the N- and C-termini of a core (Figure 1.13B). The core moiety consists of a sequence that is modified by a protein of interest, and a recognition domain, which changes its affinity for the substrate sequence, dependent on the modification. A drawback of

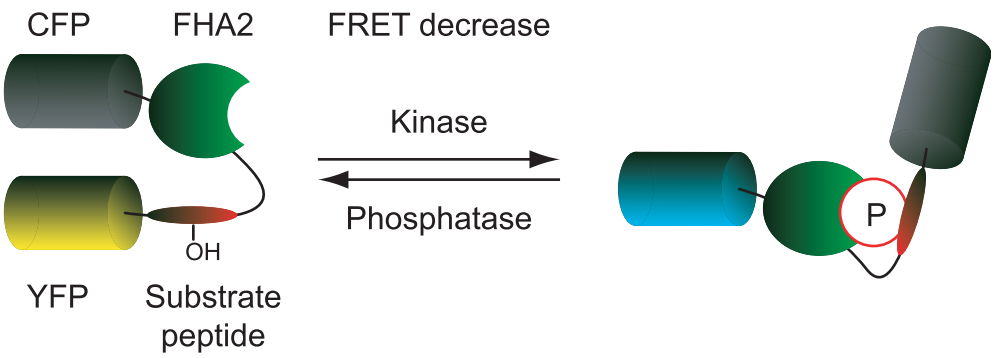

Figure 1.14: Design and proposed mechanism of CKAR. A recognition domain (green) and a PKC substrate sequence are flanked by CFP and YFP as FRET pair. The recognition domain binds to the substrate sequence after phosphorylation. This alters the structure of the probe and consequently the FRET of the fluorophores. A FRET decrease reports kinase activity.

such designs is that employed recognition domains may interact with endogenous substrates. For example, the original cameleon also bound to endogenous calmodulin and thereby decreased the probe's sensitivity. However, a design shown in Figure 1.13B is now employed in a multitude of probes, among them, reporters for cAMP,[207] methylation,[208] and kinases/phosphatases.[209-213] During the course of the work presented here, a FRET reporter for PKC based on this method was published by Violin *et al.*[214] This C kinase activity reporter (CKAR; Figure 1.14) is a generic probe based on an artificial design. CKAR's PKC sensitive moiety consists of a PKC substrate sequence with threonine as phosphate acceptor. The sequence was predicted to be an excellent substrate sequence for all PKC isoforms, but not for other kinases. An FHA2 domain is attached via a short linker to the peptide. The FHA2 domain binds to phosphothreonine with modest affinity, which guarantees access for phosphatases and therefore reversibility of the signal. The idea was that the FHA2 domain binds to the threonine after phosphorylation. A concomitant structural change of the construct invokes a change in FRET between the two flanking fluorophores, CFP and YFP. Although no PKC isozyme profile for CKAR was published, experiments that demonstrate synchronization of calcium levels and PKC activity suggest that the probe predominantly follows activities of conventional, calcium dependent PKC isozymes.

The PKC activity probe presented in this thesis is based on pleckstrin, which is believed to have no PKC isozyme preference and therefore, may also report activities of novel and atypical PKCs. The probe is based on a less common design: a core structure is equipped with two fluorophores. The core changes conformation after modification, without the need for an extra recognition domain (Figure 1.13C).

2 Aim of the project

Protein kinase C has a central role in cellular signalling, and deregulation of its activity is associated with a multitude of diseases. To investigate PKCs regulation, it is desirable to observe the kinase activity in living cells or animals, possibly in context with other parameters. Fluorescent methods are currently the only non-destructive technique to monitor cellular events with spatio-temporal resolution in single cells.

The aim of the project was to develop a novel FRET-based PKC activity sensor and to investigate its possibilities and limitations. The general design of such a probe included a kinase sensitive moiety, which was flanked by two fluorophores capable of FRET.

Genetically encoded FRET reporters have several advantages compared to other probes. For example:

- Modern techniques in molecular biology permit quick generation and optimization of reporter proteins. In contrast, chemical probes require elaborate synthesis, and even minor modifications of probes are difficult.
- Signalling sequences can be easily attached to genetically encoded reporters and direct them to specific cell compartments.
- FRET probes are independent of additional factors to exhibit a signal.

The kinase sensitive moiety of the probe had to have several features:

- PKC specificity.
- Reversibility of the modification.
- Negligible interference with cellular function.
- Conformational change after modification.

A fragment of the PKC substrate pleckstrin fulfils these requirements, promising kinase specificity and reversibility of phosphorylation. The protein is abundant in cells of hemopoietic origin, but absent in other cells. Therefore, expression of a pleckstrin fragment in most cell lines will most likely interfere minimally with cellular signalling. Residual activity of the pleckstrin fragment may be suppressed by mutations in the probe. A difference in conformation between phosphorylated and unphosphorylated probe was demonstrated by NMR structure experiments.

3 Results

3.1 Design and cloning of KCP-1

The protein kinase C activity probe consists of a core peptide-structure, sandwiched between two FRET capable fluorophores (Figure 1.13C). The probe is based on the idea that the protein conformation and therefore, the FRET signal changes upon phosphorylation of the core structure by PKC.

Core structure: The reporter's core was derived form pleckstrin, the major substrate of PKC in platelets.[96, 99, 108] Pleckstrin consists of two terminal pleckstrin homology (PH) domains flanking a central DEP (Dishevelled, Egl-10, Pleckstrin) domain (Figure 1.4). A linker harbouring three phosphorylation sites (S113, T114, and S117) is located between the N-terminal PH and DEP domain.[105, 106] NMR studies suggested that pleckstrin changes conformation after phosphorylation of these sites.[215] This reorganization was also observed when the C-terminal PH domain was deleted. It was expected that a structural change of the pleckstrin fragment would also change positions of two N- and C-terminally attached, FRET-capable fluorophores. A change in their relative geometry is concomitant with a change in FRET efficiency.

Fluorophores: Two fluorescent proteins were chosen as FRET partners. As donor, a green fluorescent protein variant, GFP^2, was selected. The fluorophore is excited with violet light either by appropriate band pass filters or a 405 nm diode laser. The emission band of GFP^2 at 515 nm overlaps perfectly with the excitation band of enhanced yellow fluorescent protein (EYFP) or Citrine, the acceptors of choice (Figure 3.1A).[216]

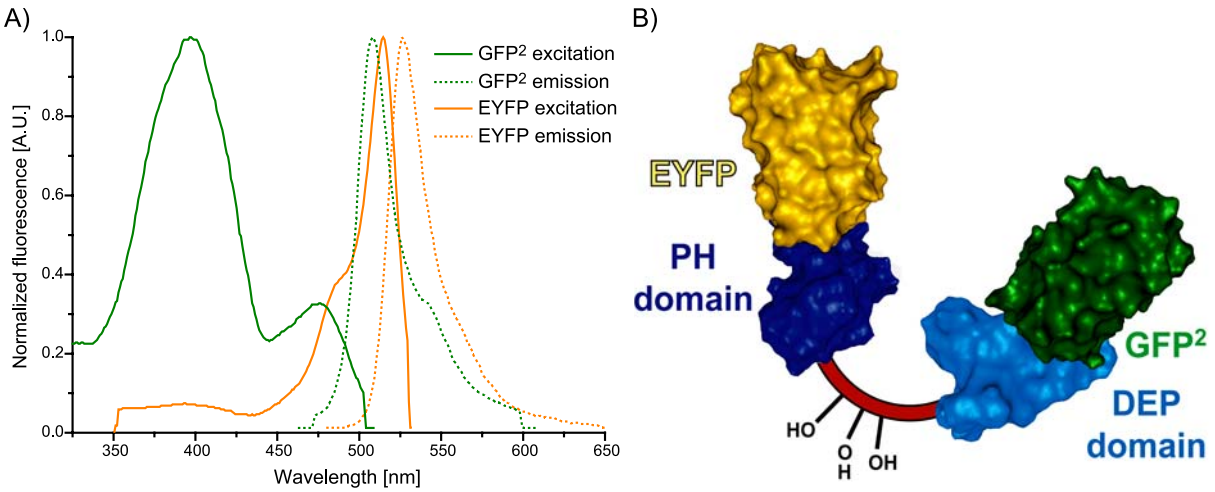

Figure 3.1: A) Emission and excitation spectra of GFP^2 and EYFP. The large overlap of GFP^2 emission and EYFP excitation make these fluorophores an excellent FRET pair. B) Design of KCP-1: two fluorophores flank a PKC sensitive moiety.

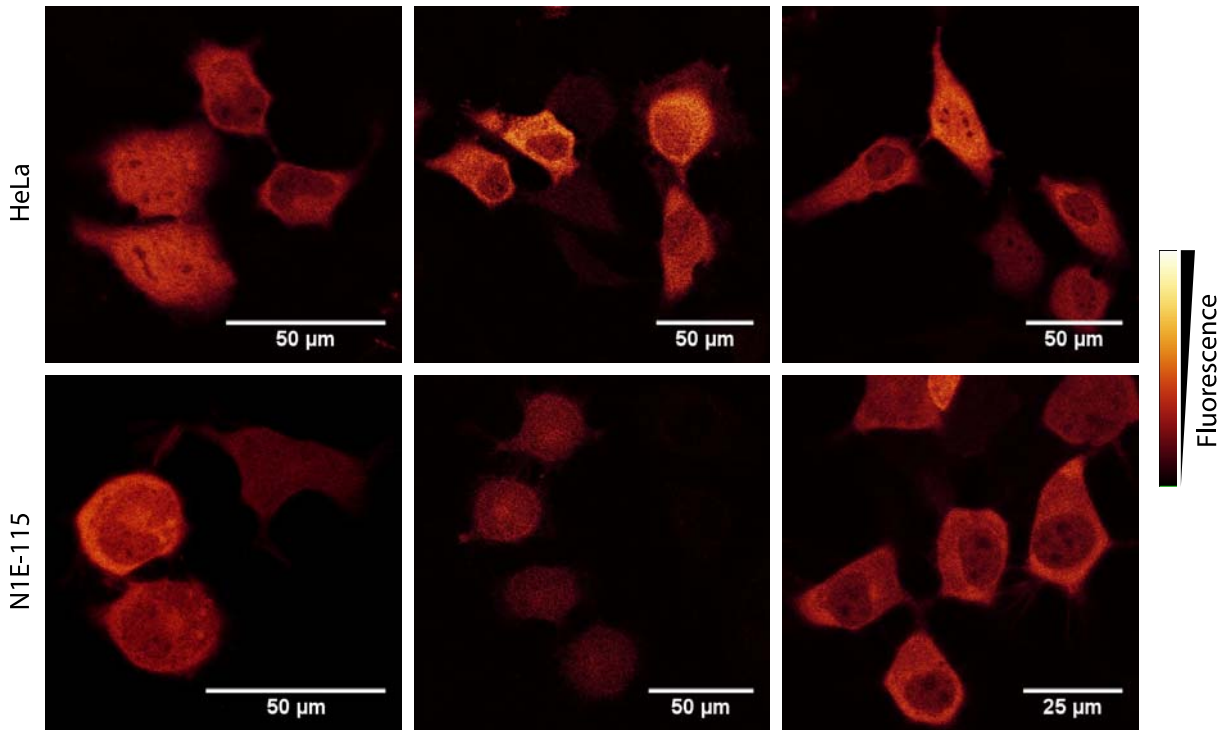

Figure 3.2: HeLa and N1E-115 cells expressed KCP-1 primarily in the cytosol.

Cloning and transfection: The probe was named kinase C probe 1 [KCP-1 or KCP-1(YFG2); YF: EYFP and G2: GFP^2] and has the design shown in Figure 3.1B. cDNAs coding single moieties were assembled in a mammalian expression vector, derived from the commercially available pEYFP-C1 vector.[217] The resulting vector was readily transfected into HeLa and N1E-115 neuroblastoma cells. Both cell types expressed the probe primarily in the cytosol (Figure 3.2). Two HeLa cell lines stably expressing KCP-1 were generated (HeLa/ASI and HeLa/ASII), indicating that KCP-1 was not toxic to cells.

In collaboration with Gunter Stier (Michael Sattler's group, EMBL), a bacterial expression vector that encoded KCP-1 was prepared. This allowed KCP-1 expression and purification from *E.coli* for *in vitro* experiments.

3.2 In vitro Experiments

3.2.1 Phosphorylation assays with □-32P-ATP

The purified protein was used to test KCP-1 performance *in vitro*. KCP-1 specificity for PKC isozymes was tested together with Alexander Gasch (Michael Sattler's group, EMBL). Recombinant KCP-1 was treated with PKCδ, PKCε, PKCη, PKCθ, or PKCζ in the presence of γ-^{32}P-ATP. Histone H3 phosphorylation was

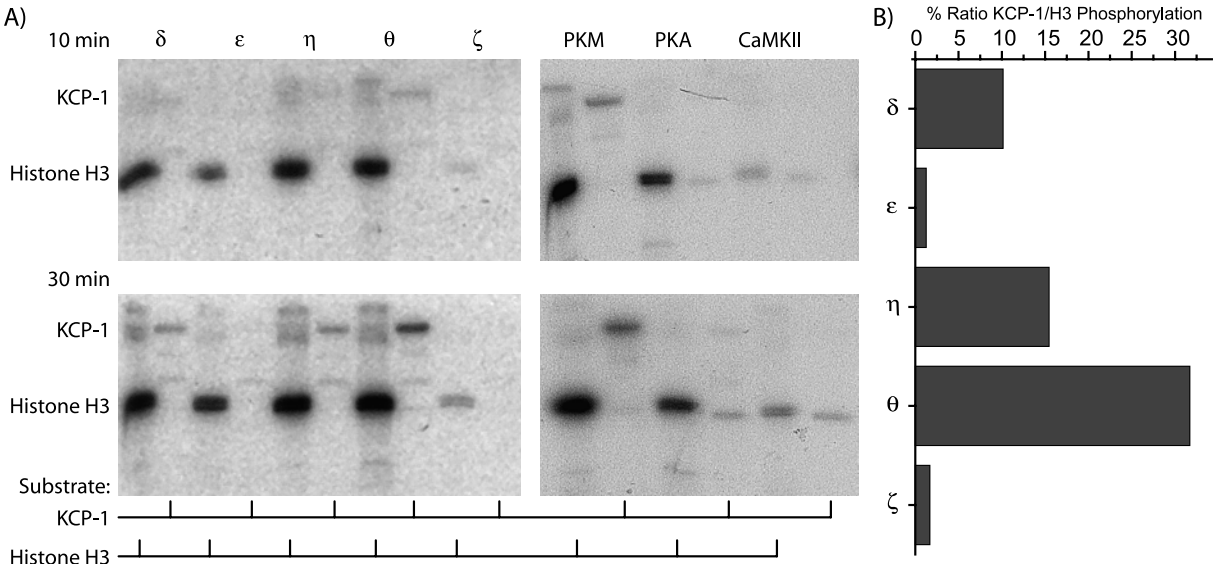

Figure 3.3: A) KCP-1 was phosphorylated by several PKC isoforms; among these, PKCθ was the most active. PKA and CaMKII showed only minor or no kinase activity with KCP-1. B) PKCθ was two to three times more active than other PKC isozymes (phosphorylation normalized to kinase activity with Histone H3 as substrate).

used as an isozyme activity control. Autoradiography was made from an SDS-PAGE gel, loaded with the phosphorylation products (Figure 3.3A). This experiment did not show PKC isozyme specific phosphorylation of KCP-1, but did demonstrate a preference for PKCθ. After KCP-1 phosphorylation was normalized to H3 phosphorylation, PKCθ was two to three times more potent than PKCδ or PKCη (Figure 3.3B). However, the reactions were performed according to manufacturer's recommendations and were not optimized for the substrates. Therefore, these values do not fully clarify isozyme preferences *in vitro* or *in vivo*.

The *in vitro* probe was further used to test for PKC specificity over PKA or CaMKII phosphorylation. SDS-PAGE and autoradiography showed no CaMKII and only very minor PKA activity with KCP-1 as substrate (Figure 3.3A). Recent results showed that the probe was not a substrate for protein kinase B (PKB), Aurora A and Aurora B kinases.[218]

Such experiments were also conducted with a PH-DEP construct lacking the fluorophores and gave results comparable to KCP-1.[219] In addition, these experiments included the conventional PKC isoforms α, βII, and γ, which gave phosphorylation levels similar to PKCδ. It can be expected that KCP-1 exhibits behavior similar to the PH-DEP construct for these PKC isoforms.

3.2.2 Fluorimeter experiments

FRET changes of KCP-1 following phosphorylation were monitored in a fluorimeter. The catalytic subunit of PKC (PKM) was used for phosphorylation, since it was constitutively active and required only Mg^{2+} as cofactor.[11] The experiments were therefore independent of calcium, lipids and lipid vesicles, which were needed for PKC holoenzyme activity assays.[54] KCP-1, purified from a bacterial protein preparation, and commercially available PKM may have contained residual protease activity. Therefore, protease inhibitors were included in the experiments. The addition of bovine serum albumin (BSA) stabilized the reaction mixture, possibly by providing hydrophobic surfaces or by titrating away protease activity. An emission spectrum from 490 - 540 nm was recorded once every 90 seconds. GFP^2 and EYFP fluorescence was integrated over 490 - 510 nm and 520 - 540 nm, respectively.

The absolute fluorescence intensities increased over time, which could be attributed to continuous maturation of fluorophores.[220] After kinase addition, FRET increased as shown by a positive ratio change, with reduced emission of GFP^2 and increased emission of EYFP (Figure 3.4A, black and red traces). From the fluorescence curves, the isosbestic point was determined to be 515 ± 1 nm. Fluorescence measured at this wavelength was not affected by PKM/ATP treatment nor did it change during trypsin cleavage of the probe (Figure 3.4A, green trace). Fluorescence spectra that were normalized to 515 nm emission directly showed the

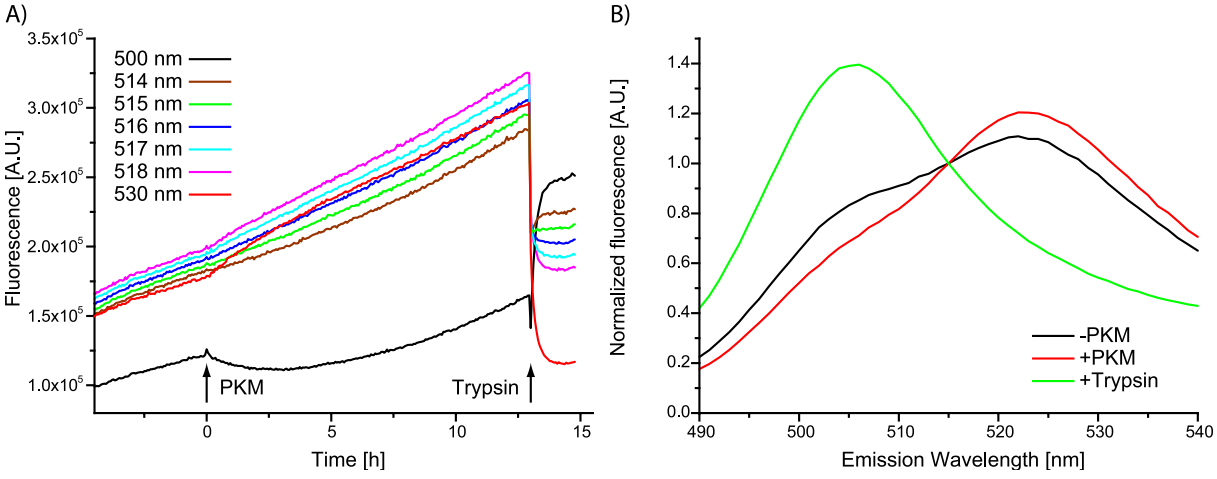

Figure 3.4: A) Fluorescence traces of different wavelength during *in vitro* phosphorylation of KCP-1 in the presence of PKM and ATP. Fluorescence increased during time, probably due to fluorophore maturation. When this background increase was subtracted, then fluorescence at 500 nm and 530 nm decreased and increased, respectively, due to larger FRET. In contrast, fluorescence at 515-516 nm was constant; this is the isosbestic point of the probe. B) Fluorescence spectra, normalized to 515 nm, of KCP-1 before and after phosphorylation and after trypsin cleavage. Unphosphorylated KCP-1 had a high initial FRET, which further increased with phosphorylation.

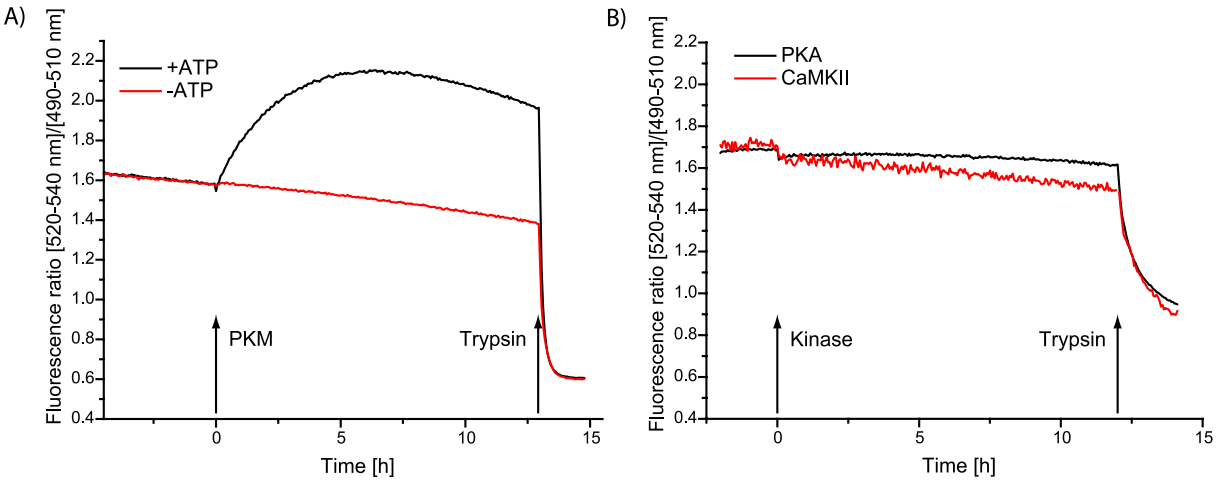

Figure 3.5: A) The fluorescence ratio increased only in the presence of PKM and ATP during *in vitro* reactions. B) PKA and CaMKII showed no activity with KCP-1 as substrate. The slow ratio decrease observed in all experiments was attributed to residual protease activity or different maturation kinetics of the fluorophores.

high initial FRET of KCP-1 (Figure 3.4B).

KCP-1 was fully phosphorylated in the presence of PKM and ATP after 5 hours. The FRET ratio increased 1.4 fold from 1.6 to 2.2 (Figure 3.5A). No FRET change was observed when ATP was absent, suggesting that phosphorylation of KCP-1 was responsible for the observed change. Trypsin treatment proteolytically cleaved KCP-1, but did not affect the fluorophores. After cleavage, the dyes were independent moieties and showed no FRET. Trypsin treatment showed a basal fluorescence ratio of 0.6, demonstrating that the unphosphorylated probe already exhibited relatively high FRET with a ratio of 1.6 (2.8 fold the basal level). It follows from this experiment that optimization of FRET change may involve decreasing the initial FRET efficiency of the unphosphorylated probe.

Preactivated CaMKII or the catalytic subunit of PKA gave virtually no responses (Figure 3.5B). These results support the probes specificity for PKC as observed in the autoradiography-assays described above.

3.3 Characterization of KCP-1 in live cell experiments

Live cell experiments were performed in HeLa and N1E-115 neuroblastoma cells. N1E-115 cells were imaged on a Leica SP2 confocal microscope, except as otherwise indicated. Cells were transfected overnight with a mammalian vector carrying the KCP-1 gene. Cells were starved in HEPES buffer before the experiments to minimize basal PKC activity, and imaged at room temperature or 37°C. No difference between results obtained under these conditions was detectable.

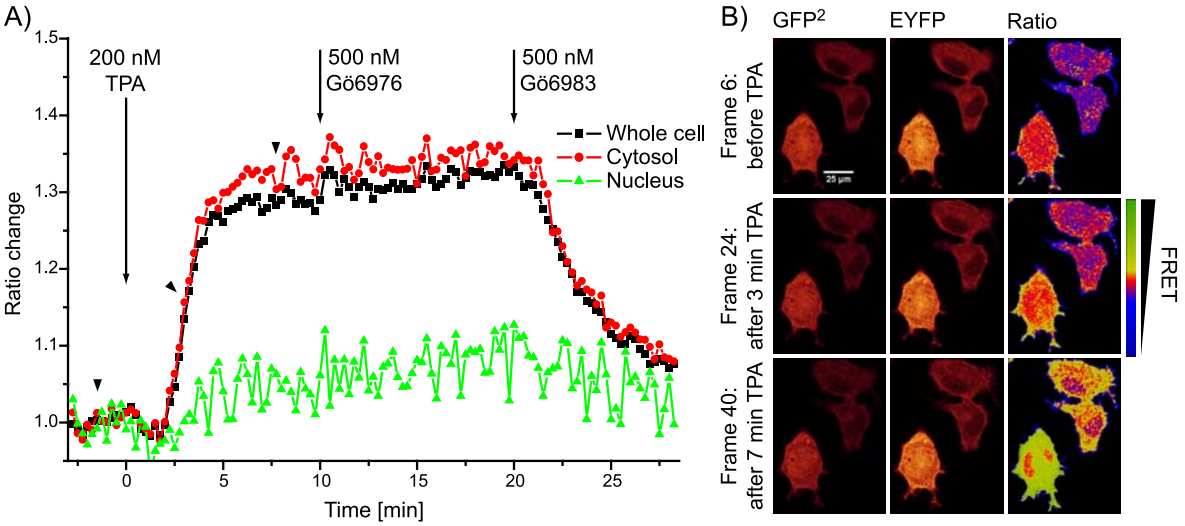

Figure 3.6: A) KCP-1 changed FRET efficiency after activation of PKC with TPA. Gö6976, a specific inhibitor for conventional PKCs did not influence the signal. The FRET change was reverted only after PKC inhibition with Gö6983, an inhibitor for all PKC isozymes. B) A change of FRET was observed in the cytosol but not in the nucleus.

Approximately ten minutes prior to experiments, cell dishes were removed from the incubator to allow temperature equilibration with the environment. GFP^2 and EYFP fluorescence was measured and a ratio value (hereafter called ratio for simplicity), was calculated. A change of this ratio was indicative for a change in FRET.

PKC activating phorbol ester (e.g. 12-*O*-tetradecanoylphorbol 13-acetate, TPA, also known as phorbol 12-myristate 13-acetate, PMA)[45] treatment led to a rapid FRET increase with an offset of approximately 2 minutes (Figure 3.6A). This delay of the response could be attributed to diffusion of TPA in the plasma membrane. Only after TPA binding was PKC activated and KCP-1 phosphorylated KCP-1, thereby inducing the FRET change.

FRET changes were observed in the cytosol and not in the nucleus (Figure 3.6B). The TPA induced FRET increase was reversed when the PKC-specific inhibitor Gö6983[50] was administered (Figure 3.6A). The FRET decrease after PKC inhibition was assumed to result from phosphatase activity, which removed phosphates from KCP-1 and reversed the probe's conformation to the original unphosphorylated state. This experiment demonstrated that KCP-1 was a reversible probe that reported active and inactive states of PKC. FRET changes after TPA treatment varied but averaged between 30 - 50%, with a signal to noise ratio in the order of 6:1.

To confirm that phosphorylation of S113, T114, and S117 was responsible for the FRET change in KCP-1, the amino acids were mutated to three glycines or

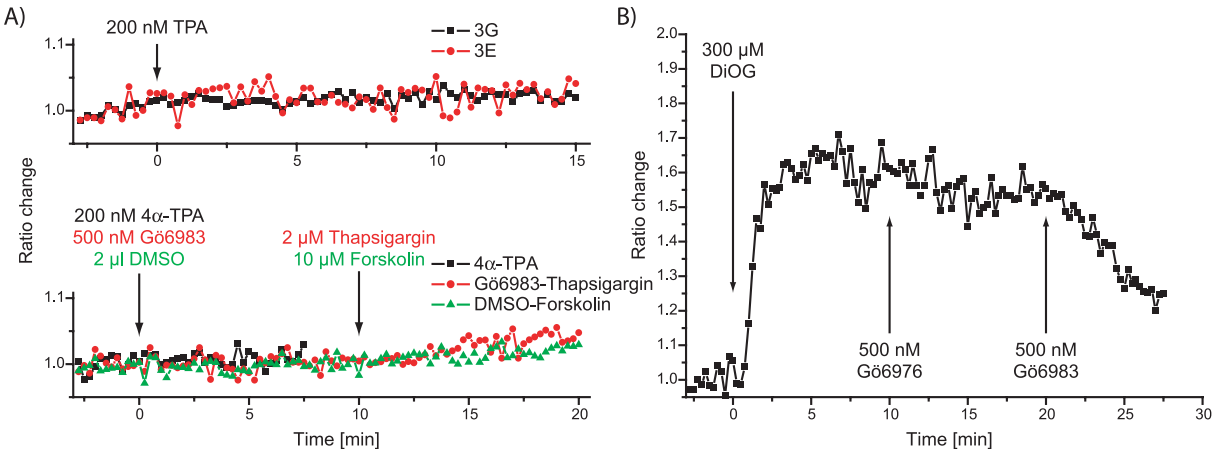

Figure 3.7: A) Mutation of S113, T114, and S117 to glycines or glutamates rendered the probe insensitive to TPA induced PKC activity (upper panel). KCP-1 showed no FRET change after cell treatment with inactive 4α-TPA, vesicle control (DMSO), or after activation of PKA and CaMKII (lower panel). B) KCP-1 reported PKC activation by DiOG, a short chain DAG derivative. (HeLa cells)

glutamates (constructs KCP-1/GGG and KCP-1/EEE, respectively). These mutations rendered the probe unavailable for phosphorylation. Neither construct responded to TPA, proving that these amino acids were the essential phosphate acceptors (Figure 3.7A, upper panel).

Treatment of the cells with 4α-TPA, which did not activate PKC, dimethylsulfoxyd (DMSO), the solvent for several drugs, or forskolin,[221] which activated protein kinase A (PKA), gave no FRET change (Figure 3.7A, lower panel). Similarly no FRET change was observed when cells were first treated with Gö6983 to block PKC activity and then with thapsigargin,[222] which elevated cytosolic Ca^{2+} concentrations and activated calcium dependent kinases like calcium/calmodulin dependent kinase (CaMKII). These experiments demonstrated that KCP-1 was not susceptible to PKA or CaMKII activation and were in accordance with the *in vitro* studies presented above.

A 30 µM dose of 1,2-di-*O*-octanoyl glycerol (DiOG), a soluble short chain diacylglycerol (DAG) derivative, gave a maximal KCP-1 response (Figure 3.7B). In contrast, thapsigargin, which should activate Ca^{2+} dependent PKC isozymes, led only to a slow, intermediate response. Subsequent TPA treatment augmented the ratio change (Figure 3.8A). It is interesting to note that the KCP-1 response after thapsigargin treatment could not be reversed by Gö6976, a specific inhibitor for conventional, Ca^{2+} dependent PKCs.[49] Therefore, thapsigargin indirectly activated calcium independent PKC isozymes, for example by calcium mediated hydrolysis of phosphatidylcholine (PC) to DAG.[41] PC degradation is a slow process, responsible

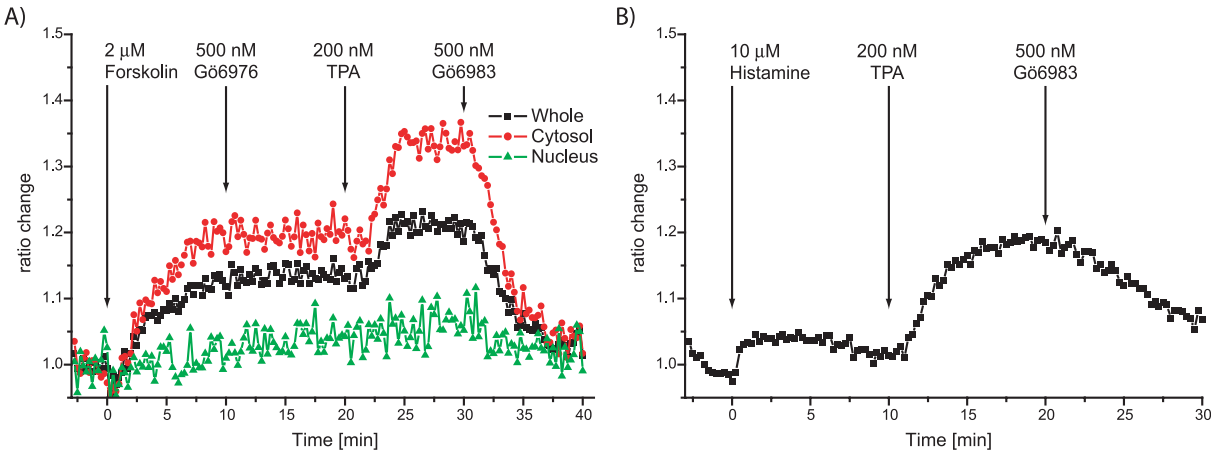

Figure 3.8: A) Activation of cells with thapsigargin resulted in an intermediate response which could be elevated by TPA treatment. The thapsigargin response could not be reversed with Gö6976. B) Histamine gave a lower response as compared to a maximal signal obtained after TPA (HeLa).

for sustaining DAG levels after cell stimulation.[40] Such kinetics could be reflected in the slow KCP-1 response after stimulation with thapsigargin.

More physiological PKC responses were expected with histamine stimulation of HeLa cells. This led to an immediate, but smaller FRET change relative to TPA (Figure 3.8B). The quick response contrasted TPA experiments, which showed offsets between TPA addition and KCP-1 response. One possible explanation is that histamine-activated cell receptors were in close proximity to PKC activating factors. This spatial organization allows for the immediate response of a cell to stimuli and avoids diffusion dependent delays, like that observed with TPA stimulation.

Stimulation of N1E-115 cells with bradykinin gave a transient FRET change that reached a maximum after approximately two minutes, followed by a decrease to the original FRET level within five to fifteen minutes (Figure 3.9A). This demonstrated that KCP-1 could dynamically monitor activation states of PKC.

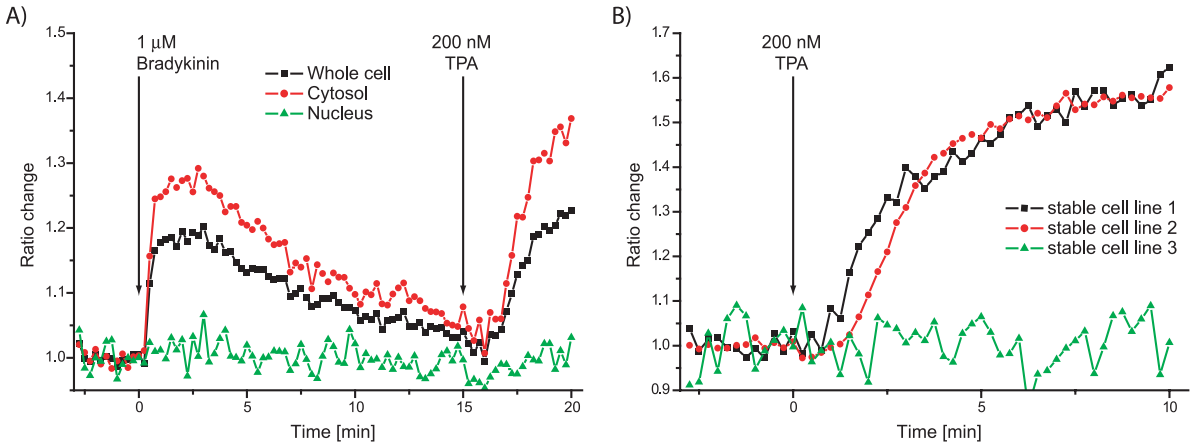

Figure 3.9: A) Bradykinin resulted in a transient KCP-1 response whose maximum is similar to levels induced by TPA. B) Two out of three generated HeLa cell lines stably expressed KCP-1.

Two HeLa cell lines stably expressing KCP-1 were generated, showing that KCP-1 was not toxic to cells. The establishment of a stably transfected N1E-115 cell line failed using standard protocols. Experiments with the stable HeLa cell line gave robust responses after histamine or TPA induced PKC activation (Figure 3.9B). These cell lines could be used for the screening assays (see below) or long term PKC activity monitoring, such as investigation of PKC activity during the cell cycle.

3.4 Technical aspects

The calculated ratios of EYFP and GFP[2] fluorescence can be influenced by the method used to acquire and calculate data. Aspects that might influence the results are discussed below. As example, a time course of HeLa cells stimulated with histamine and subsequently TPA was chosen. The recorded images contained bright and dim cells (Figure 3.10). A medium bright cell (cell 1 in Figure 3.10A) was arbitrarily chosen as reference to compare the influences of different factors.

For better comparison between methods and traces, a Z-value was calculated that combined signal to background and signal to noise (S/N; standard deviation) levels. The value was originally introduced to evaluate high-throughput screenings (HTS),[223] but can be applied to judge the quality of FRET change traces:

$$Z = \frac{|S_s - S_b| - 3\times(SD_s + SD_b)}{|S_s - S_b|} = 1 - \frac{3\times(SD_s + SD_b)}{|S_s - S_b|}$$

S_b and S_s are the mean values for the FRET level before and after stimulation (b: baseline, s: signal) and SD_b and SD_s are the respective standard deviations. The

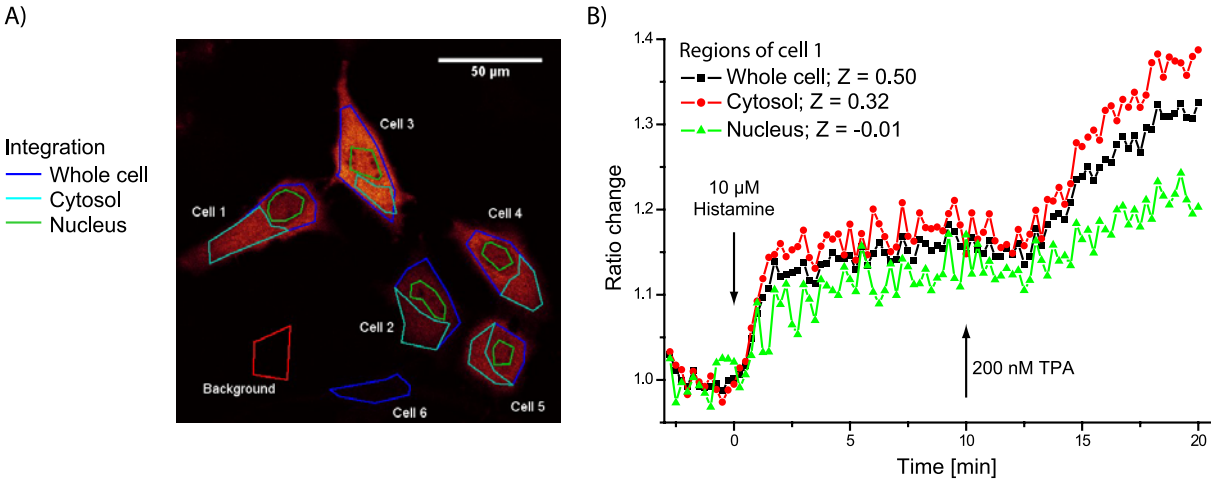

Figure 3.10: A) HeLa cell image from the experiment chosen to compare different aspects of data evaluation. B) FRET changes are very similar when measured in the cytosol and the whole cell. KCP-1 reports minor PKC activity in the nucleus of the chosen cell.

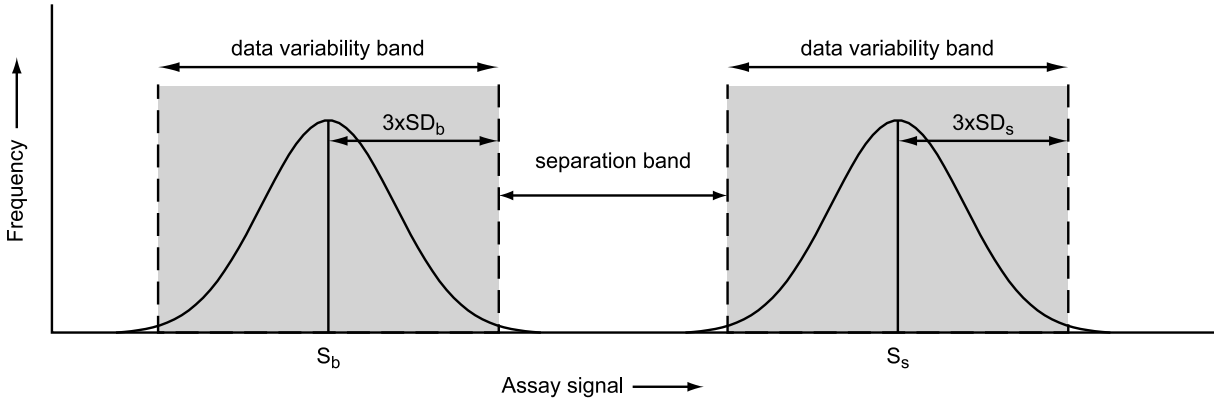

Figure 3.11: Different variable used for calculation of the Z-value. This value relates the separation band of two signals to their standard deviation. (Image adapted from reference [223])

equation relates the effective separation band between two signals (signal difference minus three times the sum of the standard deviations) to the change of signal (Figure 3.11). The factor '3' defines the data variability band and ensures a data confidence of 99.73% (0.27% of data points can be expected to be outside this range). Such a noise band is used in HTS.[224] A factor '2' would result in 95.35% confidence. An excellent signal (large change, low noise) is represented by a Z-value close to 1. A negative Z indicates a signal of low quality (small change, high noise).

Relevant Z-values were calculated and placed in the respective figures. Z-values were calculated with mean values and standard deviations from ten data point before and after cell activation. Only constant signals with an easily accessible standard deviation were used. Mean values and standard deviations of transient signals were not useful for calculation.

3.4.1 Region of interest definition

The choice of the region of interest (ROI), from which a mean fluorescence value is calculated, can contain a whole cell (cytosol and nucleus) or the cytosol only. Setting a ROI over a nucleus was not desired, since significant FRET changes could not be detected in this region. The difference between the values obtained from ROIs including the whole cell and cytosol alone was minimal (Figure 3.10B). Signals from the whole cell gave higher Z values than signals from the cytosol, probably due to larger ROI and concomitant lower noise. Values were calculated from ROIs covering the whole cell, since selecting such ROIs was easier and faster. Moreover, this process could be automated by using software to apply a threshold to images and automated area recognition. However, traces for ROIs covering the whole cell, only

cytosol, and only nucleus were inserted in several diagrams. A signal difference between cytosol and nucleus indicated that the cytosolic signal was real and not an artefact.

3.4.2 Choosing cells and normalizing ratio values

Optimal results were obtained from cells with moderate fluorescence. Ratio traces from dim cells showed high noise, whereas bright cells exhibited very low noise, but also a lower signal (Figure 3.12A). Bright cells often showed no FRET change and the influence of very high expression level of KCP-1 to cellular responses cannot be estimated.

EYFP/GFP^2 ratio values differed from cell to cell and made a direct evaluation and comparison difficult. Therefore, ratio values were normalized to the mean of starting values obtained before any drug addition. Z values were not affected by this operation.

Non-normalized traces showed that KCP-1 followed the dynamics of the phosphorylation level and could not report the absolute status of PKC activity. For example, an unstimulated cell (Figure 3.12B, cyan trace) gave the same absolute ratio value (1.3) as a different cell that had been treated with histamine (Figure 3.12B, red trace). Therefore, these two phosphorylation states could not be distinguished on basis of the EYFP/GFP^2 ratio alone, but as a change of the ratio over time.

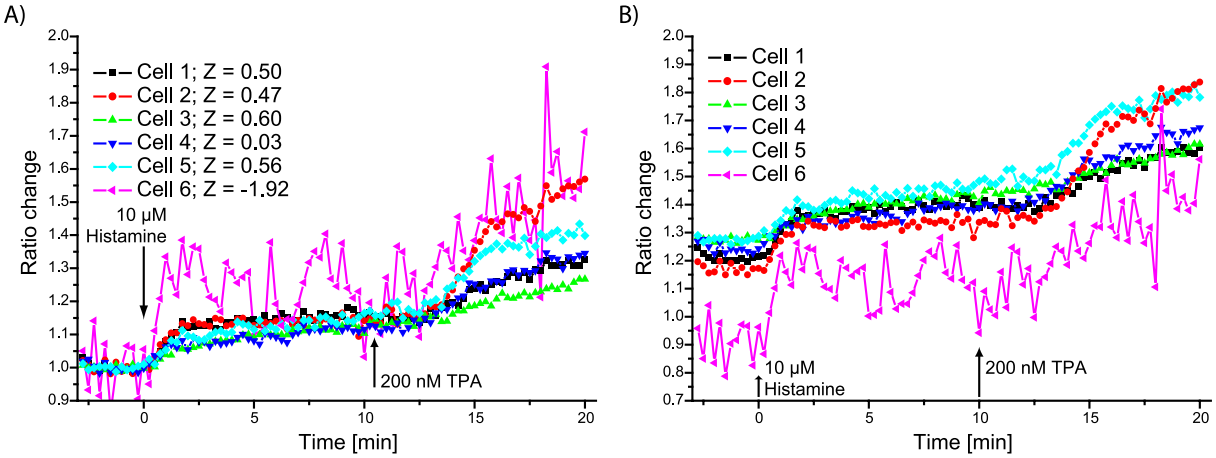

Figure 3.12: A) HeLa cells (same as in Figure 3.10A) exhibited similar responses, except when cells were very bright or very dim cells. B) Cells have divergent EYFP/GFP^2 ratio levels. Therefore, a signal value cannot be used to judge an activity state of PKC in cells. KCP-1 can report only changes in PKC activity.

3.4.3 Subtracting background values

To compare FRET values from different sources, a correct background subtraction was necessary.[225] Although no large difference was evident between values obtained with and without background subtraction (Figure 3.13A), this step was included in data processing. A background value for every frame was calculated from a ROI in an area containing no cell. This procedure increased the noise of the traces and therefore, background subtracted traces had lower Z-values.

3.4.4 Linear unmixing of the fluorophores

GFP^2 emitted substantially in the EYFP detection channel, and also EYFP fluorescence could be recorded in the GFP^2 channel (Figure 3.13B). Ratio values calculated with linear unmixing[225, 226] of the two fluorophores resulted in higher signals, but also in higher noise (Figure 3.13A). Therefore, the Z-value and the quality of the signals did not change. However, linear unmixing was always applied for the GFP^2/EYFP pair, when measured on a Leica SP2 confocal microscope, but not for other fluorophore pairs introduced below.

The ratio value r was calculated as $r = \frac{I_2 - k_1 \times I_1}{I_1 - k_2 \times I_2}$, with I_1 and I_2 being the fluorescence values from GFP^2 and EYFP channels, respectively, and k_1 and k_2 were the cross emission coefficients for GFP^2 and EYFP into the EYFP and GFP^2 detection channels, relative to the GFP^2 and EYFP detection channels, respectively.

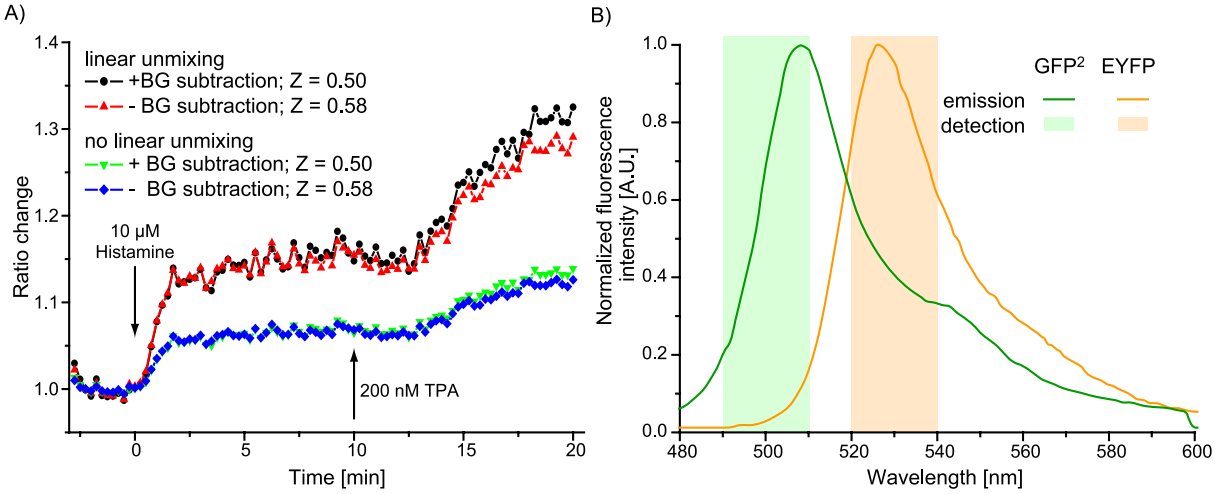

Figure 3.13: A) Procedures like background subtraction or linear unmixing had only minor effects on the data. The relative signal when no unmixing was applied was smaller, but had also lower noise and the quality of the signal did not change (similar Z-value). B) GFP^2 emits substantially into the EYFP detection channel. Therefore, linear unmixing was applied to the recorded signal of both GFP^2 and EYFP detection channels.

The constants k_1 and k_2 were 0.80 and 0.15, respectively, for Leica SP2 experiments, provided that the fluorescence detecting photomultiplier tubes (PMT) had same sensitivity (voltage).

3.4.5 Ratio calculation using ImageJ or Origin

The EYFP/GFP[2] emission ratio could be obtained either by image processing or by fluorescence intensity data processing.

In the first method, all operations (median filter, background subtraction, unmixing, and ratio calculation) on the recorded image stacks were performed with the public domain image processing software, ImageJ.[227] The result was a new image stack that represented EYFP/GFP[2] ratio for every recorded pixel and time point. Images were processed with a median filter to remove extreme pixel values.

For numerical data processing, fluorescence intensity data were obtained from the unprocessed original microscope images. ROIs were set and mean values, representing fluorescence intensities, were calculated. This raw data was processed (background subtraction, unmixing, ratio calculation, and normalization) with the scientific analysis program "Origin".[228] Origin's script programming language provided easy and fast data processing, including Z-value calculation.

No significant difference was detected between the methods of analysis (Figure 3.14A) and the latter approach was chosen. This enabled re-evaluation of the original single channel fluorescence data. Further, image processing is computer intensive and the process easily exceeded the memory size of a standard computer and was therefore impractical. However, the advantage of image processing was that FRET changes could be spatially resolved, an important feature.

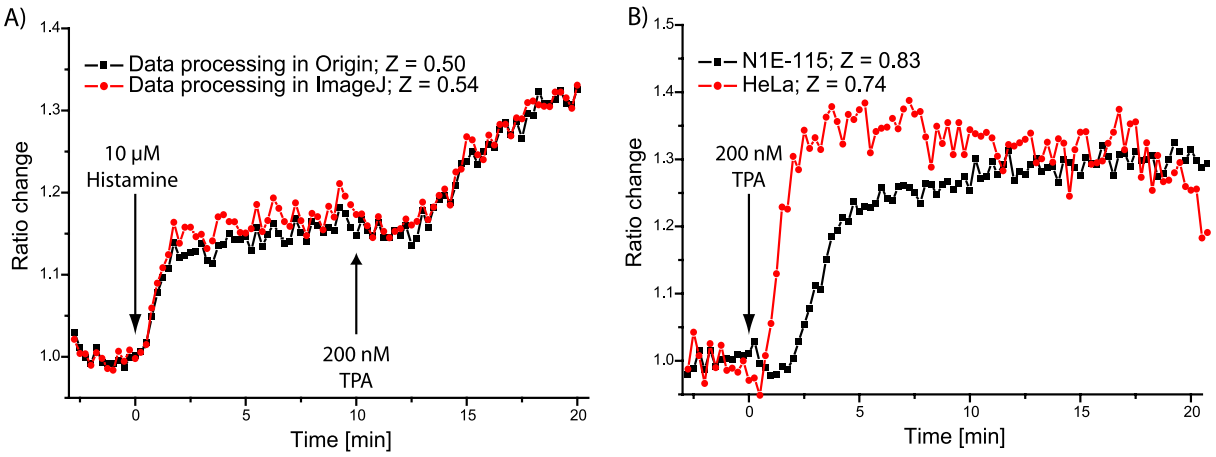

Figure 3.14: A) Data processing of pixel values in Origin, or image processing with ImageJ produced similar results. B) Both HeLa and N1E-115 cell lines produced similar results.

3.4.6 Cell Types

For experiments, human HeLa cells and murine N1E-115 neuroblastoma cells were used. Stimulation with TPA led to comparable signals in both cell lines (Figure 3.14B). Morphologically, HeLa cells were relatively flat, whereas N1E-115 cells were cylinder-shaped. Sample drifts in z direction (focus shifts) were problematic, since this reduced available cell area for evaluation. Thus, N1E-115 was the favoured cell line, since a shift along the z axis did not bring the focus plane out of a cell.

3.4.7 Microscopy

Experiments were performed on confocal (Leica SP2 AOBS and Zeiss LSM Meta) and wide field (Zeiss Axiovert equipped with a Visitron filter changer unit) microscopes.

KCP-1 was excited with a 405 nm diode laser on confocal microscopes. The Leica SP2 AOBS system[216] allowed detection of wavelength limits from 490 - 510 nm for GFP^2 and 520 - 540 nm for EYFP. The settings used with the Zeiss LSM Meta[229, 230] were 488 - 510 nm and 520 - 542 nm for GFP^2 and EYFP, respectively. Another feature of the Zeiss LSM Meta was spectral unmixing, which ideally provided images showing pure GFP^2 or EYFP fluorescence. Data obtained with the two confocal microscopes were similar in ratio and signal to noise (Figure 3.15A).

The wide field system was equipped with an HBO lamp. The excitation light was selected with a 405/20 nm filter and was separated from fluorescent light with a 425 dclp dichroidic long pass mirror. Fluorescence light was imaged with a charged

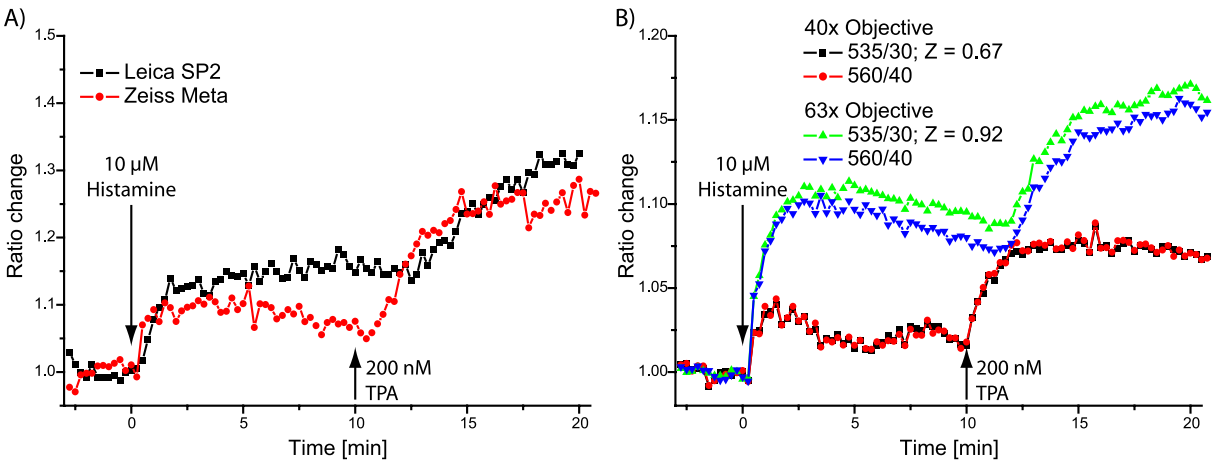

Figure 3.15: A) Both confocal microscopes produced similar results (63x objective). B) Data recorded on a wide field system had very low noise. Due to smaller projections of 40x objectives and concomitant smaller ROIs, corresponding traces exhibited larger noise.

coupled device (CCD) camera after a band pass filter. GFP^2 emission was selected with a 500/20 band pass filter and EYFP was imaged with a 535/30 or 560/40 band pass filter. Changes in ratio values and signal to noise were similar for various filters used for EYFP detection (Figure 3.15B). For imaging, the 535/30 band pass filter was used, since its transmission window is closer to the EYFP emission maximum, and therefore, yielded brighter images than those recorded with a 560/40 band pass filter.

Data recorded with the wide field microscope had higher Z-values compared to experiments performed on confocal microscopes. Compared to 40x objectives, a 63x objective gave better Z-values, probably due to larger ROIs and concomitant lower noise.

3.5 Difficulties with live cell imaging

Several factors could impair live cell experiments. Hardware failures, like computer or laser malfunction, could not be predicted, nor avoided.

Drugs were added as solution in 100 µl medium with a pipette. Care was taken, not to touch the cell dish with the pipette, since this abruptly caused large and often uncorrectable focus shifts.

Focal shifts during time course experiments diminished integratable cell areas for evaluation. Slow focus shifts could be attributed to thermal imbalances.

Some cell batches showed a very high noise for the ratio values. This was observed for all experiments on that day. No cause of this effect could be determined.

A fast ratio increase, which stabilized after 10 to 15 recorded frames, was observed in experiments performed during summer and probably was associated with air conditioning. This was corrected by setting the temperature above 25°C.

3.6 Engineering the probe

3.6.1 The truncated probe, KCP-2

Pleckstrin contains a linker between the central DEP and the C-terminal PH domain, which harbours seven acidic amino acids. These residues putatively interact with the N-terminal PH domain or sense the phosphorylation status of the sequence located between N-terminal PH and DEP domain. A part of this linker (18 amino acids including five acidic amino acids) was present in KCP-1, but was deleted in the

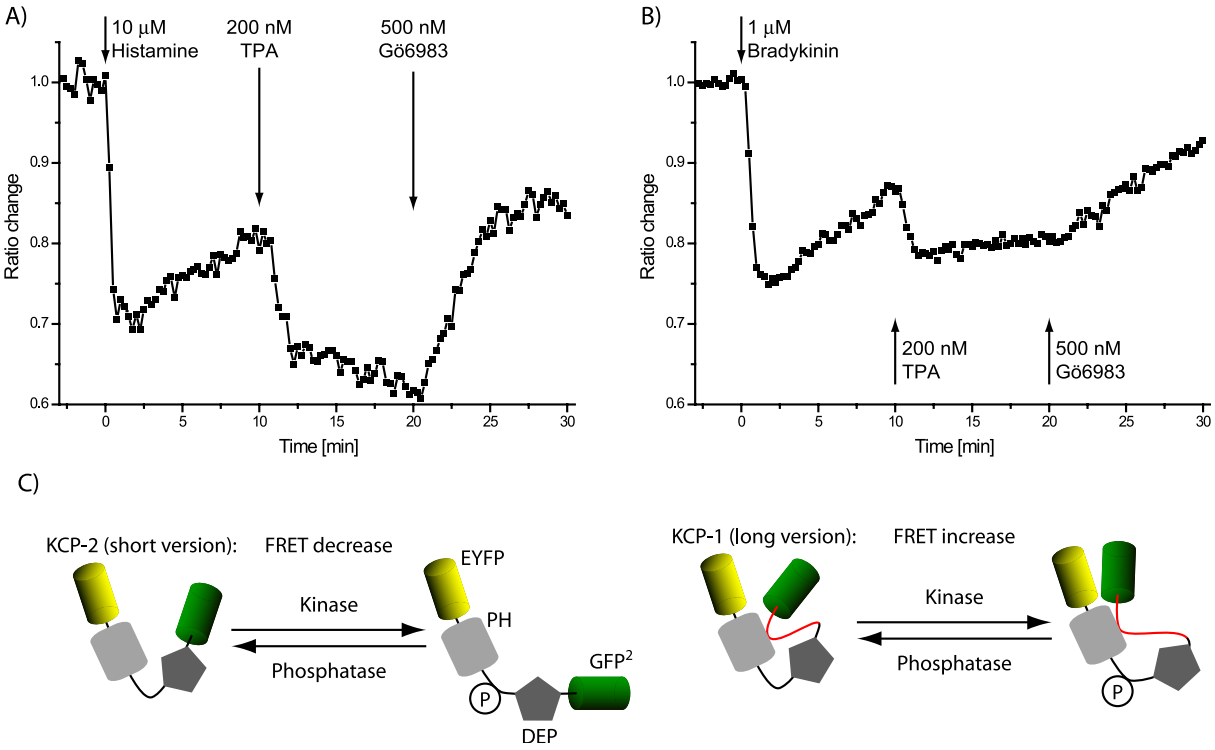

Figure 3.16: An 18 amino acid linker was deleted in the shortened probe, KCP-2. It reports PKC activity, but shows a negative FRET change in contrast to KCP-1 (A [HeLa] and B [N1E-115]). C) Models for structural rearrangements in KCP-1 and KCP-2. In both probes reduces phosphorylation the interaction between PH and DEP domain. This causes in KCP-2 separation of both fluorophores, whereas in KCP-1 both dyes reduce their distance. Such a mechanism reduces FRET efficacy in KCP-2, while KCP-1 exhibits higher FRET efficiency after phosphorylation.

new construct, KCP-2.

The new probe, KCP-2, also reported TPA-, bradykinin-, or histamine-stimulated PKC activity (Figure 3.16A and B); however, in contrast to KCP-1, FRET decreased upon PKC activation and increased after PKC inhibition. This demonstrated the structural importance of the 18 amino acid linker and ongoing experiments performed by Justin Brumbaugh are currently elucidating the mechanistic significance of the sequence.

Recent NMR structural studies showed that in both the short and the long unphosphorylated PH-DEP constructs (lacking fluorophores), the two domains interact. In the phosphorylated constructs the domains do not.[231] A structure and position for the flexible 18 amino acid linker could not be determined by NMR experiments. The results for the short construct are in good agreement with the observed FRET change: a closed, unphosphorylated state with high FRET opens upon phosphorylation, separating the N- and C-terminal ends and attached fluorophores. FRET between them is therefore diminished (Figure 3.16C, left part). An explanation for the FRET increase after phosphorylation for KCP-1 is not as

straight forward. One model is that the 18 amino acid linker interacts with the PH domain after KCP-1 phosphorylation and increases FRET by drawing the fluorescently tagged termini closer together (Figure 3.16C, right part).

3.6.2 Variations of the fluorescent proteins

The chosen FRET partners GFP^2 and EYFP are not commonly used. In fact KCP-1 is the first published probe employing these dyes. Another FRET reporter using the same dyes system was only recently published.[232]

The most frequently used fluorescent proteins for FRET purposes are enhanced cyan fluorescent protein (ECFP), as donor, and EYFP as an acceptor moiety. ECFP can be excited with standard laser lines around 450 nm and the emission maxima of ECFP and EYFP are well separated (Figure 3.17A). These two features make it easy to image ECFP/EYFP on a wide range of widefield and confocal microscopes. To test the KCP-1 construct with these dyes, GFP^2 was replaced by ECFP. In the course of generating the new probe, also EYFP was substituted by Citrine, an EYFP variant which is less environmentally sensitive.[149]

The new probes KCP-1(CiCF) (Ci: Citrine; CF: ECFP) and KCP-2(CiCF) have the designs as shown in Figure 3.17B. Intriguingly, KCP-1(CiCF) gave no signal and KCP-2(CiCF) gave only a weak FRET decrease after cell stimulation with TPA (Figure 3.18A and B). According to calculations (Timo Zimmermann, EMBL Heidelberg), it is possible that KCP-1(CiCF) would give similar responses as KCP-1,

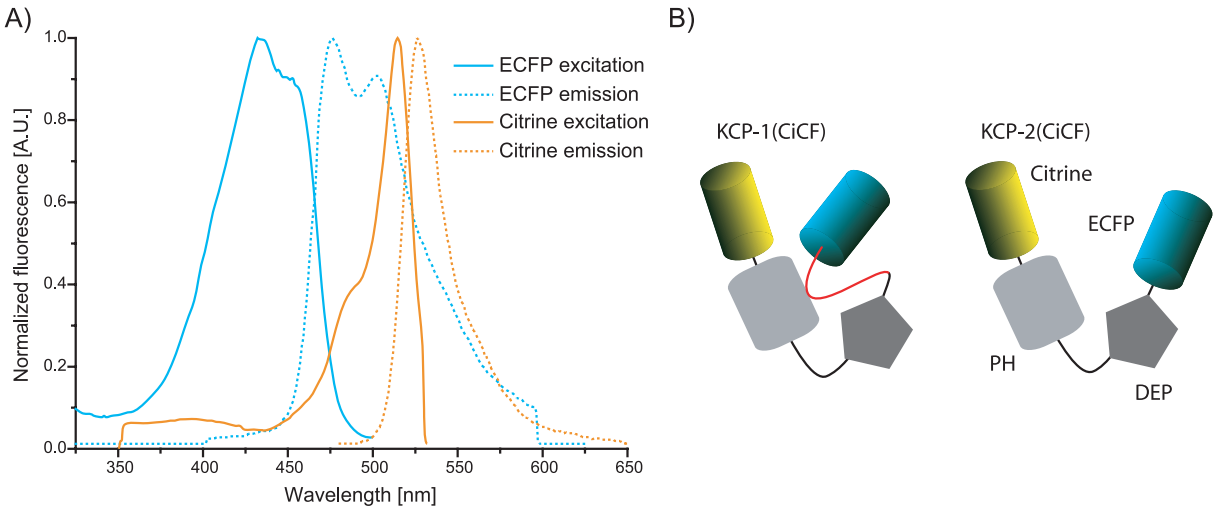

Figure 3.17: A) Excitation and emission spectra of ECFP and Citrine. The emission maxima of ECFP and Citrine are better separated than those of GFP^2 and EYFP. However, the overlap of donor emission and acceptor excitation is larger in the GFP^2/EYFP FRET pair than in ECFP/Citrine. B) Schematic structure of the probes with ECFP and Citrine as FRET partners.

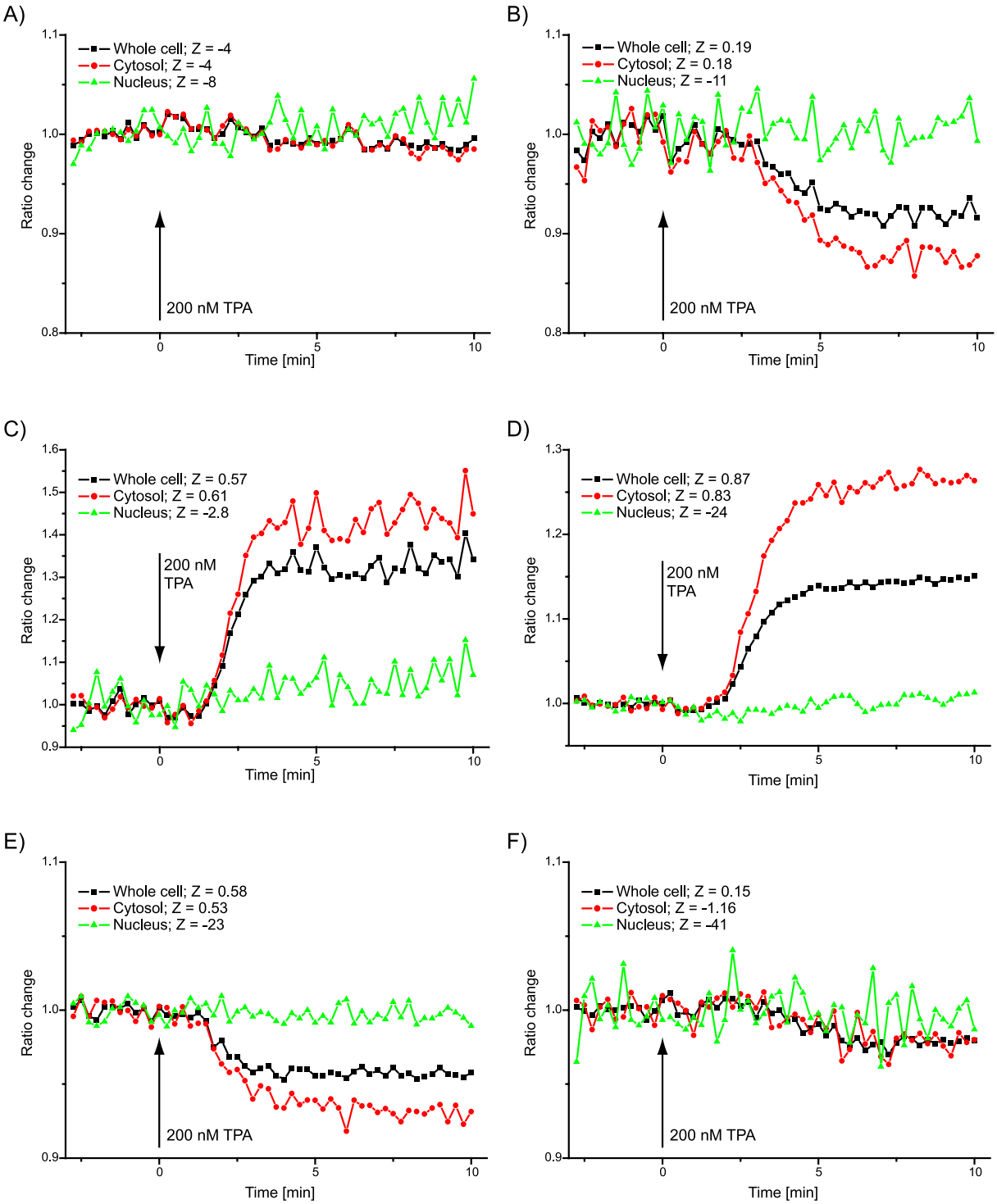

Figure 3.18: Responses of probes based on KCP-1 and KCP-2 with different fluorophore substitutions. A) KCP-1(CiCF), B) KCP-2(CiCF), C) KCP-1(YFG2), D) KCP-1(CiG2), E) KCP-2(CiRF), and F) KCP-1(CiRF). Abbreviations for the fluorophores: Ci = Citrine; CF = ECFP; G2 = GFP^2; RF = mRFP, YF = EYFP.

if the fluorophores were not hindered in their rotation. Apparently, this is not true for KCP-1: differences in the dipole-dipole orientations may explain the contrasting results obtained in experiments that employed GFP^2/EYFP or ECFP/EYFP as FRET pairs. To exclude the possibility that exchanging EYFP to Citrine influenced the

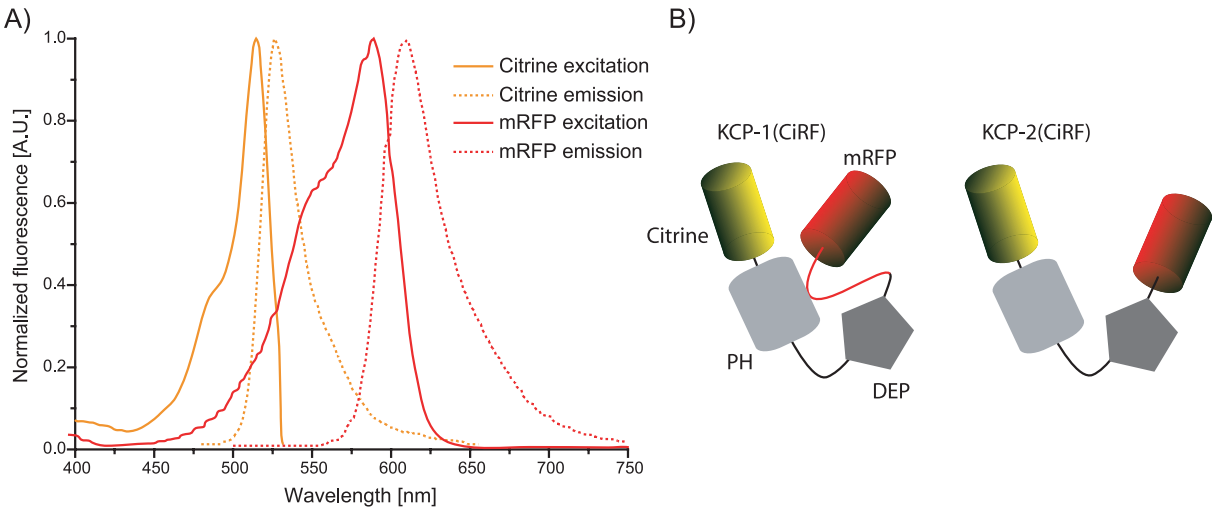

Figure 3.19: A) Excitation and emission spectra of Citrine and mRFP. The overlap between Citrine emission and mRFP excitation is small and low FRET efficiency was expected. B) Schematic representation of the probes with Citrine and mRFP as fluorophores.

FRET readout, also the EYFP in KCP-1 was switched with Citrine (⇨ KCP-1(CiG2)). However, this probe gave similar ratio changes as KCP-1 with better signal to noise ratio (Figure 3.18D).

Construction of a probe carrying longer wavelength fluorophores was attempted by using Citrine and mRFP (monomeric red fluorescent protein)[143] as FRET partners. Although the overlap integral between donor emission and acceptor excitation was small (Figure 3.19A), a change in FRET was detected with the shortened probe derived from KCP-2 (⇨ KCP-2(CiRF); Figure 3.19B and Figure 3.18E), but not in the long version (⇨ KCP-1(CiRF); Figure 3.19B and Figure 3.18F). Probes that are excited and emit with longer wavelength might prove useful for imaging PKC activity in tissue or even whole animals, since red light can penetrates deeper in tissue than blue or green light.

3.6.3 Altering the phosphorylation sequence

Mutation of the phosphate acceptor amino acids

KCP-1 has three phosphate acceptor amino acids (S113, T114, S117, short: STS [amino acid numbering of pleckstrin was retained for easier identification]),[105, 106] and therefore yields a phosphorylation reaction kinetic of at least third order. This makes the probe unsuitable for kinetic studies. Simpler kinetics are expected, if only one phosphate acceptor amino acid is present. Mutation of each of the three amino acids phosphorylated by PKC to alanines or glutamates allowed for a screen for an

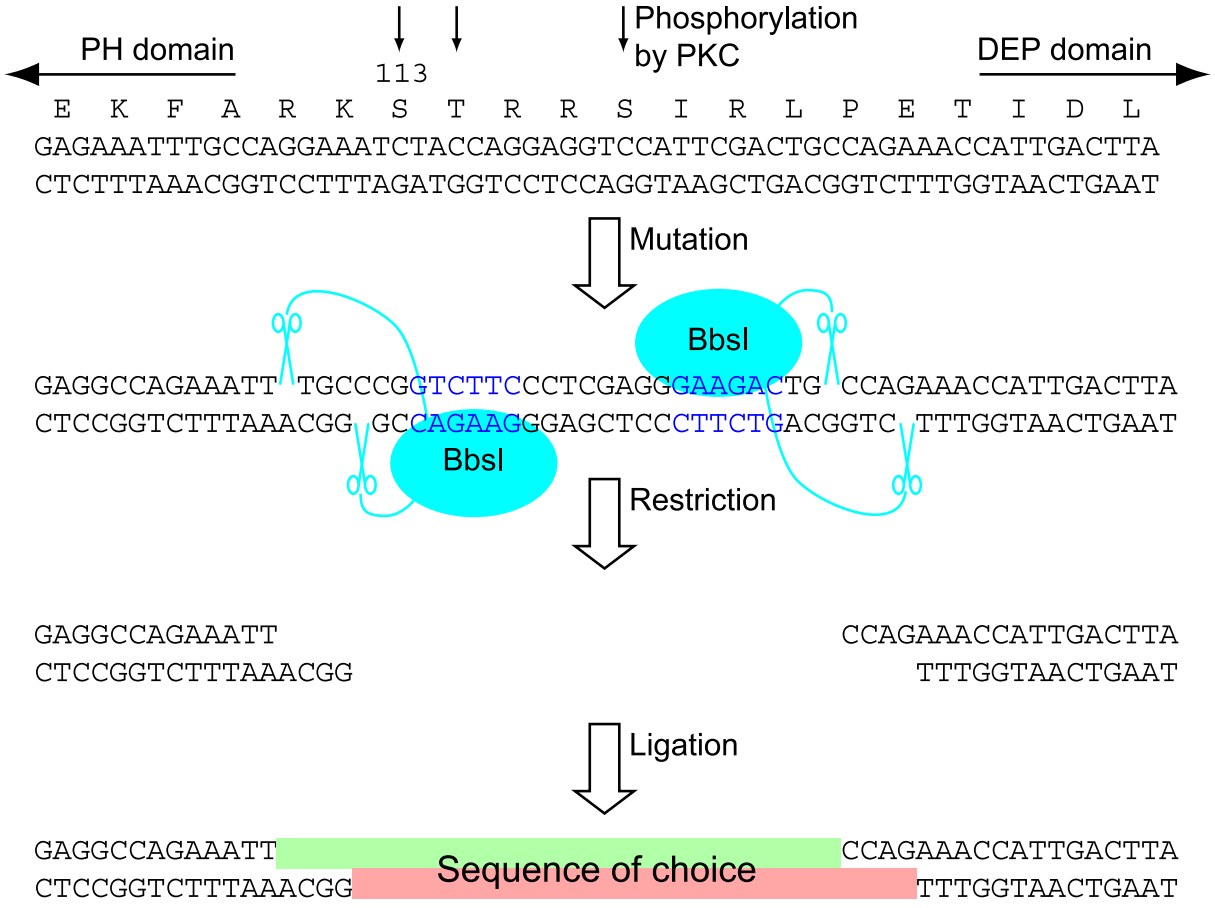

Figure 3.20: Cloning system for efficient mutation of KCP-1's kinase substrate sequence. The native sequence was substituted by a dummy sequence that could be completely excised with BbsI. In a last step, a sequence of choice was introduced.

optimized probe. The mutation S/T→A and S/T→E simulated unphosphorylated and phosphorylated amino acids, respectively.[105] To generate the set of KCP-1 mutants in an efficient way, a vector was designed, in which the original coding sequence for the phosphorylation site was substituted by a dummy sequence that was excised completely with the enzyme BbsI. Oligo-DNA duplexes could be inserted into this vector, replacing the original phosphorylation sequence with a mutated sequence of choice (Figure 3.20). This system allowed for maximal freedom in choosing desired linker sequences and most mutations in the PKC substrate were introduced with this system.

All mutations generated are shown in the table in Figure 3.21A. N1E-115 cells were transfected over night and imaged on a confocal microscope. Following a three minute baseline period, cells were stimulated with 200 nM TPA. After an additional 10 min, PKC was inhibited by Gö6983 and monitored for another 10 min.

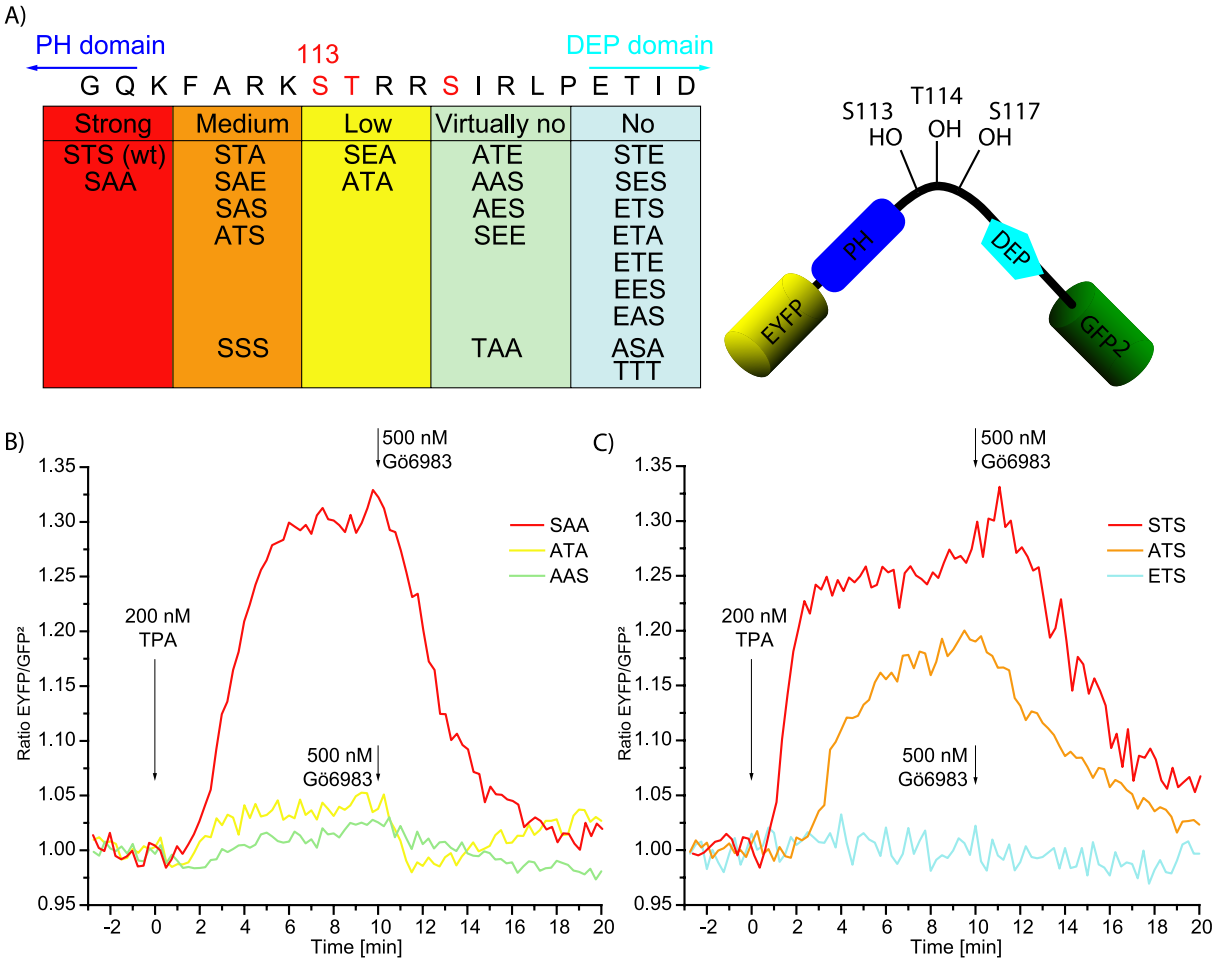

Figure 3.21: A) Constructs with alterations to the substrate loop were classified according to maximal FRET change after PKC activation with TPA (right: schematic representation of KCP-1). Z-values were omitted since these could not be calculated consistently (no stable level after TPA). Comparison of the series SAA, ATA, AAS (B) and STS, ATS, ETS (C) shows that phosphorylation of S113 is necessary and sufficient to result in a maximal FRET change.

As Figure 3.22 shows, only the mutant SAA exhibited maximal FRET change, comparable to that of the wild type sequence STS. This demonstrated that phosphorylation of S113 was necessary and sufficient to invoke maximal FRET change. Phosphorylation of the three hydroxy amino acids contributed to FRET changes to a varying extent. The maximal FRET levels observed were SAA >> ATA > AAS and STS > ATS > ETS (Figure 3.21B and C) which suggested that the FRET change contributions due to phosphorylation were S113 >> T114 > S117. Introducing glutamate at any position diminished or extinguished KCP-1 response. Also the alterations S113T (TAA) and T114S (ASA) virtually abolished ratio changes. This may reflect serine and threonine preference of the phosphorylating kinases and suggests that S113 and T114 could be substrates for distinct PKC isozymes.

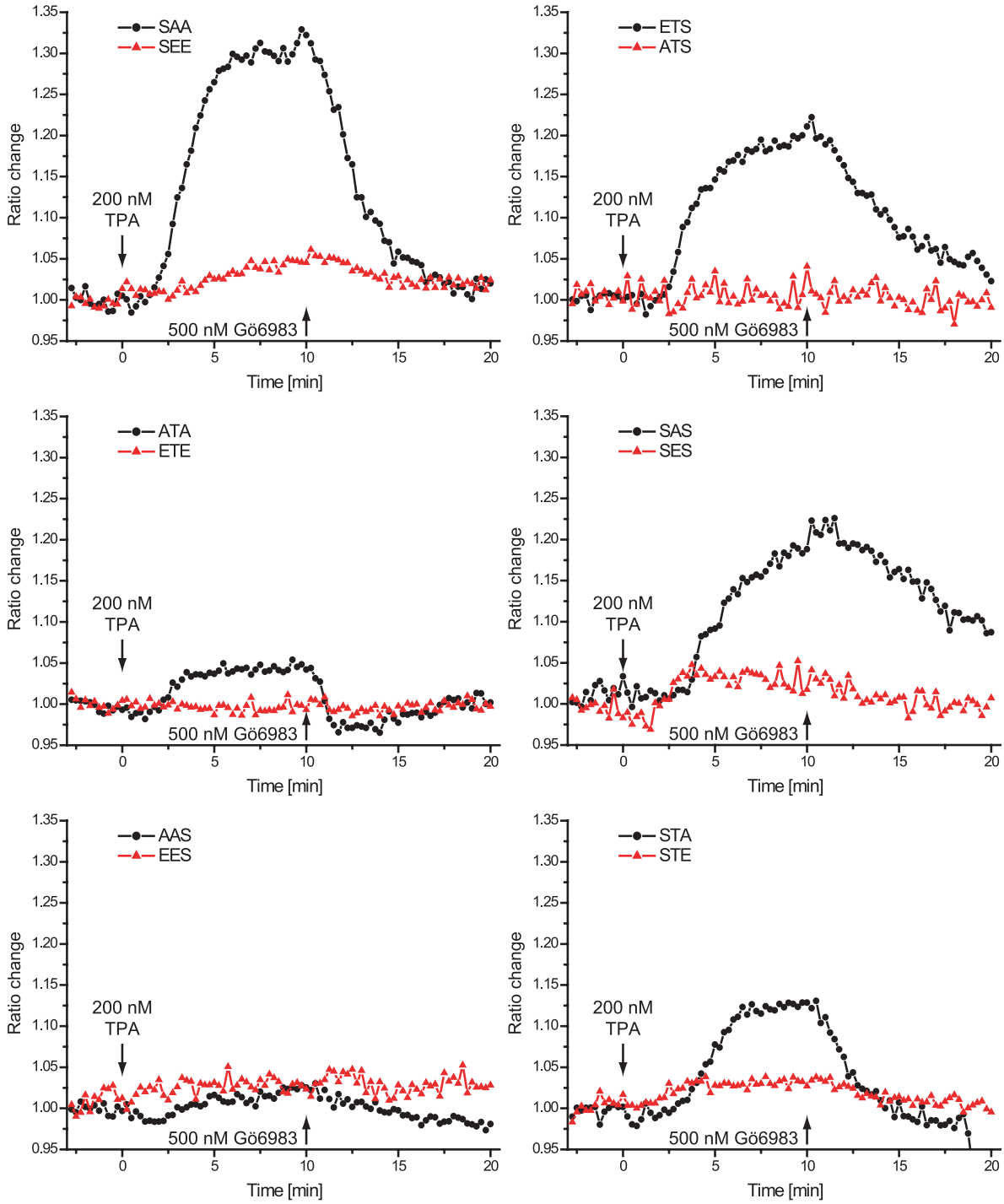

Figure 3.22: Data traces from single and double alanine and glutamate mutants that were measured in N1E-115 cells. After three minutes baseline period, PKC was activated with TPA. Subsequently, after 10 min Gö6983 was added to inhibit PKC. Phosphorylation of S113 was necessary and sufficient for a maximal FRET change. Introduction of one glutamate diminished or extinguished responses.

In vitro assays, performed by Alexander Gasch (Michael Sattler's group, EMBL) showed that recombinant PH-DEP constructs carrying alanine or glutamate substitutions, but with at least one phosphoacceptor amino acid remaining, were still substrates for PKCδ and residual hydroxy amino acids were phosphorylated.[233] Therefore, it could be concluded, that the lack of FRET change response was not

due to an artefact arising from reduced ligand-protein interaction. Instead, it seems possible that FRET changes, and therefore conformational rearrangements, were influenced by mutating the hydroxyl amino acids to alanines or glutamates.

These results suggested that S113 may have a key function in pleckstrin activation, whereas T114 and S117 could assume a regulatory role. However, previous investigations could not detect a functional difference between the phosphate acceptor amino acids.[105]

Novel substrate loops

The permutation studies discussed above demonstrated that the phosphorylation of one amino acid was sufficient to induce a maximal FRET change. Further experiments were conducted to test whether the substrate sequence could be altered to sequences suitable for recognition by other kinases. This approach targeted sequence specificity of a kinase's catalytic site.[234] However, some kinases also carry additional elements that recognize structural features of substrate proteins and thereby enhance specificity.[81, 235, 236] The following experiments address the substrate sequence only, since no alteration of a second recognition site occured. The cloning system introduced above (Figure 3.20) was used to insert the peptide sequences shown in Table 2.1.

Substrate sequences for CaMKII, PKA, or PKB were inserted to test if the sensor could be altered for use with various kinases.

Sequences with known specificities for particular kinases were chosen for first round selection: Autocamtide2 for CaMKII,[237] Kemptide for PKA,[238] and Crosstide for PKB.[239] None of these constructs showed a significant FRET response after

KCP-1	QKFA RKSTRRSIRL PETI	KCP-1	QKFA RKSTRRSIRL PETI
Autocamtide2	QKFA LRRQETVDAL PETI	Kemp1	QKFA RKSLRRASRL PETI
Crosstide	QKFA RPRTSSFAEL PETI	Kemp2	QKFA RKSLRRAIRL PETI
Cross1	QKFA RARTSSRIRL PETI	Kemp3	QKFA RKSLRRASLL PETI
Kemptide	QKFA RKSLRRASLG PETI	Kemp4	QKFA RKSLRRASFL PETI
2xKemptide	QKFA RRASLRRASL PETI	Kemp5	QKFA RKSLRRASFF PETI
PKA1	QKFA RRRRSRRASL PETI	Kemp6	QKFA RKSLRRASLF PETI
PKAPKC	QKFA KRSTRRSVRL PETI	Kemp7	QKFA RKSLRRLSFF PETI
ACh	QKFA RRSSSRRIRL PETI	Kemp8	QKFA RKSLRRALFL PETI
H2B	QKFA RKRSSRRIRL PETI	Kemp9	QKFA RKALRRASLL PETI
		Kemp10	QKFA RKELRRASLL PETI
		Kemp11	QKFA RKSLRRAALL PETI
		Kemp12	QKFA RKALRRAALL PETI

Table 2.1: Sequences inserted to alter kinase specificity of KCP-1. Autocamtide2 and Crosstide/ Cross1 are known substrates for CaMKII and PKB, respectively. The other sequences target PKA specificity. The sequences QKFA and PETI are part of KCP-1 and were not altered.

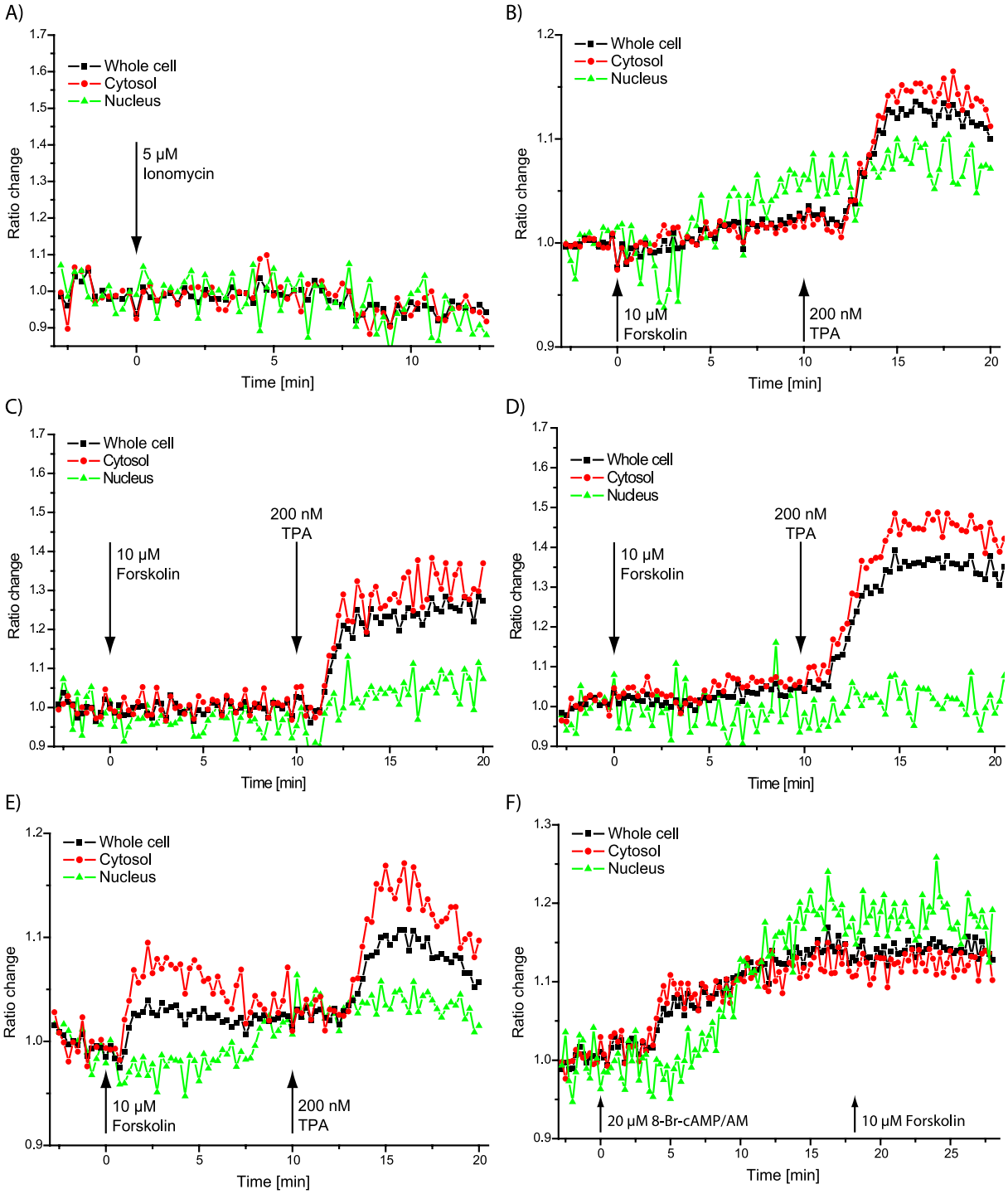

Figure 3.23: Data traces from probes with substrate loops engineered to extent kinase specificity. Most mutants were not sensitive to tested kinases (for example Autocamptide2, A). Mutants of the Kemptide sequence kept PKC sensitivity (B: Kemptide; C: H2B; D: Kemp1). The construct Kemp3 showed PKA activity in cytosol immediately after kinase activation with forskolin (E) or 8-Br-cAMP/AM (F). After a delay, PKA activity was also reported in the cytosol.

activation of the specified kinase (for example Figure 3.23A). Only Kemptide showed a minor FRET change after PKA activation. This construct kept partial sensitivity for PKC in living cells (Figure 3.23B), probably due to unaltered S113, which was the essential phosphate acceptor in KCP-1.

Since PKA is closely related to PKC (40% amino acid identity in the catalytic domain),[67] the Kemptide construct was more extensively explored to test the feasibility of altering substrate specificity. The following sequences were introduced (Table 2.1): 2xKemptide (double, shortened Kemptide), Kemp1 - 8 (hybrids of the KCP-1 sequence and Kemptide), ACh (a sequence derived from acetylcholine receptor), H2B (derived from histone 2B), PKA1 and PKAPKC (both sequences derived from a phosphorylation sequence database; the latter is known to be phosphorylated by PKA and PKC).[240, 241] These constructs showed partial responses to PKC stimulation (for example see Figure 3.23B - D).

Cells expressing PKA probes were stimulated with forskolin to elevate cyclic AMP levels and thereby activate PKA.[50] Subsequent treatment with TPA tested for residual PKC sensitivity. Only Kemp3 responded to forskolin and TPA. The signal following forskolin was approximately 1/3 to 1/2 of that induced by TPA (Figure 3.23E). This mutant was a reporter for PKA and PKC activity. FRET ratio rose immediately after forskolin stimulation in the cytosol, and following a delay of approximately five minutes in the nucleus. This delay probably represents the time it takes for the separation of PKA's catalytic subunit from the regulatory domain and subsequent diffusion of the catalytic subunit into the nucleus.[242, 243] Similar results were obtained with PKA activation with 8-Br-cAMP/AM, a direct activator of PKA (Figure 3.23F).[244, 245] PKC stimulation with TPA affected the FRET ratio in the cytosol, but not in the nucleus in accordance with previous experiments.

Kemp3 was further modified to obtain a PKA specific probe that lacked PKC sensitivity. The Kemp3-sequence (RKS^{113}LRRAS^{118}LL) contained S113, which was also the crucial phosphate acceptor in KCP-1, and S118. Both were the putative substrates for PKC and PKA, respectively. These residues were the major kinase substrates since replacing them by alanines (Kemp12: RKA^{113}LRRAA^{118}LL) extinguished responses to PKA and PKC stimulation. Therefore, mutation of one of these serines was expected to enhance specificity for PKA or PKC. Indeed, changing S118 to alanine (Kemp11) yielded a construct that responded to PKC but not to PKA stimulation. In contrast, alteration of Kemp3's S113 to alanine (Kemp9: RKA^{113}LRRAS^{118}LL) or glutamate (Kemp10: RKE^{113}LRRAS^{118}LL), rendered the probes virtually insensitive to both PKA and PKC stimulation. It seems that S113 is required for Kemp3 to be a substrate for PKA. The implications of these results remain to be resolved. However, these experiments showed that it is possible to

extend the kinase sensitivity of KCP-1 mutants. Alterations to the substrate loop tested the significance of single amino acids in substrate recognition. For example, the mutation R119L (Kemp1 ⇨ Kemp3) diminished responses to TPA and L120G (Kemp3 ⇨ Kemptide) virtually abolished signals induced by forskolin. The latter mutation may reflect secondary structure disruption caused by glycine. In the future, systematic mutation for each amino acid could help to elucidate its function and importance in pleckstrin and in novel kinase probes.

3.6.4 Mutations in the PH domain

An EGFP/pleckstrin fusion protein translocated from the cytosol to the plasma membrane when activated by PKC. Translocation was reverted after PKC inhibition with Gö6983 (Figure 3.24). Therefore, localization in the cytosol or at the plasma membrane reflected low and high PKC activity, respectively, and EGFP tagged pleckstrin could be used as a PKC activity reporter in fluorescence microscopy.

Also, in some experiments little translocation of KCP-1 was observed. This did not depend on the experimental setup, but on intangible parameters like cell batch. Since KCP-1 is a ratiometric construct, meaning that donor and acceptor fluorophores were in a constant 1:1 ratio, artefacts in the fluorescence ratio due to concentration variations were excluded.

Nevertheless, to avoid potential problems associated with the cytosol/plasma membrane translocation of KCP-1, the PH domain was mutated to eliminate its ability to recognize phospholipids. In the phospholipid-binding cavity, basic amino acids

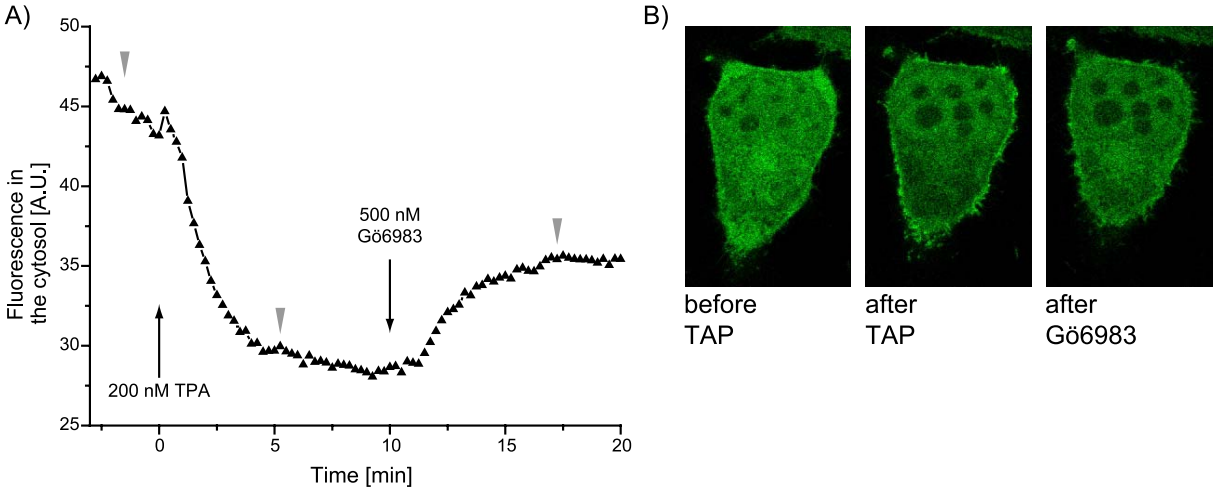

Figure 3.24: A) Fluorescence of EGFP-pleckstrin measured in the cytosol. The fusion protein translocated from the cytosol (B, left) to the plasma membrane after PKC stimulation (B, middle). Gö6983 inhibited PKC, the fusion protein was dephosphorylated by phosphatases, and relocated to the cytosol (B, right). Gray arrows indicate time points corresponding to the right pictures.

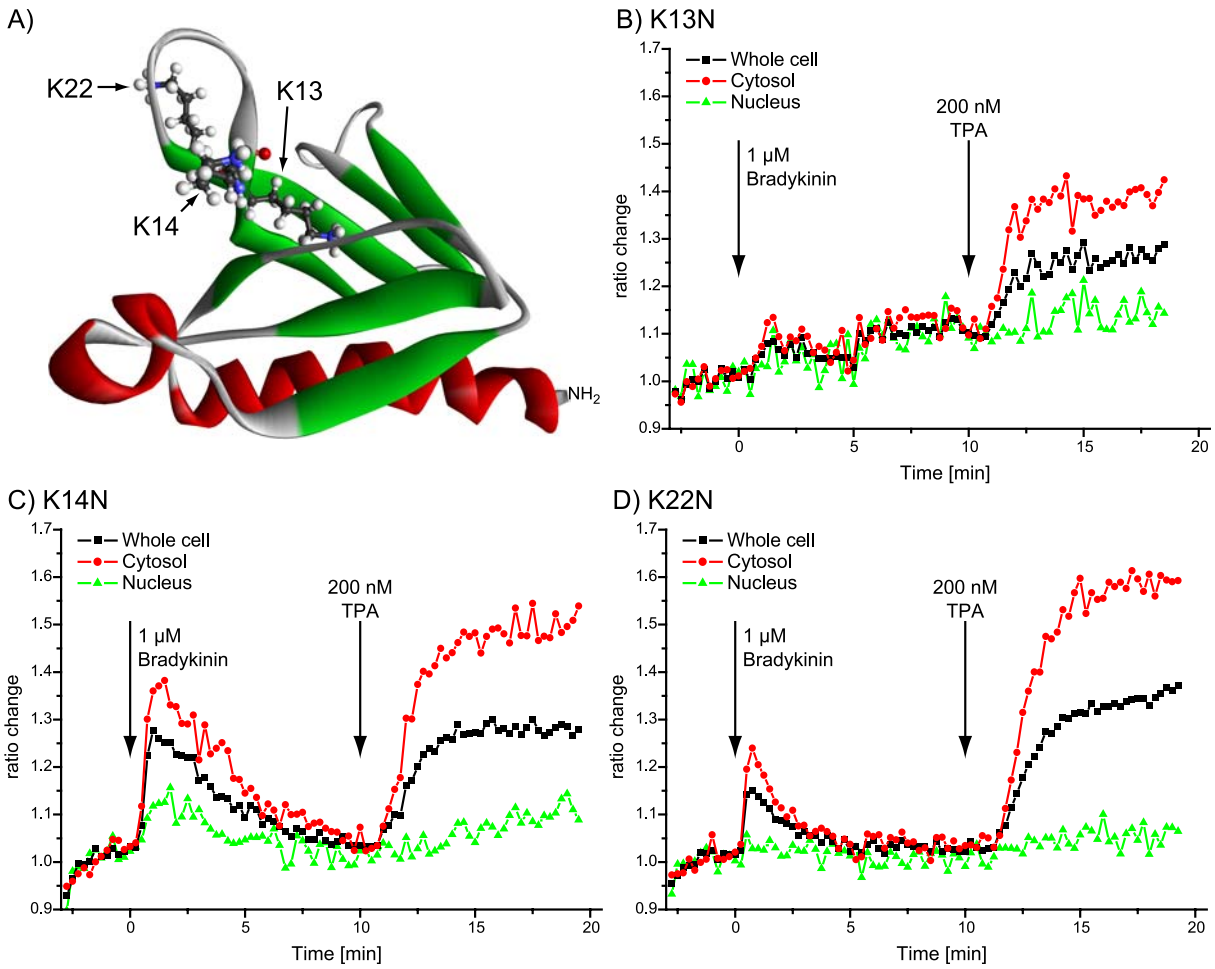

Figure 3.25: A) Positions of K13, K14, and K22 in the N-terminal PH domain of pleckstrin. The mutations K13N, K14N, or K22N render the PH domain unable to bind to the plasma membrane after pleckstrin activation. KCP-1/SAA/K13N (B) did not report bradykinin induced PKC activity, whereas KCP-1/SAA/K14N (C) and KCP-1/SAA/K22N (D) showed responses similar to KCP-1.

(Figure 3.25A), which are known to be crucial for membrane targeting of the PH domain, were altered to aspartates.[246] The mutations K13N, K14N, and K22N were introduced into KCP-1/SAA and gave the constructs KCP-1/SAA/K13N, KCP-1/SAA/K14N, and KCP-1/SAA/K22N. These probes carried only the crucial phosphorylation acceptor and lacked phospholipid-binding abilities of PH domains.

KCP-1/SAA/K14N and KCP-1/SAA/K22N responded normally to bradykinin, DiOG, or TPA, but KCP-1/SAA/K13N was virtually insensitive to bradykinin and DiOG (Figure 3.25B - D). A FRET change could only be observed with TPA. The implications of these results remain to be resolved; potentially K13 was an interaction partner for the C-terminal 18 amino acid linker.

Neither of the new probes showed translocation after cell stimulation: single dye fluorescence traces of unmodified KCP-1 (Figure 3.26A) showed changes due to FRET, which were superimposed with changes due to translocation. Both effects

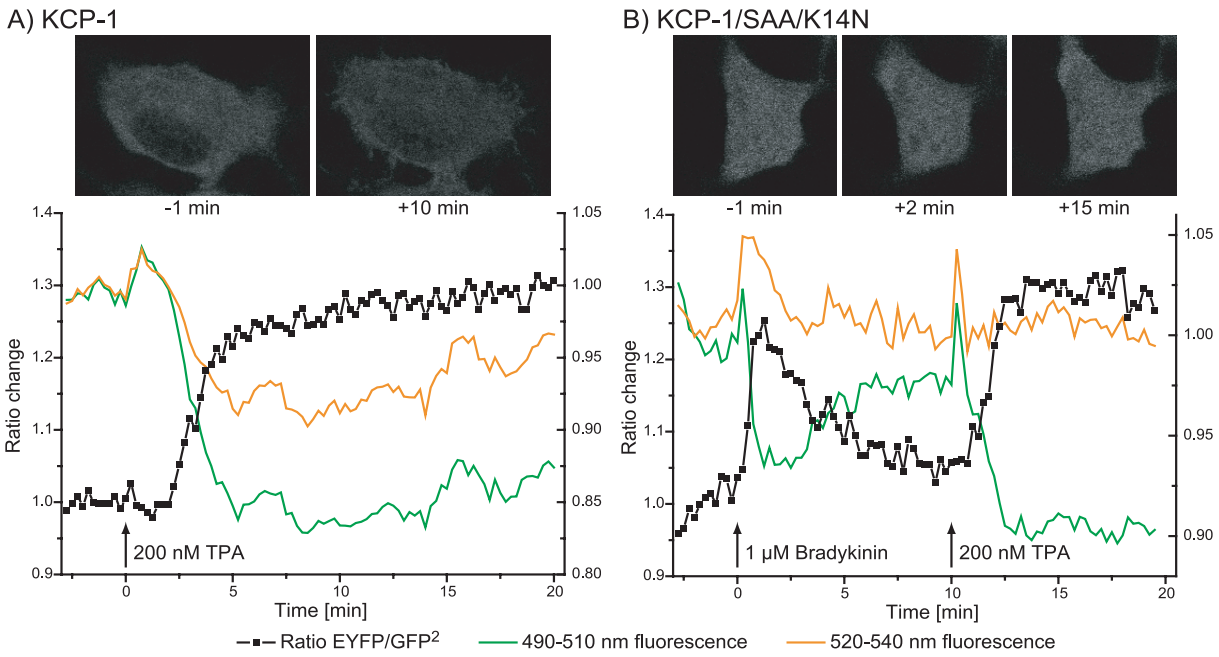

Figure 3.26: Fluorescence traces of KCP-1 (A) were dominated by translocation (when observed). In contrast, KCP-1/SAA/K14N (B) did not translocate after PKC activation.

resulted in decreased fluorescence in both GFP^2 and EYFP channels. In contrast, KCP-1/SAA/K14N showed diminished GFP^2 emission but constant EYFP emission after cell stimulation (Figure 3.26B): no translocation of the construct was observed. From theory, it was expected that increased FRET was accompanied with increased fluorescence in the EYFP detection channel. However, GFP^2 fluorescence decreased with increasing FRET. Since GFP^2 substantially emitted into the EYFP detection channel, reduced GFP^2 fluorescence in this channel compensated for increased EYFP fluorescence, and no change was observed for data that were not unmixed.

3.6.5 Parallelization of construct testing experiments

As shown above, a multitude of probes were tested, and innumerable more probes should be generated for further characterization. Performing individual experiments with each probe is time and resource consuming. Also, it is difficult to compare experiments between different cell batches. Parallel acquisition of experimental data would make the experiments faster and easier. This would also allow better comparison between constructs.

Cell arrays, with localized cell patches expressing different constructs, in conjunction with a semi-automated microscope for batch processing, provided such a system. Cell arrays were produced by spotting (Figure 3.27A) mixtures of plasmids with transfection reagent on welled coverslips (Figure 3.27B). These were seeded

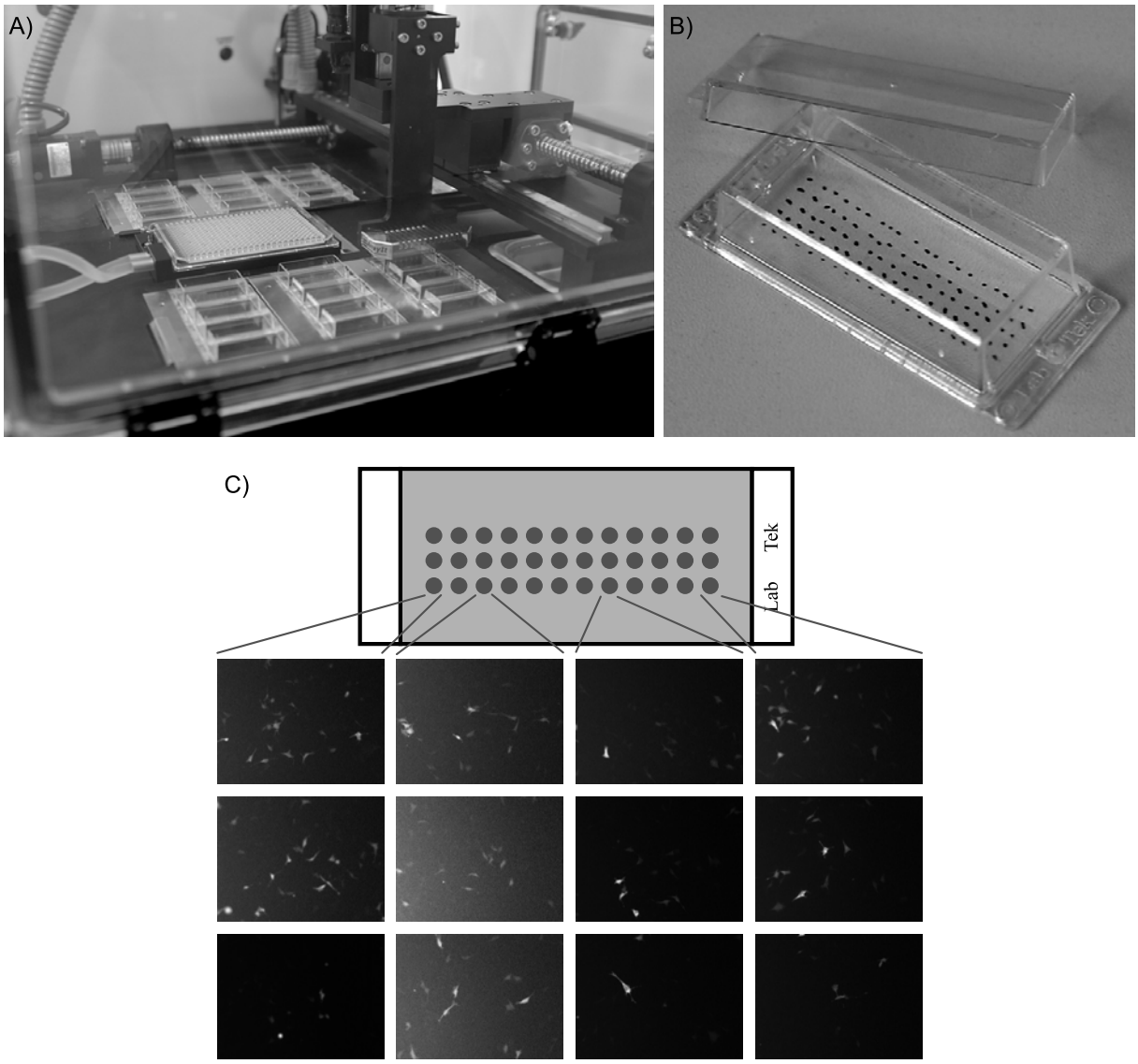

Figure 3.27: System for spotting DNA on welled coverslips. The spotter (A) distributes mixtures of cDNA and transfection reagent on welled coverslips (B; dark spots symbolize DNA spots). Cells are seeded in these coverslips and get transfected (C).

with a cell suspension. Cells attached to the coverslip, were transfecteded with DNA on individual spots, and expressed the corresponding protein. This generated an array of cells expressing different reporter proteins (Figure 3.27C).[247] Since every spot, or cell patch, can carry a plasmid for a different probe, simultaneous evaluation of up to 150 constructs could be possible.

Optimal transfection reagents, DNA concentrations, and an optimal mixing protocol were selected in preliminary experiments. Pre-activation of Lipofectamin 000, subsequent DNA incubation, and addition of further components provided the best transfection efficiency of HeLa cells. Additional components werefibronectin,[248] a small protein that improved cell adhesion and attracted cells to the spots, and

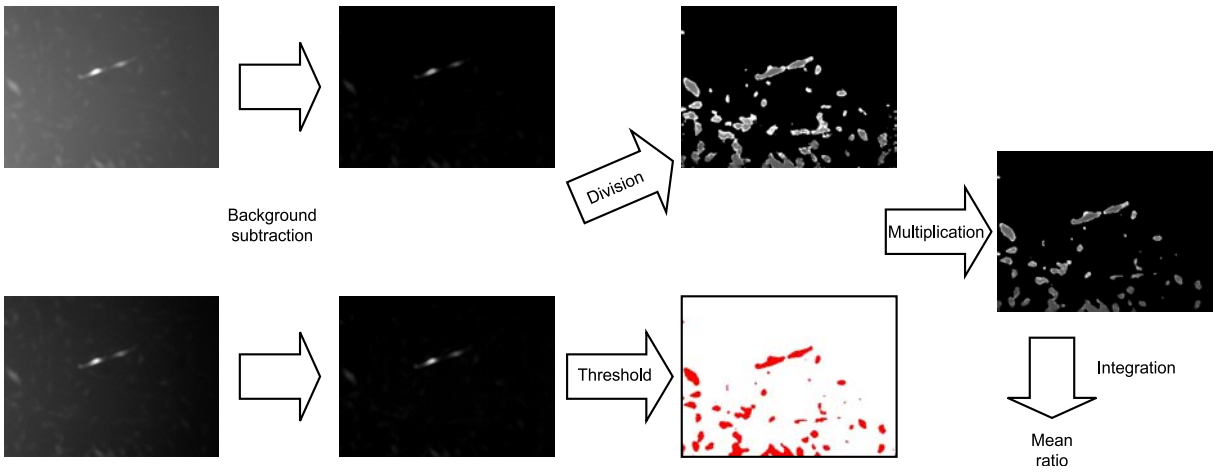

Figure 3.28: Schematic of steps involved in processing images acquired on a Visitron wide field system. This method permitted high throughput batch evaluation.

gelatine that generated a mesh in which complexes of DNA and transfection reagent were sequestered. The amount of DNA was less important to transfection efficiancy, and good results were obtained with DNA isolated with QIAGen Minipreps from 3 ml over night bacteria cultures. DNA concentrations ranged from 0.2 - 0.7 µg/µl.

A Visitron wide field microscope with a 10x objective was used for imaging. This system had an automatic stage and was temperature controlled. The image acquisition with wide field microscopes (~0.5 sec) was faster than with confocal microscopes (~15 sec), an important factor for imaging several spots in parallel.

The feasibility of the approach was initially tested with six constructs, each spotted at six sites. HeLa cells were plated and transfected over night in OptiMEM. The medium was exchanged to HEPES imaging buffer, and cells were equilibrated for two hours. The coverslip was then mounted on the microscope stage and cell patches were selected manually. Images from the GFP^2 and the EYFP channel were recorded to obtain initial values from untreated cells. Then TPA was added, and after ten minutes incubation, a second set of images was acquired. Comparing fluorescence ratio values before and after TPA showed FRET changes.

Background was subtracted from all images, $EYFP/GFP^2$ ratio images were calculated, and a threshold to select cells and to set the background to null (‘not a number’) was applied. The mean pixel intensity over a whole picture was calculated. The mean value represented the average ratio of $EYFP/GFP^2$ fluorescence in one image (Figure 3.28).

One set of mean values was obtained for every DNA spot before (*preRatio*) and after (*postRatio*) PKC activation by TPA. The values *preRatio* and *postRatio*

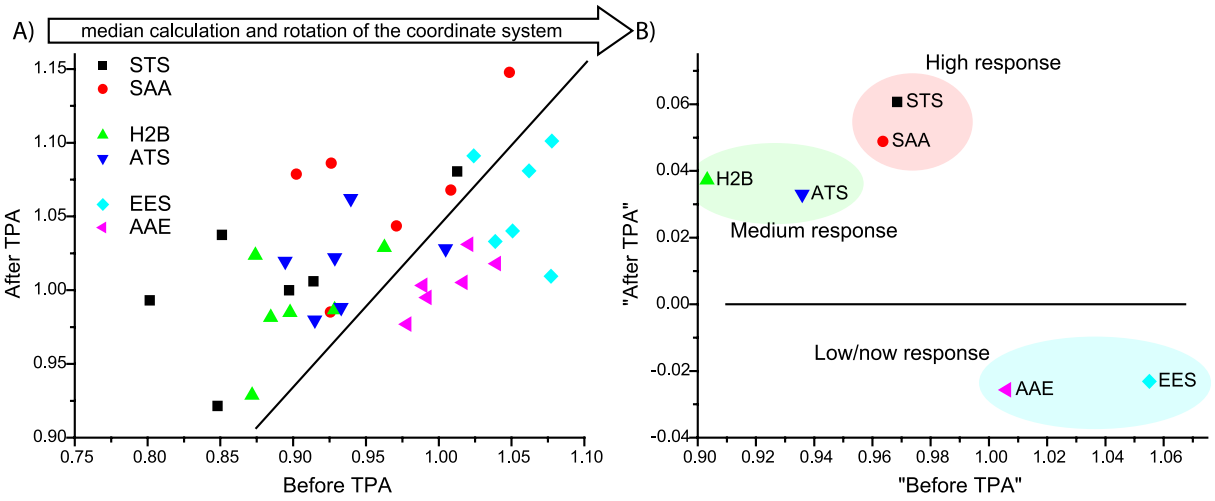

Figure 3.29: Results from a coverslip experiment with six mutants. The same DNA was spotted at six sites of the coverslip. The directly obtained scatter plot is difficult to interpret (A). Median values for equal identical spots and rotation of the coordinate system helps to identify constructs with large (red), medium (green), and no response (blue).

were placed on the abscissa and the ordinate of a scatter plot. Probes with a positive or negative FRET change appear in the upper left or lower right area of the diagram, respectively. Constructs not reacting to stimulation appear in the middle area of the diagram, ideally located along a straight line, representing different, but unchanged FRET levels. To simplify the data analysis in the diagram, the coordinate system of the scatter plot could be rotated. Then, spots indicating a FRET change or no FRET change were located above or below the abscissa, respectively.

Since a semi-automated approach was chosen and single imaging sites were not inspected visually, not every image gave applicable values. To compensate for this, a median value for sites expressing the same construct was calculated for both *preRatio* and *postRatio*.

A pilot study included constructs carrying mutated STS sequences as described above. The constructs KCP-1/STS and KCP-1/SAA were positive controls, KCP-1/ATS and KCP-1/H2B showed a medium FRET change, and KCP-1/EES and KCP-1/AAE exhibited no FRET change. Figure 3.29 shows that different responses are distinguishable and cluster in different areas.

Analysis performed in this manner might not give time resolved values and cannot serve for quantitative comparison between different constructs, but could help to quickly and efficiently identify functional probes for further investigation. The assay screens at least 20 constructs in triplicate in the same time usually needed to examine a single construct using the conventional method (30 min).

Time resolved experiments are also possible, when the time required for visualizing all of the spots does not exceed an appropriate time resolution. For example, imaging of 27 sites could be performed within one minute. This time resolution was 4 times lower than single construct analysis, but was sufficient to permit resolution of the transient bradykinin response. When a lower time resolution is needed, as for TPA or forskolin treatment, longer periods can be tolerated and more constructs can be screened in parallel. Therefore, this method will allow efficient screening for a multitude of constructs under identical conditions.

3.7 Applications of KCP-1

3.7.1 Drug screening possibilities

Deregulation of protein kinase C activity has been associated with a wide range of physiological symptoms. Potent activators of PKC, like phorbol esters (TPA), are tumour-promoters.[26, 249] Therefore, PKC is a valuable drug target,[27, 31, 250, 251] and high throughput *in vitro* assays are available to identify PKC inhibitors.[166, 252, 253] However, experiments showed a large discrepancy between reaction kinetics of KCP-1 phosphorylation *in vitro* and *in vivo* (compare Figure 3.5A and Figure 3.6A). Therefore, screening assays that employ live cells have major advantages compared to *in vitro* experiments. A multi-well plate, seeded with cells expressing KCP-1 and imaged with an automatic microscope, supplied an appropriate system.

HeLa cells that stably expressed KCP-1 were grown in 96-well plates, which were directly mounted on the microscope (Visitron). The software (Metamorph)[254] was equipped with a screening capability, which can either use predefined plate layouts or user-specific array patterns. EYFP/GFP^2 ratios were obtained after image background subtraction, ratio calculation (EYFP/GFP^2), cell segmentation, and pixel values averaging over a whole image.

First, several objectives were tested. Only air objectives (5X, 10X, 32X) were considered since the chosen plates were made from plastic and had an inappropriate optical density for high refractive oil immersion objectives.

Ten wells with two imaging sites each were evaluated using the 10X and 32X objective, twenty wells with one imaging site were evaluated for the 5X objective. Each site was imaged three times. After image acquisition and processing, calculation of median and standard deviation of the values from the three time points,

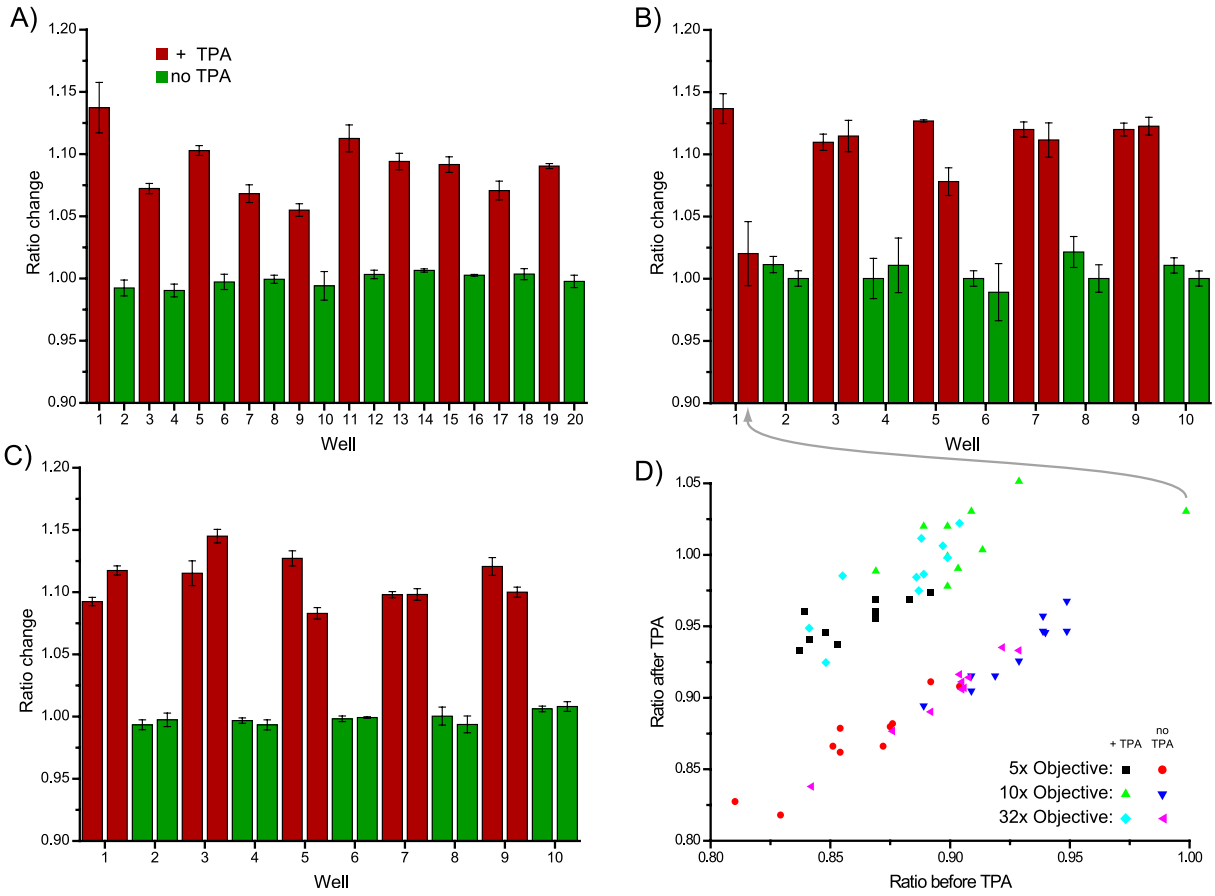

Figure 3.30: Initial screening experiments tested several objectives (A: 5x; B: 10x; C:32x). All objectives gave similar results. One false negative result in (B) can be directly identified in a scatter plot (D) as a non-clustering data point.

two EYFP/GFP[2] ratio values (*preRatio* before TPA and *postRatio* after TPA treatment) and their standard deviations were obtained for each imaged site. The values *postRatio* were normalized against *preRatio* for a bar graph representation. This quotient is approximately “1”, in case of no FRET change and should be higher or lower for a positive or negative FRET change, respectively (Figure 3.30A-C). From the 60 data points obtained, only one value was false negative. A scatter plot revealed that the ratio value in this case did not cluster with the others, and should not be considered (Figure 3.30D). For this data point, a very large and bright cell dominated the measurement. This example showed the advantage of scatter plots over bar diagrams.

Although all objectives tested gave acceptable results, a 10x objective was selected, since it offered appropriate brightness and field of view. The 5x objective had lower aperture and the 32x objective could image only a limited number of cells in one field. Furthermore, since the focal depth of the 10x objective is higher than of a 32x objective, autofocusing for single spots was omitted.

Next, 80 wells of a 96-well plate were loaded with cells expressing KCP-1 (16 wells could not be assessed with the automated microscope stage). 50% of the wells were treated with TPA and five were pretreated with the PKC inhibitor Gö6983 (pattern in Figure 3.31A). Images were taken before and after TPA treatment at four sites per well. After image processing, medians were calculated for each well from the respective ratio (*preRatio* and *postRatio*). Images that showed no cells and therefore, lacked ratios, did not contribute to the calculation. The quotient *postRatio*/*preRatio* was calculated (displayed as false colour hue in Figure 3.31B) and thresholded to separate positive and negative signals. Since the threshold is set arbitrarily, it could be adjusted to obtain an optimized result (Figure 3.31C) and minimize false negative and false positive hits (Figure 3.31D and E). However, this is not a valid method for compounds of unknown effect. Again, a scatter plot of

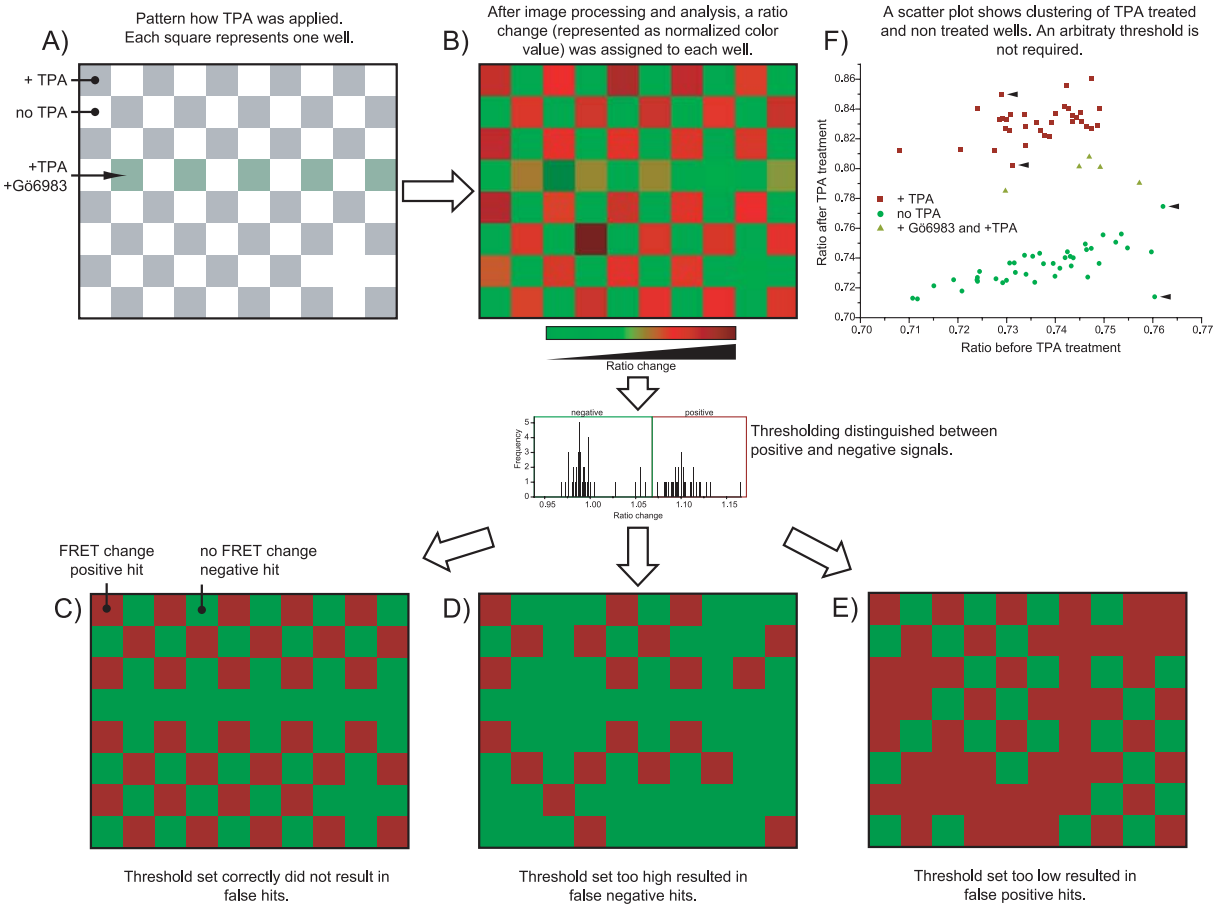

Figure 3.31: A) Parallel evaluation of 80 wells, half of them loaded with TPA (gray). In addition, 5 wells were treated with Gö6983 (green). B) The change in emission ratio was calculated for every well. Subsequent thresholding separated positive from negative hits. The threshold could be set to obtain optimized results: positive (red) and negative (green) hits (C) represent the pattern of TPA and Gö6983 loading (A). Another threshold resulted in false negative and false positive hits (D and E). F) A scatter plot omitted a threshold and positive and negative hits were directly identified. The four data point with highest and lowest y-values are indicated by an arrow. When these data points were omitted in Z-value calculations, Z = 0.53, which qualifies the method for industrial applications.

postRatio against *preRatio* is the best way to analyse the data (Figure 3.31F). Wells that were treated with and without TPA were readily distinguished. Autofluorescence of Gö6983 might explain the fact that Gö6983/TPA treated wells did not group with results from unstimulated cells.

To judge the quality of the assay, a Z-value was calculated as introduced above.[223] Since the formula for the Z-value considers only one dimension of the data points, y-values were used. Therefore, the coordinate system of the scatter plot was rotated (here 33° counter-clockwise) to produce minimal standard deviation of the y-values. The mean values of data points from TPA- and not TPA-treated wells gave S_s and S_b, respectively, and their standard deviations SD_s and SD_b. A Z-value of 0.39 was calculated, indicating that the assay's separation band between positive and negative signals is too small to be used in an industrial HTS. However, when the four data points with extreme values (minimal and maximal y-values for negative and positive controls; marked with an arrow in Figure 3.31F) are excluded in the calculation, Z = 0.53. Therefore, the assay has the potential to qualify for industrial screenings upon further optimization.

This assay system was used to screen 16 compounds in quadruplet. The drugs were randomly chosen from SiLib, a commercially available compound library.[255] TPA, DMSO, 4α-TPA, and Gö6983 were added as positive, neutral, and negative controls. Images were taken before treatment (*preRatio*) and ten minutes after the compounds were added (*postRatio1*). A scatter plot (*preRatio* versus *postRatio1*; Figure 3.32A) showed activators of PKC as non-clustered data points located near the positive TPA control (data point c1 in Figure 3.32). Next, TPA was added to activate PKC in each well. After ten minutes another image set was recorded (*postRatio2*). In a scatter plot of *postRatio2* against *preRatio* (Figure 3.32B), non-clustering data points represented PKC inhibitors close to the negative control Gö6983 (data point d1 in Figure 3.32). The 4α-TPA and DMSO neutral controls did not show an activating or inhibitory effect on PKC and clustered with compounds without effect as expected (Figure 3.32). The compounds a4 and c8 did not group with the other compounds and a PKC activation effect could be expected; however, there is a shift of the data points *preRatio*/*postRatio1* and *preRatio*/*postRatio2* as observed with non-interacting but not with interacting compounds (compare the large shift of the DMSO control a1 and the little shifts of activator TPA or inhibitor Gö6983

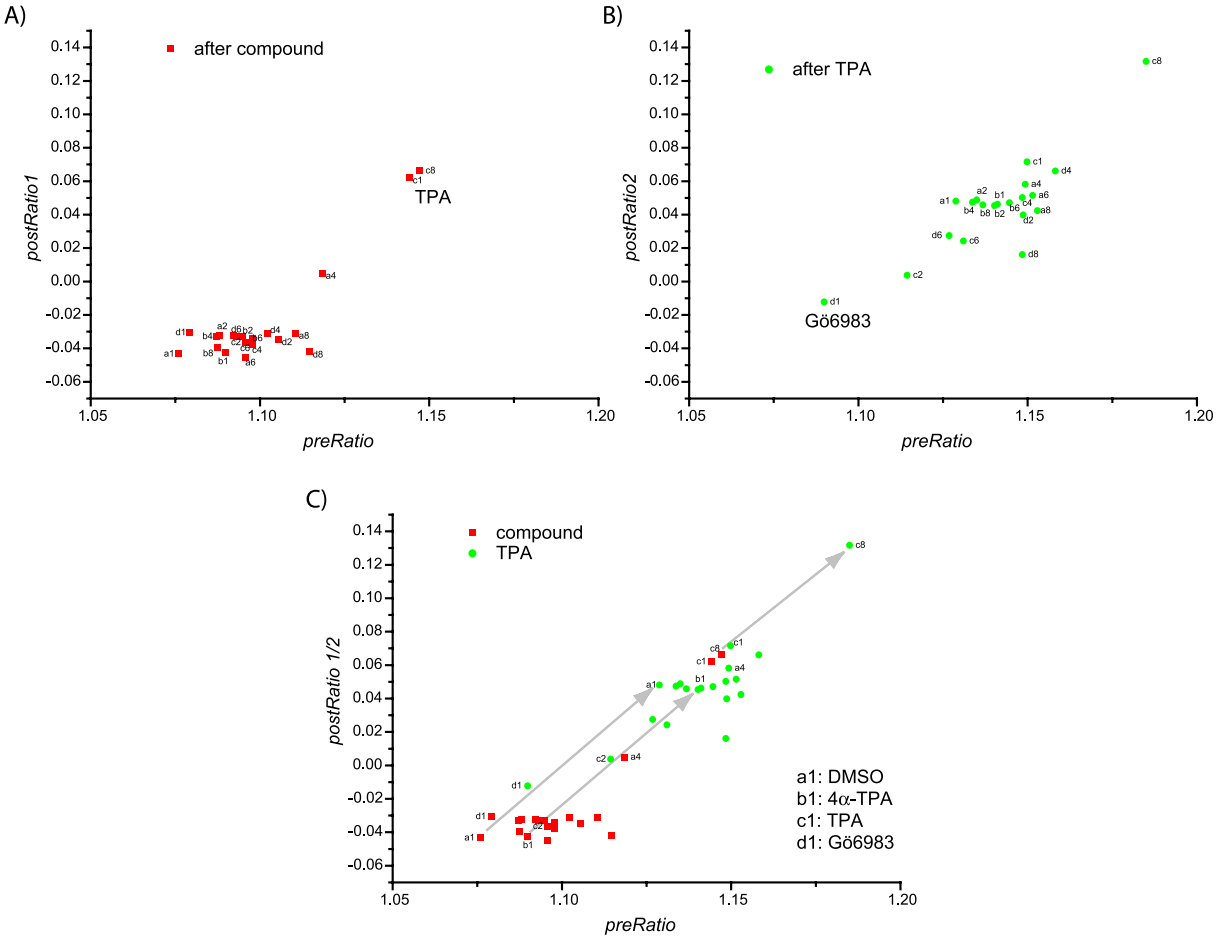

Figure 3.32: Screen of 20 compounds. A) Addition of the compounds identified activators (e.g. TPA). B) After subsequent TPA treatment, PKC inhibitors, like Gö6983, can be recognized. C) When a data point shifts after addition of drug *and* TPA, then the compound has probably no effect, but is fluorescent. Compounds used are listed in the experimental part.

in Figure 3.32C). This suggested that compounds a4 and c8 did not have an effect on PKC activity. These candidates had a red colour in solution, and the compounds' fluorescence interfered with that of KCP-1, obscuring the calculated values.

These experiments demonstrated that KCP-1 could be used on an automated screening system employing live cells. Activators and inhibitors of PKC were reliably identified, and fluorescent compounds were detected.

3.7.2 Multiparameter imaging

General aspects

Protein kinase C is one member of a complicated network of cellular signals. Examination of several parameters in parallel would help to elucidate the -interplay between components. To accomplish this, multiple fluorescent reporters, being either genetically encoded or small molecule probes have to be imaged simultaneously

using microscopes that allow for segmentation of distinct fluorescent properties.[256]

The feasibility of multiparameter experiments was tested using the signalling cascade that activates PKC. This cascade is initiated when an agonist binds to a cell receptor, phosphatidylinositol 4,5-bisphosphate (PIP_2) and phosphatidylcholine (PC) are cleaved to DAG and *myo*-inositol 1,4,5-trisphosphate (IP_3), and the latter releases calcium. DAG and calcium activate PKC (Figure 1.1).[37, 38, 40, 257]

The following identifies and describes several reporters that can be used to monitor different parameters involved in PKC activation:

- PKC: FRET change of KCP-1.
- Calcium: Small molecule dyes that change spectral properties are commonly used as calcium sensors. For the presented experiments, the dye fura red was chosen because it emits in the far red and interfered minimally with other probes.[164] Another reporter was fluorescent protein fused to the C2 domain of PKC.[39] This probe translocated from the cytosol to the plasma membrane upon Ca^{2+} binding. (ECFP-C2)
- PIP_2: PH domain of phospholipase δ1 (PLCδ1) tagged with a fluorophore. This domain recognized PIP_2 at the plasma membrane and translocated to the cytosol after PIP_2 breakdown.[178-181, 183-185] (mRFP-PLCδ1PH)
- DAG: A fluorophore labelled C1a domain of PKC residing in the cytosol but that translocated to the plasma membrane when DAG was present.[186] (ECFP-C1a, C1a-mRFP)

Plasmids encoding EGFP-PLCδ1PH, C1a-EGFP, ECFP-C1a, and C2-ECFP were gifts from K. Jalink, T. Meyer, and T. Gadella. These plasmids were either used directly or were templates for the assembly of mRFP fusions of C1a and PLCδ1PH.

Experiments based on translocation probes required the ability to distinguish between cytosol and plasma membrane during fluorescence measurements. In HeLa cells, although the translocation could be readily recognized by visual inspection, it was difficult to set computational meaningful regions of interest since fluorescence signals from the cytosol and the plasma membrane superimposed. Therefore, most experiments were performed with N1E-115 cells, which were comparably thick and where cytosol could be distinguished from the plasma membrane without difficulty.

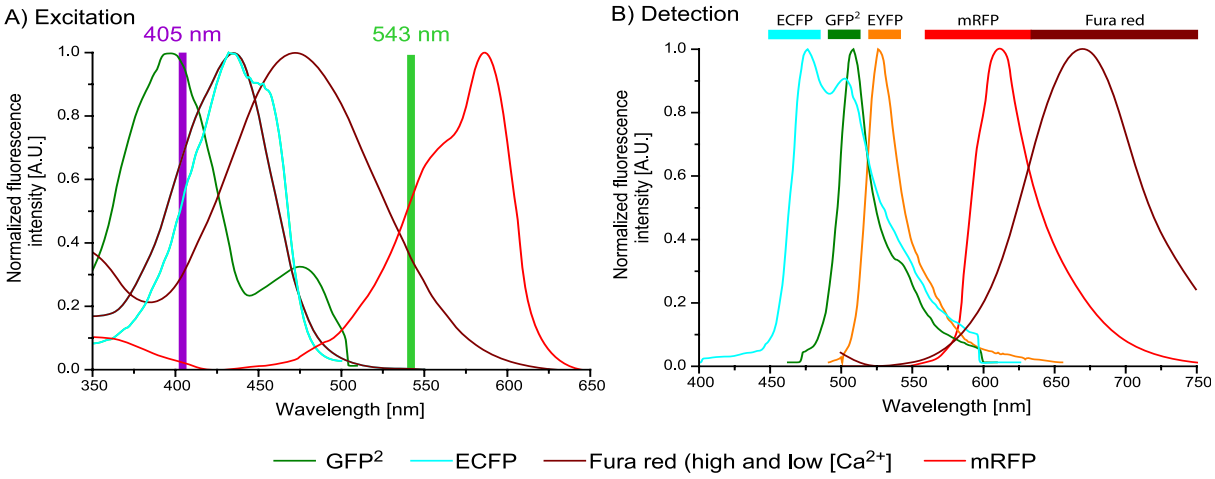

Figure 3.33: A) Excitation spectra of ECFP, GFP^2, fura red, and mRFP. The first three dyes are excitated simultaneously with a 405 nm diode laser, while mRFP (and also fura red) is imaged with the 543 nm line of an He/Ne laser. B) Emission spectra of the dyes and limits for the detection channels.

The signal of translocation probes (C1a, C2, and PLCδ1PH domain fusions) were measured as increase or decrease of fluorescence in the cytosol. Translocation of the probes from the cytosol to the plasma membrane or *vice versa* was easily followed by visual inspection. Unlike the cytosolic area, applying a ROI over a section of the plasma membrane was difficult due to cell movement. Therefore, a static ROI was not suitable to measure fluorescence in the plasma membrane.

Different GFP variants were used as fluorophores. Since KCP-1 already uses GFP^2 and EYFP, the remaining available FP variants were cyan (ECFP) and red (mRFP) fluorescent proteins. Blue FP (EBFP) had poor optical properties (bleaches easily, low quantum yield).[125, 133] The microscope of choice was the Leica SP2 AOBS, which enabled unrestricted choice of detection ranges. Laser wavelengths, detection channels, excitation and emission spectra are shown in Figure 3.33.

Imaging of ECFP was performed in parallel to KCP-1 (or GFP^2) during fluorophore excitation with a 405 nm. The ECFP emission spectrum was broad and overlapped substantially with GFP^2, and to a lesser extent, with EYFP emission. Therefore, it was necessary to select cells with relative low ECFP expression compared to KCP-1. In principle, linear or spectral unmixing could be applied to correct for fluorescence cross talk in the raw images. However, automated algorithms, such as the spectral unmixing capability of the Zeiss LSM Meta microscope ("online fingerprint"),[226, 229, 258] usually provided satisfactory results only when the different dyes concentrated on distinct localizations. For the components ECFP, GFP^2, and EYFP linear unmixing was a more direct method and was applied

with crosstalk coefficients, which were adjusted where necessary.

Parallel imaging of KCP-1 and mRFP tagged proteins did not require fluorescent unmixing. The large spectral distance between fluorophore emissions prevented crosstalk between KCP-1 and mRFP. A caveat was that mRFP had to be excited with a 543 nm (or even worse a 532 nm) laser, which was close to the EYFP detection channel (520-540 nm). This made parallel imaging impossible and prevented simultaneous imaging during one scan. The fluorophores had to be imaged successively by switching microscope settings (laser lines, detection channels) either between lines or frames during acquisition. This limited the time resolution, which could be corrected by faster imaging at the cost of image quality (higher data noise). A 560 nm laser would solve this problem.

The calcium sensor fura red was ideally excited at 452 nm, where its excitation efficiency did not change with different calcium levels.[164] A loss of fluorescence was indicative for higher calcium levels. In contrast, when fura red was excited at 405 nm, in parallel with ECFP and GFP^2, fluorescence levels increased with calcium concentration. Fura red's maximum emission was at 670 nm, but its emission band was very broad and emitted substantially in the GFP^2 and EYFP detection channels. Therefore, it was important that cells were not strongly stained with fura red. Since both mRFP and fura red were excited at 543 nm, imaging these dyes in one cell was difficult. Even in experiments which combined high mRFP expression and low fura red labelling, fluorescence detected in the mRFP emission channel was dominated by fura red fluorescence and linear unmixing was impossible.

Imaging of several fluorophores in parallel was a challenge. In addition to experimental problems discussed above, further difficulties were apparent. In particular, few cells expressed FP tagged proteins in an appropriate balance. Even when this was achieved, all probes were required to give a reasonable response. Often, meaningful signals could be recognized only after image analysis. Therefore, only a handful from more than 70 experiments gave applicable results.

Multiparameter experiments

An initial experiment employed KCP-1 and C1a-mRFP in order to detect PKC activity and DAG build up. DiOG was added to HeLa cells (DiOG was shown to invoke a rapid FRET response [see above] and was known to bind the C1a domain). C1a gave an immediate signal, whereas KCP-1 ratio change was delayed by

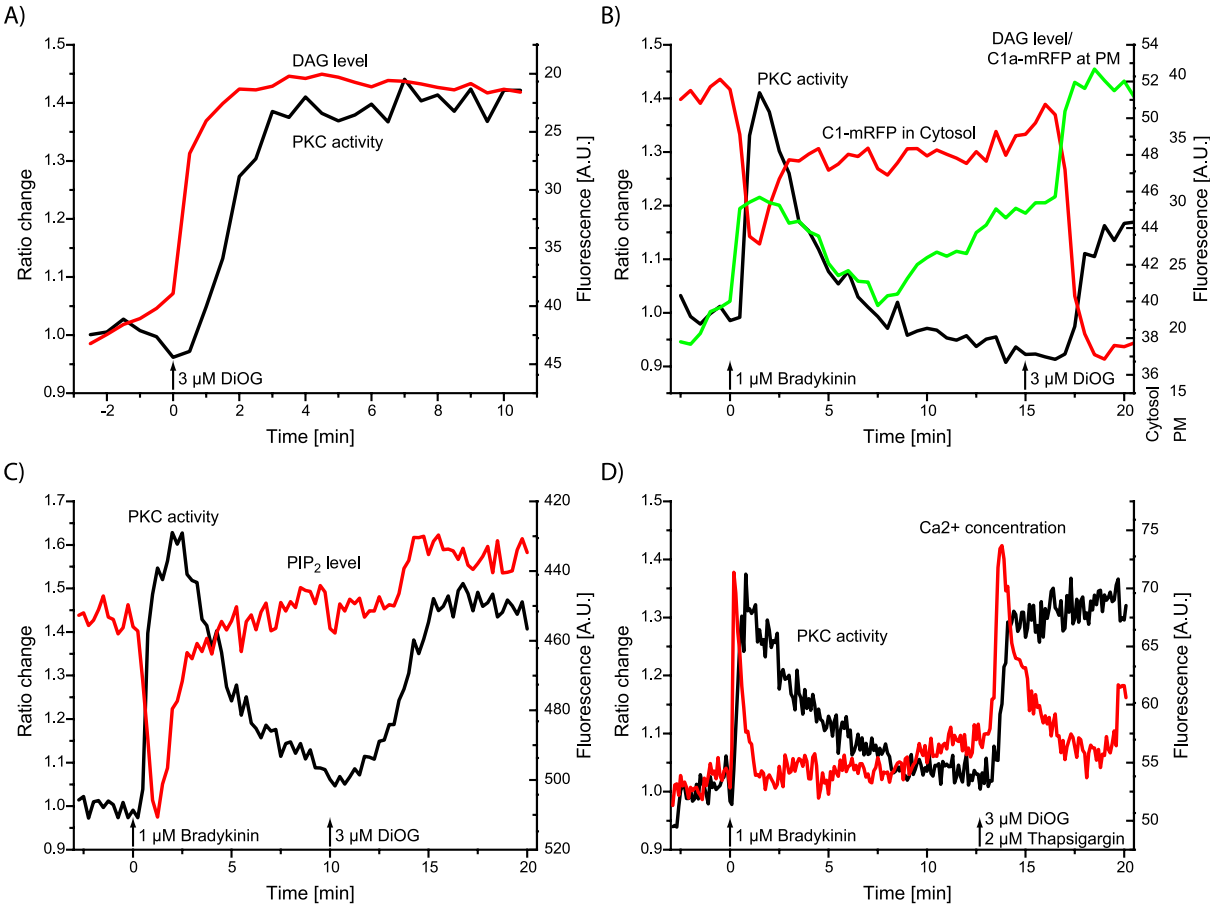

Figure 3.34: Dual parameter experiments. A) PKC was not immediately activated after DAG addition, probably due to diffusion effects (DAG: C1a-mRFP; PKC: KCP-1). B) The C1a-mRFP fusion construct shows different signals from the cytosol and the plasma membrane. The signal from the plasma membrane parallels PKC activity (KCP-1). C) PIP_2 levels (mRFP-PLCδ1PH) show a short breakdown after cell stimulation with bradykinin, in contrast to sustained PKC activity (KCP-1). D) Bradykinin induced a very sharp calcium spike (fura red), whereas thapsigargin had a longer lasting effect.

approximately one minute (Figure 3.34A). This demonstrated that although DAG was present in the plasma membrane, PKC was not directly activated. In contrast, histamine treatment prompted an immediate signal from the C1a domain and KCP-1. This supports the concept that DAG, as proposed for TPA above, must diffuse in the membrane to locate and activate PKC, while histamine was faster and activated PKC more directly, for example by direct receptor/PKC contact.

In an experiment with an mRFP tagged C1a domain, fluorescence in the cytosol as well as in the plasma membrane was evaluated. Surprisingly, both signals did not appear in parallel (Figure 3.34B, red and green trace). The cytosolic signal reverted faster than that of the plasma membrane. A possible explanation is that the depleted cytosolic pool was partially refilled with C1a-mRFP protein from the nucleus. Furthermore, a membrane derived signal is more direct (the monitored compound, DAG, is synthesized in the membrane), whereas a cytosolic signal is indirect: loss of

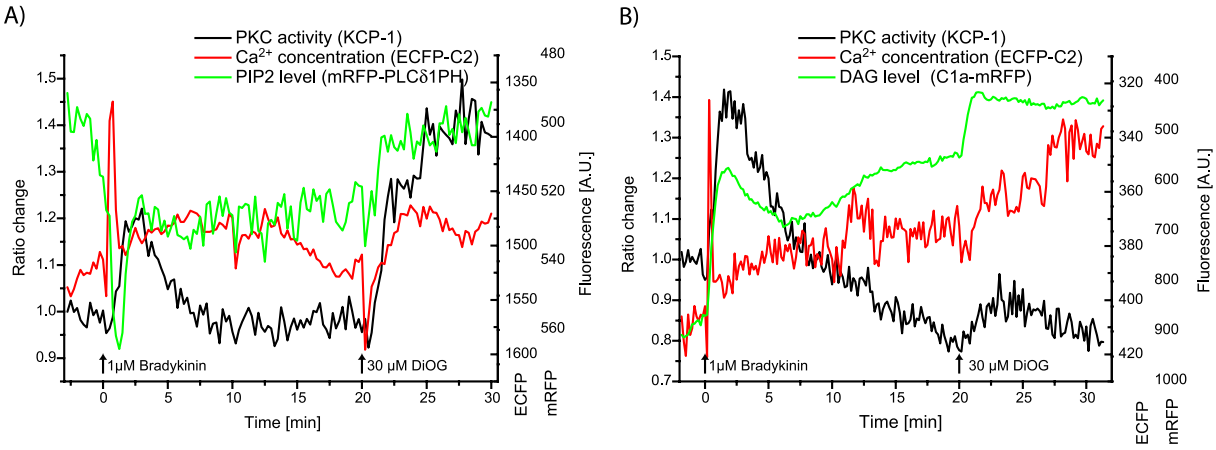

Figure 3.35: Triple parameter experiments. A) Bradykinin induces a short calcium spike, which is paralleled by PIP_2 breakdown. PIP_2 is hydrolysed to IP_3, which releases calcium. B) A calcium spike reverts faster than KCP-1 reaches its maximal response. The KCP-1 signal is paralleled by DAG concentrations. This may indicate that KCP-1 primarily reflects activities of novel PKCs.

fluorescence is caused, because elsewhere (here: in the plasma membrane) the compound of interest is generated. Therefore, a signal measured in the plasma membrane might reflect DAG concentration more appropriately than data collected in the cytosol.

Experiments with KCP-1 and mRFP tagged C1a- or PLCδ1PH-domains showed that PKC activity paralleled DAG presence (Figure 3.34B) but not PIP_2 breakdown (Figure 3.34C) after bradykinin stimulation of N1E-115 cells.

In experiments using bradykinin, KCP-1 response was not coupled to changes in Ca^{2+} levels, which were observed with fura red. Bradykinin induced a very rapid calcium spike in N1E-115 cells,[259-262] which virtually reverted before KCP-1 reported maximal PKC activity (Figure 3.34D). This result implied that KCP-1 primarily monitored activities of calcium independent PKC isozymes.

Three-parameter experiments were conducted as proof of principle. It was shown that KCP-1, ECFP, and mRFP fluorescence could be monitored in parallel and that distinct results could be obtained (Figure 3.35).

As in the two-parameter experiments shown above, bradykinin treatment of N1E-115 cells led to a Ca^{2+} spike, as followed with ECFP tagged C2 domain. The response of KCP-1 paralleled DAG concentrations in the plasma membrane. Again, the PIP_2 signal reverted faster than DAG levels. This means that DAG is formed via other pathways, most likely by phosphatidylcholine hydrolysis. Fluorescent probes that monitor PC levels would complete a set of reporter molecules that could shed light on the complete signaling cascade that leads to PKC activation (Figure 1.1).

4 Discussion

4.1 Introduction

Protein kinase C occupies key functions in a multitude of cellular pathways and is a popular focus for research. Commonly used radioactivity assays on cell lysate are unfavorable for several reasons and no safe and simple method existed to monitor real-time PKC activity in living cells.[54] Such assays measure PKC activity only in *in vitro* extracts of an ensemble of cells and cannot resolve spatiotemporal PKC activities in single living cells. In addition, the use of radioactivity is hazardous.

The FRET-based kinase C probe, KCP-1, and related constructs, provide the means to observe PKC activity in living cells with fluorescence.

4.2 Design of the probe

In KCP-1, two fluorescent proteins flank a PKC specific pleckstrin fragment,[108] which changed conformation after phosphorylation.[215] These two features of the fragment promised *a priori* both specificity and signal, in contrast to *de novo* designed FRET-reporters. The fluorophore pair GFP^2/EYFP was chosen because donor emission and acceptor excitation overlap perfectly for FRET applications.[216]

Generic FRET reporters employ substrate recognition domains, for example, M13 binds to Ca^{2+}/calmodulin in the calcium reporter cameleon. These motifs can also bind to endogenous substrates in cells. This may lower the probe's sensitivity and may interfere with cellular signaling.[203, 204, 206] Such recognition domains were omitted in KCP-1 and therefore, minimal interference with cellular proteins was expected. Potential signaling domains in KCP-1 are a PH and a DEP domain. These domains mediate phospholipid binding and/or protein-protein interactions in wild type pleckstrin. Alterations in these domains can be used to inactivate these functions for the probe, since their cellular performance is not required for KCP-1's function. Therefore, KCP-1 mutants can be generated that avoid additional cellular interaction, other than PKC and phosphatase activity.

4.3 Fluorimeter experiments

KCP-1 phosphorylation was monitored *in vitro* in a fluorimeter. After addition of active kinase, the ratio of GFP^2/EYFP emission increased from 1.6 to 2.2, and after cleavage of the probe with trypsin decreased to 0.6 (Figure 4.1). The fluorescence spectrum of phosphorylated KCP-1 exhibits virtually no peak at the GFP^2 emission

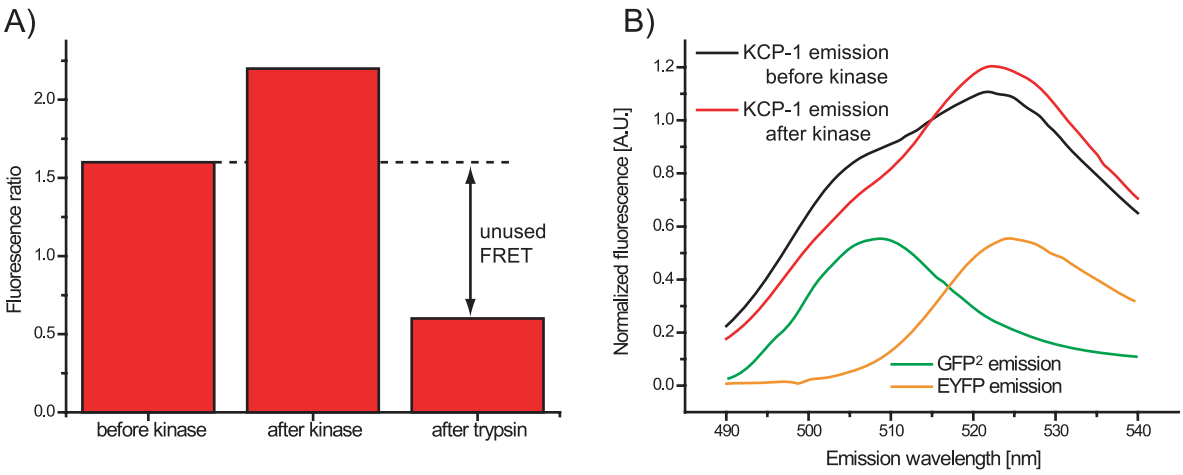

Figure 4.1: A) Fluorescence ratio values (EYFP over GFP^2) of KCP-1 before and after kinase (PKM) treatment. The FRET efficiency increased after phosphorylation. Trypsin released both fluorophores and no FRET occurred. Decrease in FRET demonstrated that unphosphorylated KCP-1 exhibited high FRET efficiency. B) Emission spectra of KCP-1 before and after phosphorylation. The probe shows strong EYFP fluorescence. For comparison, GFP^2 and EYFP spectra are shown.

maximum, but shows strong EYFP fluorescence. This suggests that phosphorylated KCP-1 has almost maximal FRET efficiency. As such, a larger FRET change cannot be achieved by increasing FRET efficiency. Instead, the initial FRET efficiency of the unmodified probe must be reduced. This is feasible since trypsin cleavage of the probe showed a minimal emission ratio of 0.6. Reduction of initial FRET efficiency may be obtained by altering the N- and/or C-terminal linker between the probe's pleckstrin fragment and the fluorophores. Elongation of the linkers may increase the distance of both fluorophores and therefore, reduce FRET efficiency.

4.4 Characterization of KCP-1

KCP-1 reported PKC activity after cell stimulation with drugs or mitogens, like phorbol esters, histamine and bradykinin. Activation of PKA or CaMKII did not produce a signal, reflecting KCP-1's specificity for PKC over PKA and CaMKII. Alternation of the putative phosphate acceptor amino acids to glycines or glutamates destroyed KCP-1's sensitivity, demonstrating that phosphorylation of at least one of these amino acids (S113, T114, and S117 in pleckstrin) was responsible for the FRET change.

Phosphorylation of pleckstrin is thought to be PKC isozyme unspecific.[107] In contrast, *in vitro* phosphorylation of a pleckstrin fragment (PH-DEP)[219] or KCP-1 showed that both were preferred substrates for PKCθ, but not for, e.g. atypical PKC isozymes. However, *in vivo* selectivity cannot be deduced from these experiments

since subcellular distribution and additional binding partners determine PKC specificity in living cells.

Live cell stimulation with thapsigargin[222] transiently elevates cytosolic calcium concentration for approximately five minutes (see Figure 3.34D). Activities of the calcium-dependent, conventional PKCs should follow calcium levels; however, the KCP-1 signal increased within five minutes to reach a plateau. The signal could not be reverted by specific inhibition of conventional PKCs. This experiment suggested a) that thapsigargin activated non-conventional PKCs, for example by calcium-initiated hydrolysis of phosphatidylcholine to DAG[41] (a slow process) and b) that KCP-1 was not sensitive to conventional PKCs. It must be recognized that these experiments report only activities of PKC isozymes that were active in the observed cells. However, a PKC isozyme profile of the cells was not available and published data were inconsistent.[43, 263]

To characterize effectors of KCP-1, i.e. which PKC isozyme activities are observed with KCP-1, experiments employing either cell lines deficient in specific PKC isoforms, or PKC isozyme specific RNA interference (RNAi)[264, 265] experiments should be performed in future. The technique used for the KCP-1 mutant screen can be beneficial in such experiments. Instead of a DNA array, an siRNA array is spotted on welled coverslips.[266] These are seeded with cells that stably express KCP-1. For each spot, one or more specified PKC isozymes are suppressed by siRNAs. Evaluation of experiments with diverse PKC activators would reveal PKC isozyme preference of KCP-1. To complement knock-down experiments, knock-in experiments can also be performed. For example, *Drosophila* Sf9 cells, have no endogenous PKC activity, but could be cotransfected with KCP-1 and single PKC isozymes. Activation of the PKC isozyme would directly show KCP-1's selectivity. Moreover, in conjunction with KCP-1's related probes that are mutated in the phosphorylation loop (KCP-1/SAA, KCP-1/ATA, and KCP-1/AAS) these experiments could show if the different phosphorylation sites in KCP-1 are targeted by different PKC isoforms. Such may clarify regulation and function of pleckstrin.

4.5 Comparison of KCP-1 and CKAR

CKAR is another PKC activity FRET reporter that was recently developed.[214] For comparison, KCP-1 and CKAR were expressed in N1E-115 neuroblastoma cells, which were stimulated with bradykinin and subsequently with TPA (Figure 4.2). Both

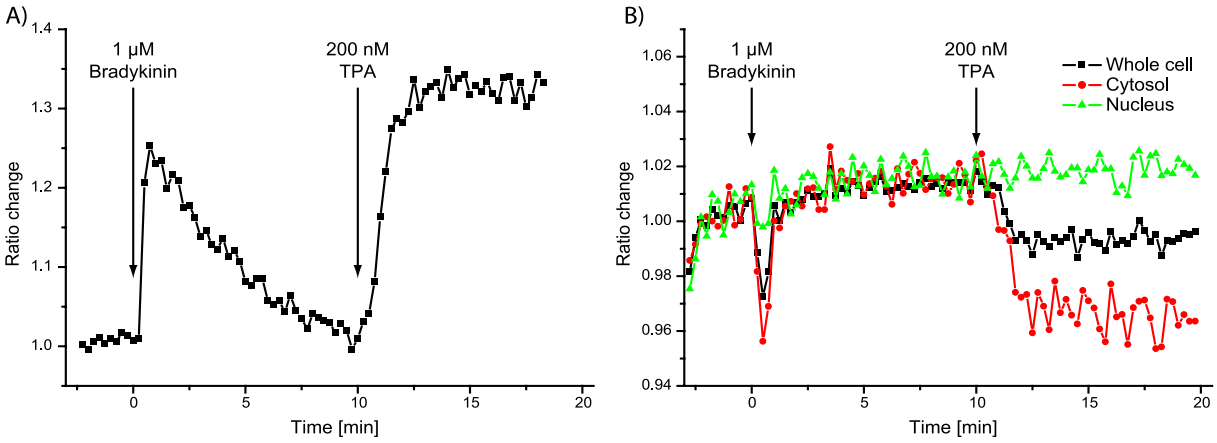

Figure 4.2: KCP-1 (A) and CKAR (B) were expressed in N1E-115 cells. Stimulation with bradykinin shows that KCP-1 reports sustained PKC activity, but CKAR exhibits a short pulse. This may represent different PKC isozyme preference.

probes reported a transient bradykinin signal and a stable TPA response. FRET changes for both probes following TPA and Gö6983 treatment were similar (data not shown). CKAR may have reached a maximal signal slower and reverted more quickly after PKC inhibition, however such differences were marginal. Striking was the difference in the bradykinin signal, which occurred faster, but with shorter duration for CKAR than for KCP-1. The kinetics of the signal resembled that of calcium spikes observed after bradykinin treatment in the multiparamter experiments; in contrast, KCP-1's signal paralleled DAG levels. KCP-1 and CKAR are obviously phosphorylated by different PKC isoforms and/or have different kinetic parameters for phosphorylation/dephosphorylation. Comparison of responses induced with bradykinin suggests that CKAR is preferred by calcium-dependent PKC isozymes, whereas KCP-1 is predominantly phosphorylated by calcium-independent, novel PKC isoforms. The contribution of phosphorylation by atypical (calcium and DAG independent) PKC isozymes cannot be judged based on these experiments. CKAR's preference for conventional PKC isozymes is also supported by experiments that demonstrated synchronism of calcium levels and (reported) PKC activity.[214] Experiments with Madin-Darby canine kidney (MDCKII) cells also show that both PKC activity probes report activity of different PKC isozymes; CKAR, but not KCP-1 reported TPA induced PKC activity (data not shown) in this cell line. A PKC isozyme profile of MDCKII cells would help to evaluate these results. One possible explanation is that these cells express conventional but not novel PKC isoforms. However, such speculations must be confirmed in future.

KCP-1's and CKAR's isoform preference should be tested in experiments such

as those proposed above (e.g. siRNA experiments). If the probes have different kinetics for different isozymes then they can be used in parallel experiments to distinguish activation of distinct subsets of PKC. While the origin of both probes' signal is not fully understood, the parallel employment of KCP-1 and CKAR will give a more complete picture than experiments performed with just one probe. For such experiments, both reporters could be labeled with orthogonal sets of fluorophores, which permit parallel imaging in single living cells.

4.6 KCP-1 mutants

Mutants of KCP-1 were generated to investigate the effects of altering the linker between DEP and C-terminal PH domain, color variations of the fluorophores and changes in the phosphorylation loop.

4.6.1 Linker region

KCP-1 included 18 amino acid of the stretch that separates DEP and C-terminal PH domain in pleckstrin. NMR experiments with pleckstrin fragments suggested that this linker was important in structural rearrangements of pleckstrin invoked by phosphorylation.[267]

This linker was deleted from KCP-1 to generate a new probe, termed KCP-2. KCP-2 reported TPA, bradykinin or histamine stimulated PKC activities, but, in contrast to KCP-1, exhibited a FRET efficiency decrease after phosphorylation.

From these results and comparative NMR analysis of pleckstrin fragments, a model for structural changes in pleckstrin was developed. The model proposes that phosphorylation diminishes interactions between the PH and DEP domains. Both domains separate which increases the distance and/or orientation between the termini. This is reflected by a decrease in FRET efficiency in KCP-2. In contrast to KCP-2, KCP-1 has an 18 amino acid linker separating DEP domain and fluorophore. The stretch may interact with the PH domain and functions like a lever: repellent forces (separation of DEP and PH domain) on one side (near the DEP domain) induce a decrease of the distance between N- and C-terminus, and attached fluorophores. Consequently FRET efficiency increases. Such a model could not be verified by NMR experiments since the structure of the flexible 18 amino acid linker could not be determined. An NMR structure of KCP-1 would be desirable, but is not feasible due to the high molecular mass of the construct (82 kDa; NMR methods can

currently resolve protein structures of 50 kDa). Substitution of KCP-1's fluorescent proteins with small molecule dyes would result in probes that are suitable for NMR experiments. Structural information from such probes can then be correlated to FRET efficiency changes and a model for the function of KCP-1 can be established. Small fluorophores could be introduced in KCP-1 by several techniques like native chemical ligation, tetracystein/FlAsH technique, and other commonly used protein labeling techniques (e.g. thiol-reactive iodoacetamides).

X-ray structure analysis of phosphorylated and unphosphorylated KCP-1 and KCP-2 may give insight into the structural basis of FRET efficiency change for these two probes: however, it will remain unclear if the location of the flexible linker is affected by crystal-energetic effects. Furthermore, atomic resolution is not needed and crystallization of large polypeptides is typically difficult. The method of choice to detect domain organization of the probes is small angle x-ray scattering (SAXS).[268] This method permits structural analysis of protein domains in solution and could report directly the interdomain geometry of the probes' fluorophores, depending on phosphorylation states. Such experiments would eventually help to clarify pleckstrin's mechanism and function and could correlate structural changes in the PKC activity probes to FRET changes.

4.6.2 Color variations

KCP-1 and KCP-2 were equipped with GFP^2 and EYFP as a FRET pair, whereas CFP and YFP are the standard FRET partners used in most published procedures. To put KCP-1 and KCP-2 into this context, the donor fluorophore, GFP^2, was exchanged to ECFP and the acceptor dye, EYFP, was altered to Citrine, a close relative with equal spectral properties, but lower dependency on the environment (i.e. pH and ion concentration).[149]

Results obtained with ECFP/Citrine equipped probes – KCP-1(CiCF), KCP-1(CFCi), and KCP-2(CFCi) – were surprising: The KCP-1 derived probes showed only a *small decrease* of FRET efficiency, whereas FRET of KCP-2(CFCi) did not change at all after PKC activation in cells. In KCP-1, EYFP alone was substituted by Citrine (KCP-1(CiG2)) to demonstrate that this change was not responsible for a loss of signal. In fact, the probe's FRET change had a better signal to noise ratio.

FRET efficiency calculation, based on *in vitro* measured FRET efficiency change of KCP-1, estimated a similar FRET change for both GFP^2/EYFP and

ECFP/Citrine FRET pairs. However, such calculations assumed free rotation of the fluorophores and a concomitant mean dipole orientation factor $\kappa = 2/3$, which might not apply to the presented probes. Again, insight into the probes' structure will help to understand the discrepancy between model and experimental results.

Equipping KCP-1 and KCP-2 with Citrine as donor and mRFP as acceptor dye produced the probes KCP-1(CiRF) and KCP-2(CiRF). Both showed a negative FRET change as response to PKC activation in cells. KCP-2(CiRF) exhibited a stronger response. These probes are first steps to longer wavelength probes. Such probes might prove useful in living animals, where long wavelength excitation and emission enable fluorescence detection deep in tissue.

4.6.3 Mutations in the PH domain

A hallmark of phosphorylation of wild type pleckstrin is translocation of the protein to the plasma membrane, probably mediated to some extend by the N-terminal PH domain.[109, 269] Partial translocation from the cytosol to the plasma membrane was sometimes observed for KCP-1 as well. Since KCP-1 had a fixed fluorophore stoichiometry, a calculated FRET ratio was not affected by translocation. However, KCP-1 mutants were generated that were unable to bind to the plasma membrane and did not translocate. Lysines in the PH domain were mutated to asparagines that lack the phosphate interacting, ionic amino group.[246] It is reported that such mutants are still substrates for PKC.[269] These PH mutants were prepared from KCP-1/SAA, where T114 and S117 were replaced by alanines. KCP-1/SAA retained maximal FRET change after phosphorylation. The mutants KCP-1/SAA/K14N and KCP-1/SAA/K22N showed similar responses as KCP-1 and KCP-1/SAA, but showed no translocation after PKC activation.

Surprisingly, the mutation K13N in KCP-1/SAA/K13N impaired bradykinin and DiOG stimulated responses. Such behavior was not observed in experiments with respective KCP-2 derived mutants performed by J. Brumbaugh. A conclusive explanation for the effect of K13N cannot be found. One possible explanation is that the mutation K13N in KCP-1 disrupts interaction of the 18 amino acid linker and the PH domain. Then a flexible linker and attached fluorophore would have random orientation and large spatial freedom, which would not change dramatically with a structural change of the protein; a concomitant FRET change would be minor. However, KCP-1 constructs with impaired interaction of the 18 amino acid linker and

the PH domain exhibited signals similar to KCP-2.[270] Therefore, reduced contact between the 18 amino acid linker and PH domain in KCP-1/SAA/K13N cannot be the decisive reason for a diminished FRET response.

Another explanation for the effect of the mutation K13N may be that the interaction between PH and DEP domain was altered. Such an alteration could have secondary effects on the 18 amino acid linker.

It is interesting to note that the amino acid side chains of K14 and K22 are on the outside of the PH domain, but that of K13 is directed into the phospholipid-binding cavity. Whether such a difference can be associated with the distinct responses, can probably only be concluded from further structural insight into KCP-1 and related probes.

4.6.4 Phosphorylation loop

Wild type pleckstrin had three phosphate acceptor amino acids (S113, T114, and S117, short: STS), but PKC activation lead to partial phosphorylation only.[106] Mutation of one of these amino acids to glycine did not impair pleckstrin phosphorylation level or function; phosphorylation of the wild type pleckstrin is apparently redundant.[105] Similar behavior may be expected for the pleckstrin derived KCP-1 probe. Therefore, the three hydroxy amino acids of the phosphorylation loop in KCP-1 were partially mutated to find a probe with ideally only one phosphate acceptor amino acid left and maximal FRET change. Amino acids were mutated to alanines to simulate PKC insensitive amino acids and glutamates that simulated constitutively phosphorylated amino acids.[105] Glutamate was a well-suited equivalent for a phosphorylated amino acid: pleckstrin with STS mutated to glutamates was shown to be constitutively active and had similar cellular distribution as phosphorylated pleckstrin.[269] According to NMR experiments, the PH-DEP construct with three glutamates (EEE) instead of STS, had a similar structure as the phosphorylated wild type polypeptide.[215] *In vitro* experiments demonstrated that PH-DEP constructs with partially mutated STS remained substrates for PKCδ.[219] In living cells, single-site glycine mutants behaved as the wild type protein, while double-site mutants had a diminished effect.[105] Therefore, for the following discussion it may be assumed that a) glutamate was equivalent to a phosphorylated amino acid, and b) the mutants remained substrates for PKC.

A systematic screening of all mutants showed that the three phosphate

acceptor amino acids contributed to a varying extent in FRET changes. Maximal FRET changes were SAA >> ATA > AAS, SAA > SAE > SEA, and STS > ATS > ETS. From this data, the hierarchy of contribution to FRET change after phosphorylation in KCP-1 may is S113 >> T114 > S117. S113 was necessary and sufficient to invoke maximal FRET change after PKC activation with TPA. The signal of this probe, KCP-1/SAA, was comparable to that observed with KCP-1 and similar structural change can be concluded.

Interestingly, when S113 (in SAA) was substituted by threonine (TAA), FRET change was virtually abolished, although both constructs should be substrates for PKC, a Ser/Thr kinase. A similar result was found for ATA versus ASA. Such an effect might be explained by an impaired structural change, but the mutation T114S in KCP-1/SSS had only a minor impact on the FRET efficiency change (as compared to KCP-1/STS). However, more interesting is the possibility that these constructs, KCP-1/TAA and KCP-1/ASA, were worse substrates for PKC than KCP-1/SAA and KCP-1/ATA. If this were true, then both S113 and T114 would be phosphorylated by specific PKC isoforms, which would distinguish between the substrates serine and threonine. However, both mutants KCP-1/SAA and KCP-1/ATA were substrates for the same isozyme PKCδ *in vitro*, although this may not reflect behavior in live cells.

If the results obtained with KCP-1 mutants can be correlated to pleckstrin, then S113 may occupy a key role in the protein's activation or regulation. This contrasts the idea that in wild type pleckstrin S117 is the favored target for phosphorylation.[106] It was reported that phosphorylation of two amino acids is necessary to activate pleckstrin,[105] as reflected in the responses ATS >> ATA > AAS. When the three sites, STS, are substrates for specific PKC isozymes, then two distinct mechanisms could result in pleckstrin activation: a) phosphorylation of S113 suffices to invoke the maximal structural change or b) phosphorylation of T114 and S117 integrate two signals to activate pleckstrin. However, further experiments must be performed to test these possibilities.

It must be noted that not all mutants gave conclusive results. For example, it is not clear why KCP-1/STE showed no response, but KCP-1/SAE exhibited a medium TPA response; the additional phosphate acceptor, T114, should have a positive, but not a negative effect. The single constructs were tested with different cell batches and other intangible parameters may have differed. Although the assay system is

stable, differences between the constructs are not decisive. The spotting technique discussed below can be used to perform parallel experiments with the different constructs. This will generate data sets that can be compared more reliably.

4.6.5 New kinase sensitivities

Results from KCP-1/SAA demonstrated that phosphorylation of a single amino acid suffices for maximal FRET efficiency change. This led to experiments in which the wild type phosphorylation loop was exchanged for other sequences with altered kinase specificities. Substrates for various kinases related to PKC (PKA, PKB, and CaMKII) were selected. The sequences were designed to resemble known peptide substrates. However, most constructs did not show a FRET change after kinase activation.

A construct with the Kemptide sequence gained, although very little, sensitivity for PKA activation and reported TPA induced PKC activity. Single amino acids in this construct were consequently altered to produce probes with higher FRET changes. The best results were obtained when a glycine in the Kemptide sequence was mutated to leucin: the improvement may reflect glycine's tendency to disrupt a protein's secondary structure. The probe showed immediate FRET efficiency change in the cytosol and a delayed response in the nucleus. This result reflects the time required for PKA activation in the cytosol and translocation into the nucleus. Subsequent PKC activation augmented the FRET change in the cytosol, probably due to phosphorylation of S113. In KCP-1 this is an important PKC substrate amino acid and was not altered in the new PKA probe. It is interesting to note that alteration of S113 in Kemp3 to alanine or glutamate abolished the probes' responses to PKA and PKC activation.

Another approach to extend KCP-1's kinase selectivity was to insert a PKA phosphorylation sequence (Kemptide) between the 18 amino acid linker and the C-terminal fluorophore.[218] Such a probe responded to PKC and PKA with opposite FRET changes. When the PKC phosphorylation site STS was altered to AAA or EEE, then the probe lacked PKC sensitivity and responded only to PKA stimulation.[218]

Although, FRET reporters for PKA activity have already been published,[207, 209, 271] this probe is unique since it shows that KCP-1's sensitivity can be extended from PKC to PKA. It will be interesting to see if the system can be used for other kinases, or if it is restricted to PKA, a close relative of PKC.[67] Mutations in the

phosphorylation loop target only kinase specificity that is mediated via the kinase's catalytic core.[234] However, target selectivity of some kinases is guaranteed by an additional docking site.[235, 236] Docking sites bind at regions outside the phosphorylation sequence of substrate proteins. However, such interaction is not addressed by the introduced mutation system.

As demonstrated with the Kemptide sequence, a single mutation in the substrate sequence can differentiate between a functional and nonfunctional probe. Therefore, a screening system must be provided for an efficient probe development.

This was accomplished using microarrays with cells expressing defined cDNAs in conjunction with automated microscopy and image processing. Microarrays were generated by spotting of mixtures of DNA and transfection reagent on welled coverslips.[247] Such coverslips were seeded with cells, which in turn were transfected with the DNAs at a specific spot. Probes with low, medium, or high responses were distinguished using the screening system.

The capacity of these experiments is at least 60 constructs in triplicate without time-resolution, or 10 constructs in triplicate with time-resolution (1 measurement per minute and spot). Such an imaging system in combination with automated cloning will permit a medium to high throughput screening for new kinase activity reporters.

4.7 Drug screening possibilities

PKC is a key member of signaling pathways and PKC deregulation is associated with a multitude of diseases and in particular, cancer.[26] Activators or inhibitors for PKC may prove to be useful drugs.[250] Therefore, the possibility was explored whether KCP-1 can be used in a live cell drug-screening assay.

Cells stably expressing KCP-1 were seeded in 96-well plates and analyzed with automated microscope and image processing. Initial experiments demonstrated that a 10x objective offered appropriate brightness and field of view. Reproducibility and quality of the assay were tested by parallel imaging of wells with and without PKC activation. Data from TPA treated and untreated wells could clearly be distinguished on a scatter plot. A parameter, the Z-value,[223] provides a measure for the quality of a screening assay was determined to be 0.4. An assay with a value higher than 0.5 is assumed to be 'excellent'. A value of 0.5 was obtained when extreme data points were rejected. This method is not valid, but it showed that the introduced PKC assay could be used for drug screening. A small screen was

performed that included 16 random compounds and 4 control drugs. Although none of the compounds showed an effect, the control drugs behaved as expected and activating, inhibiting, and neutral compounds were distinguishable.

The stability and applicability of such an assay for high throughput screenings can be evaluated only after further experiments. Optimization of parameters, such as microscope settings, cell densities, or incubation time may further increase signal and therefore, reliability of the test. Compared to other methods, the major advantage of the proposed screening assay is the use of living cells and therefore, observation of PKC in its natural environment. Parallel read-out of a 96-well plate may even give time-resolved results from living cells. However, it is worth noting that KCP-1 probably reports activities of several PKC isozymes and can report integrated signals only. When the PKC isozyme specificity or preference of KCP-1 in living cells is resolved, a drug-screening assay employing KCP-1 may prove very valuable.

4.8 Multiparameter imaging

Insight into interplay between cellular pathways is difficult to gain when only a single parameter is monitored in live cells. Instead, simultaneous observation of concerted activities for several components can resolve a spatiotemporal mechanism of interdependent signals. Experiments must take into account cell heterogeneity and therefore, such multiplexing measurements can be performed only in single cells that simultaneously report several parameters. Spectral differentiation of fluorescent probes permits such multiparameter imaging experiments.[256]

PKC activation was chosen as a model system for multiparameter imaging. In these experiments, PKC activity was imaged using KCP-1 in conjuction with probes monitoring PKC activating signals, like calcium and DAG concentrations. An advantage of KCP-1 in multiparameter imaging was the use of GFP^2 as donor moiety, which permitted use of ECFP as an additional reporter fluorophore. In contrast, when CFP/YFP would be as FRET pair, GFP would be required to serve for other probes. However, GFP would substantially emit in the CFP/YFP-FRET probe's detection channels making signal separation impossible.

Initial experiments that monitored PKC and DAG concentration showed a delay between both signals when cells were stimulated with DAG. This demonstrated that PKC and/or DAG had to diffuse within the cytosol or the plasma membrane to associate. In contrast, cells that were stimulated with bradykinin or histamine

exhibited virtually immediate PKC activation. The KCP-1 signal paralleled DAG, but neither calcium nor PIP_2 levels. Bradykinin induced a sharp calcium spike[259-262] that reverted before maximal KCP-1 response. The difference between a short PIP_2 signal and longer sustained DAG levels demonstrated that PLC mediated PIP_2 hydrolysis was not the only DAG source. Instead, bradykinin also initiates long-lasting DAG production through other mechanisms like phosphatidylcholine metabolism.[36, 38, 40, 272] Similar data were obtained with triple parameter measurements that imaged PKC activity, calcium levels and either PIP_2 or DAG concentrations.

Taken together, these results suggest that KCP-1 primarily reflected activity of novel PKC isozymes, which require DAG, but not calcium as cofactor. The experiments demonstrated the value of multiparameter imaging by acquiring time-resolved data of parallel events from the same cell.

In addition to technical problems associated with live cell microscopy (especially focus shift or other hardware malfunction), the major problem with the experiments was insufficient spectral discrimination between different fluorophores. In particular, fura red and ECFP had very broad emission spectra and showed high fluorescence crosstalk in several detection channels. Often, such a crosstalk could not be corrected by calculation (linear unmixing). Best results were obtained from cells with low concentrations of these dyes and concomitantly reduced crosstalk. Nevertheless, the fluorescence had to be high enough to generate an appropriate signal to noise ratio. Unfortunately, a suitable stochiometry could usually be recognized only after experiments, during image processing and fluorescence unmixing. A prominent signal, like the calcium spike after bradykinin stimulation, helped to judge proper unmixing. Despite the fluorescence crosstalk, the fluorophores ECFP, KCP-1, mRFP, and fura red combined best-separated emission spectra and appropriate properties of the fluorophores (e.g. EBFP has low quantum yield and photostability).[133] However, it is desirable to have a CFP variant with a sharper emission spectrum and fewer fluorescence overlap with the GFP^2 and EYFP spectra.

Another source of error in data interpretation arises because the choice of the region of interest affects signals of probes based on translocation. In the case of DAG, a fluorescence signal obtained from an ROI over the plasma membrane lasted longer than a signal measured in the cytosol. The difference could be explained by fluorophore diffusion from the nucleus into the cytosol. The measurement of a signal

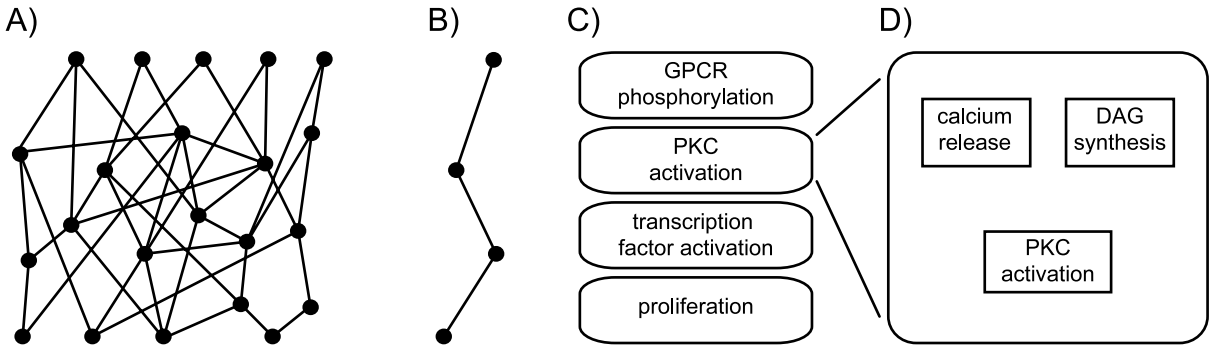

Figure 4.3: Schematic signaling network (A), which can be split into single signaling cascades (B). These in turn comprise successive modules (C). A module consists of several units (D).

derived from the plasma membrane can be difficult since the membrane is mobile and most often cannot be defined by a static ROI. Images of specific membrane stains could serve as reference, which could be applied computationally as membrane masks. This method permits automated measurement. This requires that the optical properties of such a stain interfere minimally with the fluorescence of dyes of other reporters.

In time, such multiparameter experiments will help to shed light on complex networks of signal transduction (Figure 4.3A).[273, 274] Such a network can be approached, when split into smaller, interacting components, like major signaling cascades (Figure 4.3B). The components themselves can be divided into successive modules, e.g. the activation of a specific kinase (Figure 4.3C). In a further step, the modules could be reduced to a sequence of units (Figure 4.3D), which then can be examined and understood with respect to their molecular and spatiotemporal mechanism. For example, one unit could be defined as release of a second messenger. It is important to note that module or unit boundaries are not strictly delineated, but can be arbitrarily defined and adjusted to the investigated problem. Furthermore, units and modules may be integrated in several parts of organization levels. For example, the unit “calcium release” would be a member of the modules “conventional PKC activity” and “CaMKII activity”. In turn, these modules are constituents of many signaling cascades.

A typical reference feature of one unit could be used as a hallmark for the unit’s activity. As for the definition of a unit, the selection of a reference feature depends on the demands of the performed experiment. The study of such signals would be best accomplished with fluorescent methods, since these permit multiplexed readout from live cell experiments. When all units of a module are

investigated, a typical marker for the module can be selected. This method identifies a defined signal for one component of a network. Finally, parallel observation of several such signals will give insight into the interdependence of various components of a signaling network in living cells.

However, in a primary step, the components that comprise a unit or module must be examined. Reporters like KCP-1 can help to investigate the role of protein kinase C in such efforts.

5 Outlook

KCP-1 provides a reliable tool to measure protein kinase C activity in living cells. However, several questions remain to be addressed. One of the most important questions is PKC isozyme specificity of KCP-1. Further, it will be intriguing if KCP-1 reports activity of PKCs that have low sequence homology to mammalian PKC isozymes. For example, can KCP-1 report activity of PKC in yeast, *Caenorhabditis elegans* or *Drosophila melanogaster*? Or, is KCP-1 restricted to certain PKC isozymes in mammals or vertebrates? Such questions must be clarified to identify the potential of KCP-1.

An isozyme profile of KCP-1 will help to define the probe for screening assays. As demonstrated, KCP-1 can potentially be used in live-cell screening applications for PKC activators or inhibitors. Such experiments are currently planned in cooperation with industrial partners. The use of professional platforms, like single cell based high throughput screening systems, will show whether KCP-1 suffices industrial standards. However, to meet industrial requirements, it may be necessary to enhance the signal of KCP-1. This may be achieved by using other FRET pairs, or by mutations in the probe like alterations to the linkers between the core structure and the fluorophores. A shortened version, KCP-2, may be a better candidate for such alterations because the mechanism of structural change appears simpler. Larger FRET changes may be obtained when the initial FRET efficiency of this probe is increased, for example by tandemly repeated acceptor fluorophores (larger quenching probability of the donor). Another possibility is increasing GFP's tendency to dimerize (closer distance between the FRET partners). An increased dimerization tendency will influence only the initial, high FRET efficacy, when both fluorophores are in close proximity. However, the effect will not contribute after KCP-2 phosphorylation upon separation of the fluorophores. Techniques and methods were developed that allow efficient investigation of KCP-1 and related probes. An automated cloning system will help to optimize the generation of new KCP-1 variants. The cloning system used to obtain KCP-1 linker mutants can probably be directly adopted.

A further application is use of KCP-1 as an analogue for wild type pleckstrin. Although phosphorylation of pleckstrin can be readily followed by radioactive tracing experiments, structural information is only gained *in vitro*. *In vivo* data may be obtained with KCP-1 and related constructs in the event that results can be correlated to pleckstrin. In time, this may help to elucidate the function of pleckstrin.

Finally, KCP-1 has applications in transgenic animals. Zebra fish and fruit flies (Figure 5.1) that express KCP-1 are currently under investigation. It is possible that the probe can help to understand PKC signalling in live animals.

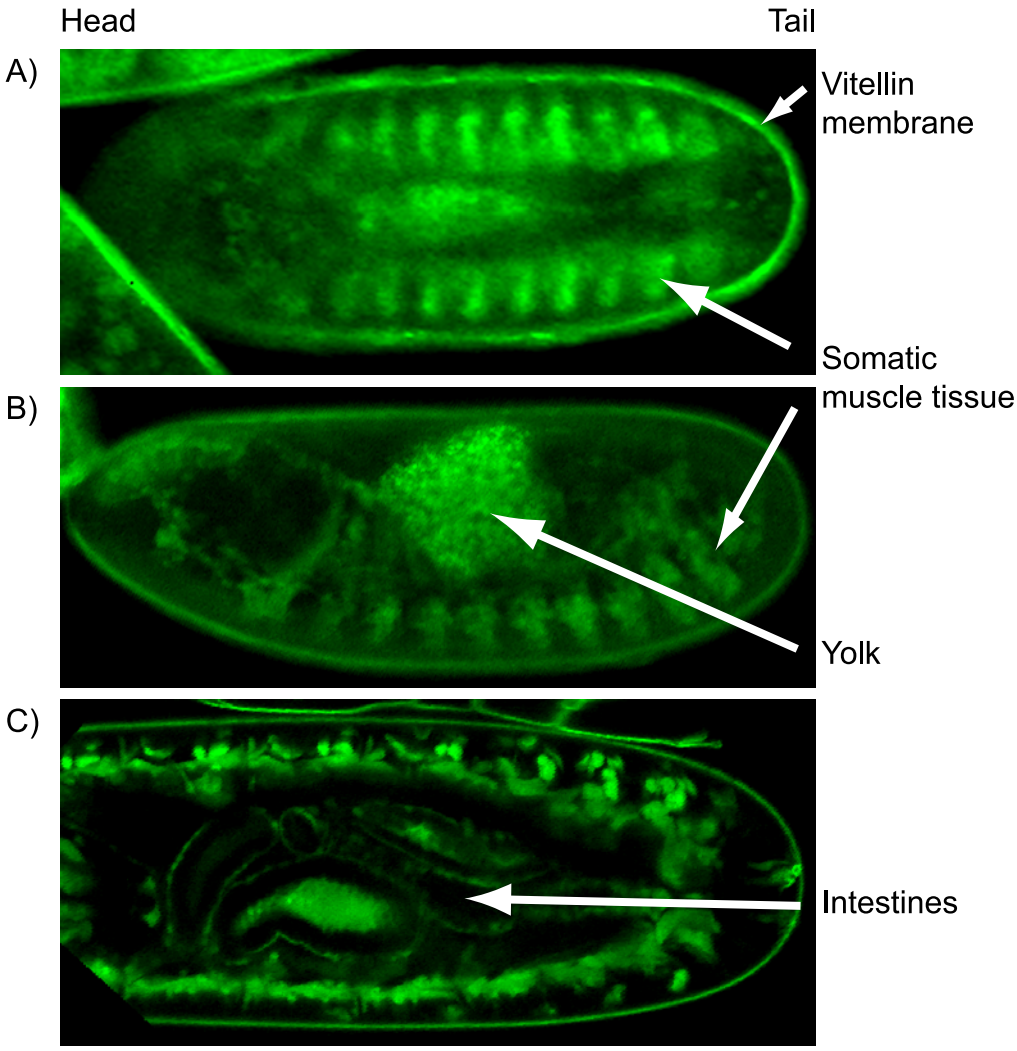

Figure 5.1: Dechorionated *Drosophila melanogaster* embryos that expressed KCP-1 in muscle tissue (generated by H. Gustafson). Ventral (A) and lateral (B) views show somatic muscle tissue. C) A dorsal view demonstrats that muscle tissue surrounded intestines. Vitellin membranes were autofluorescent. (Zeiss LSM Meta; A and B were recorded with an open pin-hole. Image C was acquired with a closed pin hole).

6 Experimental

6.1 Material and assets

Chemicals:

Agar-agar	Serva, Heidelberg, Germany
Ampicillin	Serva, Heidelberg, Germany
ATP	Sigma-Aldrich, Steinheim, Germany
$B(OH)_3$	Merck, Darmstadt, Germany
Bacto tryptone	Difco, Detroit, MI, USA
Bacto yeast extract	Difco, Detroit, MI, USA
Bradykinin	CalBioChem, Eggenheim, Germany
8-Br-cAMP/AM	Biolog GmbH, Bremen, Germany
BSA	New England Biolab, Ipswich, MA, USA
$CaCl_2$	Merck, Darmstadt, Germany
CaMKII	New England Biolab, Ipswich, MA, USA
CH_3CO_2H	Merck, Darmstadt, Germany
CO2-independent medium	Gibco, Eggenstein, Germany
Complete EDTA free Protease Inhibitor	Roche, Mannheim, Germany
Dulbecco modified Eagle's medium (DMEM)	Gibco, Eggenstein, Germany
Dimethylsulfoxid (DMSO)	Merck, Darmstadt, Germany
1,2-Dioctylglycerol (DiOG)	Fluka, Steinheim, Germany
DNA primers and oligos	MWG Biotech GmbH, Ebersberg, Germany
1,4-Dithiothreitol (DTT)	Fluka, Steinheim, Germany
Effectene	QIAgen GmbH, Hilden Germany
Ethidium bromide	Serva, Heidelberg, Germany
Ethylenedinitrilotetraacetatic acid (EDTA)	Sigma-Aldrich, Steinheim, Germany
Ethylene glycol-bis(2-aminoethylether)-N,N,N′,N′-tetraacetic acid (EGTA)	Sigma-Aldrich, Steinheim, Germany
Ethanol	Merck, Darmstadt, Germany
ExGene500	Fermentas, St. Leon-Roth, Germany
Fetal bovine serum (FBS)	Gibco, Eggenstein, Germany
Fetal calf serum (FCS)	Gibco, Eggenstein, Germany

Fibronectin	Sigma-Aldrich, Steinheim, Germany
Forskolin	Sigma-Aldrich, Steinheim, Germany
Fugene6	Roche, Mannheim, Germany
γ-^{32}P-ATP	Sigma-Aldrich, Steinheim, Germany
Gelatine	Merck, Darmstadt, Germany
Geneticin	Sigma-Aldrich, Steinheim, Germany
Glucose	Merck, Darmstadt, Germany
Glycerol	Merck, Darmstadt, Germany
Gö6976	CalBioChem, Eggenheim, Germany
Gö6983	CalBioChem, Eggenheim, Germany
HCl	Merck, Darmstadt, Germany
Histamine	Sigma-Aldrich, Steinheim, Germany
Histone H3	Sigma-Aldrich, Steinheim, Germany
4-(2-Hydroxyethyl)-1-piperazineethanesulfonic acid (Hepes)	Sigma-Aldrich, Steinheim, Germany
Ionomycin	CalBioChem, Eggenheim, Germany
K_2HPO_4	Merck, Darmstadt, Germany
Kanamycin	Serva, Heidelberg, Germany
KOAc	Merck, Darmstadt, Germany
Lipofectamine 2000	Invitrogen, Carlsbad, CA, USA
$MgCl_2$	Merck, Darmstadt, Germany
$MgSO_4$	Merck, Darmstadt, Germany
$MnCl_2$	Fluka, Steinheim, Germany
Morpholinepropanesulfonic acid (MOPS)	Sigma-Aldrich, Steinheim, Germany
NaCl	Merck, Darmstadt, Germany
NaOH	Merck, Darmstadt, Germany
Nucleotides (dNTP)	PEQlab, Erlangen, Germany
OptiMEM	Gibco, Eggenstein, Germany
pECFP	Clontech, Carlsbad, CA, USA
pEGFP	Clontech, Carlsbad, CA, USA
pEYFP	Clontech, Carlsbad, CA, USA

pGFP2	PerkinElmer Life And Analytical Sciences, Inc., Boston, MA, USA
PKA	New England Biolab, Ipswich, MA, USA
PKC isozymes	Panvera, Madison, WI, USA
PKM	CalBioChem, Eggenheim, Germany
2-Propanol	Merck, Darmstadt, Germany
Primocin	Invivogen, Toulouse, France
RbCl	Merck, Darmstadt, Germany
Restriction enzymes	New England Biolab, Ipswich, MA, USA
Shrimp alkaline phosphatase (SAP)	Fermentas, St. Leon-Roth, Germany
SiLib	SiChem, Bremen, Germany
Sucrose	Merck, Darmstadt, Germany
T4 kinase	Fermentas, St. Leon-Roth, Germany
T4 ligase	Fermentas, St. Leon-Roth, Germany
T4-polynucleotide kinase (PNK)	Fermentas, St. Leon-Roth, Germany
Taq polymerase	Roche, Mannheim, Germany
Thapsigargin	CalBioChem, Eggenheim, Germany
4β-12-O-Tetradecanoylphorbol 13-acetate (TPA)	Fluka, Steinheim, Germany
4α-TPA	CalBioChem, Eggenheim, Germany
Tris(hydroxymethyl)amino methane (Tris)	Merck, Darmstadt, Germany
Trypsin	Sigma-Aldrich, Steinheim, Germany
Trypton	Difco, Detroit, MI, USA
Zeocin	Invitrogen, Groningen, The Netherlands

Following materials and assets were used.

Bacteria (*E.coli*):

BL21(DE)	for protein expression
XL1blue	for DNA amplification

Cell lines:	
HeLa CCL-2 (human)	LGC Promochem GmbH, Wesel, Germany
MDCKII (canine)	LGC Promochem GmbH, Wesel, Germany
N1E-115 (murine)	LGC Promochem GmbH, Wesel, Germany
Centrifuge:	
Megafuge 1.0	Heraeus, Hanau, Germany
Microcentrifuge 5415C	Eppendorf, Hamburg, Germany
DNA purification kits:	
QIAquick Gel Extraction Kit	QIAgen GmbH, Hilden Germany
QIAprep Miniprep Kit	QIAgen GmbH, Hilden Germany
QIAfilter Plasmid Maxi Kit	QIAgen GmbH, Hilden Germany
DNA spotter:	
Virtek Chipwriter Compact	Eurogentec, Seraing, Belgium
Pins: PTS/PTLS 600	Point Technologies, Inc
PTS/PTLS 300	Point Technologies, Inc
Fluorimeter:	
Photon Technology International Quantamaster QM4/2000SE	PhotoMed GmbH, Seefeld, Germany
Gel chambers:	
40 ml and 80 ml chambers	EMBL mechanical workshop
Gel electrophoresis power supply:	
PowerPac Basic	BioRad Laboratories, München, Germany
Microscopes:	
Leica AOBS SP2	Leica Microsystems, Heidelberg, Germany
Zeiss LSM Meta	Carl Zeiss Mikroskopiesysteme, Jena, Germany
Visitron System:	
Zeiss Axiovert	Carl Zeiss Mikroskopiesysteme, Jena, Germany
CCD camera Coolsnap HQ	Photometrics, Roper Scientific, Inc., Trenton, NJ, USA
Filter wheel system	Visitron Systems GmbH, Puchheim, Germany
PCR machine:	
MJ Research Thermocycler PTC-200	Biozym Diagnostik GmbH, Oldendorf, Germany
Plastic ware:	

0.22 µM filter bottles	Millipore
0.3 ml thermotubes	PEQLab, Erlangen, Germany
1.5 ml micro tubes	Eppendorf, Hamburg, Germany
Cell culture flasks	Nunc, Wiesbaden, Germany
Cell dishes with glass bottom	MatTek, Ashland, MA, USA
Welled coverslides (LabTek)	Nunc, Wiesbaden, Germany
pH meter:	
Hannah Instruments pH213	Carl Roth GmbH, Karlsruhe, Germany
Pipettes:	
10 µl, 100 µl, 1ml pipettes	Eppendorf, Hamburg, Germany
Software:	
ImageJ (http://rsb.info.nih.gov/ij/)	W. Rasband, NIH, Bethesda, USA
Metamorph v6.2r4	Universal Imaging Corp., 2004
Origin v6.1	OriginLab Corporation, Northampton, MA, USA
Felix v1.41	PhotoMed GmbH, Seefeld, Germany
UV/Vis spectrometer:	
Ultraspec 2100 pro	Amersham Biosciences, Piscataway, NJ, USA
X-ray films:	
Kodak BioMax MS film	Sigma-Aldrich, Steinheim, Germany

The following vectors were kind gifts:

pmRFP-N2[143]	R. Y. Tsien, UCSD, San Diego, CA, USA
pcDNA3.1(EGFP-PLCδ1PH)[183]	K. Jalink, Amsterdam, The Netherlands
C1a-EGFP[275]	T. Meyer, Stanford, Paolo Alto, CA, USA
ECFP-C1a[256]	T. W. J. Gadella, Amsterdam, The Netherlands
C2-ECFP[256]	T. W. J. Gadella, Amsterdam, The Netherlands
CKAR[214]	A. Newton, UCSD, San Diego, CA, USA
pET9d-Pleckstrin(1-221)	M. Sattler, EMBL Heidelberg, Germany
pET9d-Pleckstrin(1-239)	M. Sattler, EMBL Heidelberg, Germany
pET9d-Pleckstrin(1-350)	M. Sattler, EMBL Heidelberg, Germany
Pleckstrin fragments containing K13N, K14N, K22N, SAA, SEE, AAS, EES, STA, STE, SAS, SES, ATS, and ETS	M. Sattler, EMBL Heidelberg, Germany

6.2 Cloning and cell culture

6.2.1 General procedures

General cloning procedures were performed according to standard protocols.[276]

Media

Agarose gels: Gels for DNA analysis were 1% (w/v) agarose in TBE.

Hepes: Live cell imaging was performed with Hepes buffer (pH 7.4) consisting of NaCl (115 mM), $CaCl_2$ (1.2 mM), $MgCl_2$ (1.2 mM), K_2HPO_4 (2.4 mM), and Hepes (20 mM).

LB: Autoclaved Luria-Bertani (LB) broth was obtained from EMBL's media kitchen. LB contained 1% (w/v) bacto tryptone, 0.5% (w/v) bacto yeast extract, and 170 mM NaCl. The buffer was adjusted to pH 7.6 with NaOH.

LB agarose plate: Agarose plates were obtained from EMBL's media kitchen. The plates were prepared with 1.5% (w/v) bacto agar in LB and antibiotics (50 µg/ml Ampicillin or 10 µg/ml Kanamycin).

SOC: SOC broth was obtained from EMBL's media kitchen. SOC medium contained 20 mM glucose, 10 mM $MgCl_2$, 10 mM $MgSO_4$, 2.5 mM KCl, 10 mM NaCl, 2% (w/v) tryptone, and 0.5% (w/v) yeast extract. SOC was adjusted to pH 7.0.

TBE: TBE buffer was used for DNA gels and electrophoresis contained 90 mM Tris base, 90 mM boric acid, and 2.5 mM EDTA.

Chemical competent bacteria for DNA transformation

Chemical competent bacteria were prepared according to standard procedures.[277]

RF1: 100 mM RbCl, 50 mM $MnCl_2$, 30 mM KOAc, 10 mM $CaCl_2$, 15% (w/v) glycerol; adjusted to pH 5.8 with 0.2 M acetic acid; RF2: 10 mM MOPS, 10 mM RbCl, 75 mM $CaCl_2$, 15% (w/v) glycerol; adjusted to pH 6.8 with NaOH.

Both buffers were sterilized by filtration through a 0.22 µm membrane and kept on ice.

A single bacteria colony was selected and grown overnight in 3 ml LB medium (containing no antibiotics) to give a starting culture. This was used to inoculate 1 l LB

broth. Bacteria were grown until the optical density of the suspension reached 0.3-0.4 at 550 nm. The broth was distributed into 50 ml tubes and kept on ice for 15 min. Then, bacteria were collected by centrifugation (1000g, 5 min, 4°C). The pellet was resuspended in 2 ml RF1. The content of 3 tubes was pooled, RF1 was added to 50 ml volume, and the mixture was incubated on ice for 10 min. Bacteria were pelleted by centrifugation (1000g, 5 min, 4°C), resuspended in 2 ml RF2 and the content of 4 tubes was pooled. RF2 was added to final 50 ml volume, and the mixture was kept on ice for 30 min. The suspension was distributed into 1ml plastic tubes, flash-frozen in liquid nitrogen and stored at -70°C.

Polymerase chain reaction (PCR)

PCR was performed in 0.3 ml PCR-tubes. The reaction mixture consisted of 1-3 units Taq polymerase, 10x buffer (100 mM Tris-HCl, 15 mM $MgCl_2$, 500 mM KCl, pH 8.3), 0.3-3 pmol 5'/3'-primer, 1-10 pmol dNTP, traces of template and water to 30 µl total reaction volume. The following cycle program was used for all PCR reactions: 94°C/5min, 4 cycles 94°C/20sec, 52°C/20sec, 72°C/1min, 21 cycles 94°C/20sec, 56°C/20sec, 72°C/1min, and finally 72°C/10min.

PCR products were analyzed and separated on 1% agarose gels.

DNA extraction from agarose gels

DNA was extracted from agarose gels with commercial kits (QIAquick Gel Extraction Kit) according to manufacturer's instructions.

Briefly, a gel slice containing DNA was excised from a gel, and dissolved in buffer ("QG") at 50°C. DNA was precipitated with 2-propanol 25% (v/v) final concentration. This solution was filtered through a membrane, which bound DNA. After washing with 70% ethanol, the DNA was eluted with 40 µl water.

Restriction

Restriction reactions were performed in 50 µl (<1µg DNA) or 100 µl (1-3 µg DNA) volume with 5 to 10 units of the used enzymes. Buffers were used according to manufacturer's instructions. Reactions proceeded for 2 hours. Shrimp alkaline phosphatase (SAP, 1 unit) was added for ½ hours when appropriate, particularly when the desired fragment was used as a vector backbone. Fragments were separated on 1% agarose gels and isolated. Separation distance was 3 cm to 6 cm.

Ligation

Ligation of DNA with T4 ligase was performed according to the manufacturer's instruction. Briefly, 1 µl (~0.1 µg) plasmid (treated with restriction enzymes and SAP), 1 µl T4 ligase (1 unit), 1 µl 10x buffer (400 mM Tris-HCl, 100 mM $MgCl_2$, 100 mM DTT, 5 mM ATP, pH 7.8) and 7 µl (~0.02 µg) restricted DNA was kept at room temperature for 30 to 60 minutes.

Transformation

Bacterial transformation was performed according to well described protocols.[277] Frozen competent *E.coli* were thawed on ice. 50 µl of the bacteria suspension was added to the ligase reaction or plasmids. After 30 to 60 minutes incubation on ice, the cells were heated for one minute to 42°C, cooled one minute on ice, and then diluted with 1 ml pre-warmed SOC medium. To improve bacterial recovery and growth, this solution was vigorously shaken at 37°C for one hour. Bacteria were then pelleted by centrifugation (2000g; 2 min) and streaked onto LB agarose plates with 50 µg/ml ampicillin, 25 µg/ml kanamycin, or 25 µg/ml zeocin.

After 12 to 16 hours at 37°C, samples of single colonies were selected and diluted in 50 µl water. 5 µl from these solutions were used for PCR reactions to screen for colonies carrying the desired construct. Bacteria from positive colonies were suspended in 3 ml LB medium containing antibiotic (100 µg/ml ampicillin, 50 µg/ml kanamycin, or 25 µg/ml zeocin), and were grown overnight at 37°C with vigorous shaking.

DNA preparation

Plasmids were isolated from bacteria with commercial preparation kits (QIAprep Miniprep Kit) according to manufacturer's instructions.

Briefly, cells were pelleted by brief centrifugation and the supernatant was removed. Then, cells were resuspended and lysed with alkaline buffer. The lysis was stopped by acidification after five minutes. This step precipitated proteins and prevented cleavage of DNA. The precipitate was separated by thorough centrifugation. The supernatant containing DNA was filter through a membrane which bound plasmids. After washing with 70% ethanol, the DNA was eluted with 40 µl water. The yield averaged 0.2-0.6 µg/µl DNA.

DNA sequencing

DNA sequencing was performed by EMBL's genomic core facility.

Antibiotic resistance genes of plasmids

Plasmids that derived from Clontech vectors (pEYFP-C1)[217] carried a gene for Kanamycin resistance. The vectors of the pET and pcDNA series had an Ampicillin resistance gene. PerkinElmers pGFP^2-C1 vector carried Zeocin resistance.

Cell culture and transfection

Propagation of cell lines was performed by Heike Stichnoth and Nicole Heath. HeLa CCL-2 and N1E-115 cells were cultured according to vendor's recommendations. Briefly, HeLa or N1E-115 cells were grown in DMEM at 37˚C in a humidified atmosphere with 5% CO_2. DMEM was supplemented with 10% FCS (for HeLa cells) or 10% FBS (for N1E-115 cells) and 0.1 mg/ml primocin. Cells were subcultured twice (HeLa) or three times (N1E-115) a week.

For microscope experiments, cells were plated in 35mm MatTek chambers. Cells were transfected overnight at 40-60% confluency with Fugene6 in OptiMEM according to manufacture's protocol.

Briefly, Fugene6 (3 µl) and DNA (0.2-1 µg) were incubated in 100 µl OptiMEM for 15 minutes. This reaction mixture was given onto cells, which were transfected overnight. For cotransfection of several plasmids, the total DNA concentration was kept constant, and amounts of single plasmids were scaled down.

6.2.2 FRET vector family

The prepared FRET vectors have a general design as shown in Figure 6.1

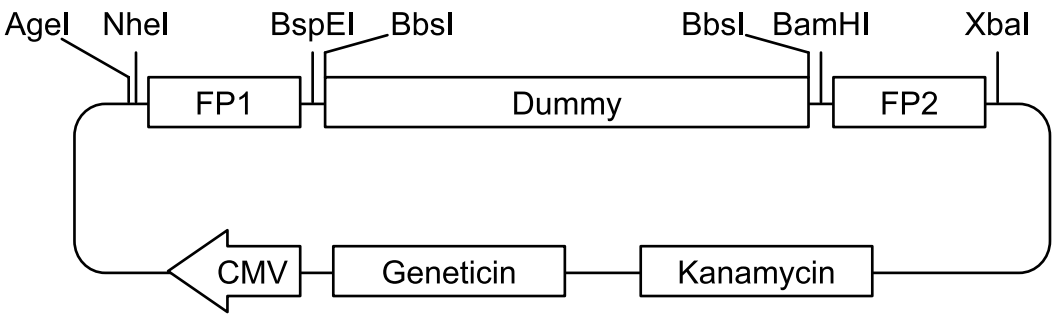

Figure 6.1: Schematic vector map of FRET vectors showing important restriction sites. The restriction enzyme BbsI completely excises the dummy sequence. The vector encodes a kanamycin resistance gene for selection of bacteria and a geneticin resistance gene for selection of eukaryotic cells. A cytomegalovirus promoter (CMV) guaranteed high expression of the FRET reporter in cells.

A dummy fragment was amplified from pleckstrin by PCR with 5'-BspEI and 3'-BamHI restriction sites (sense 5'-CCG TTC TCC GGA GCC ATG GAG TCT TCC CAA AGC GGA TCA GAG AGG GC-3'; reverse 5'-CGC AGT CAG ATC TTA GGA TCC GGT CTT CAA TGG CCT TAT TGA TAT CCC G-3'). The used primer encoded for two BbsI restriction sites, which, after cutting, produced 5'-NcoI and 3'- BamHI compatible overhangs on the vector and a 314 bp dummy fragment, which served as restriction control. Inserts were in frame with CCATGG encoding methionine (NcoI) and GGATCC encoding serine-glycine (BamHI).

Another PCR generated a fluorescent protein (FP) encoding DNA with 5'-BamHI and 3'-XbaI restriction sites from appropriate FP templates (sense 5'-CCG TTC GGA TCC ATG GTG AGC AAG GGC GAG GAG C-3'; reverse 5'-GCA GTT CTA GAT TAC TTG TAC AGC TCG TCC ATG CC-3'). Both DNA fragments were assembled into a BspEI and XbaI opened pEYFP-C1 vector. The fluorophore-encoding DNA sequences could be excised from the vector and exchanged to other moieties by using either AgeI/BspEI or BamHI/XbaI restriction for the 3'- or 5'-FP sequence, respectively. 3'-FP sequences either were obtained from commercial vectors (pEGFP-C1 series of Clontech) or were amplified by PCR (sense 5'-TGC AGC ACC GGT CGC CAC CAT GGT GAG CAA GGG CGA G-3; reverse 5'-GCT GAG TCC GGA CTT GTA CAG CTC GTC C-3'). It should be noted that AgeI and BspEI create priming overhangs. The following vectors were created via this method:

pYG	EYFP-dummy-GFP^2
pCiCF	Citrine-dummy-ECFP
pCiG2	Citrine-dummy-GFP^2
pCiRF	Citrine-dummy-mRFP

In contrast to EGFP, EYFP, ECFP, GFP^2, and Citrine, mRFP is not derived from wtGFP of *Aequorea victoria*, and therefore, its DNA sequence cannot be amplified with the above-mentioned primers. Furthermore, mRFP contained an internal BbsI restriction site, which interfered with the cloning technique described above. Therefore, silent mutations were introduced in mRFP to remove the BbsI site with the following procedure. Two fragments of mRFP were amplified by PCR from a pmRFP-N2 vector. This vector provided an XbaI restriction site after the mRFP stop codon. The primers for the N-terminal fragment (sense 5'-ATC CAC GGA TCC ATC GCC ACC ATG GCC TCC TCC GAG GAC-3'; reverse 5'-TAG CAG TGA AGA CGT TTT CTT CTG CAT TAC GGG-3') introduced 5'-BamHI and 3'-BbsI restriction sites.

Those for the C-terminal fragment (sense 5'-AAT CGT GAA GAC AAG AAA ACC ATG GGC TGG GAG GC-3'; reverse 5'-CAT TTT ATG TTT CAG GTT CAG GG-3') had a 5'-BbsI. The reverse primer annealed downstream from the XbaI restriction site. Restriction of the N- and C-terminal fragments with BamHI/BbsI and BbsI/XbaI, respectively, yielded two fragments with common overhangs created by the BbsI restriction. These overhangs were not BbsI binding sites, since this enzyme cuts outside of its recognition sequence. To obtain the general FRET vector (pCiRF) with Citrine and mRFP as FRET partners, a FRET vector with a 3'-Citrine sequence was opened BamHI/XbaI and ligated with the two mRFP fragments. Compared to other C-terminal fluorophores in the FRET vectors, pCiRF had an additional sequence (coding for the amino acids IAT) between the BamHI restriction site and the start codon of the fluorophore.

6.2.3 KCP-1, KCP-2 and other color variants

Bacterial expression vectors that carry the open reading frames for a 239 aa (amino acid) or 221 aa long N-terminal fragment of pleckstrin were a gift from G. Stier (fragments were amplified from a human cDNA preparation and cloned into a modified pET-9d vector [with C-His tag] via 5'-NcoI and 3'-BamHI restriction).

These fragments were excised with NcoI and BamHI restriction and ligated into BbsI opened FRET vectors (Figure 6.1). Using pYG and the 239 aa or 221 aa fragment resulted in the constructs KCP-1 or KCP-2, respectively. The sequence of KCP-1 (Figure 6.2) may be obtained from the EMBL Nucleotide Sequence Database or GenBank via the accession number AJ783754.

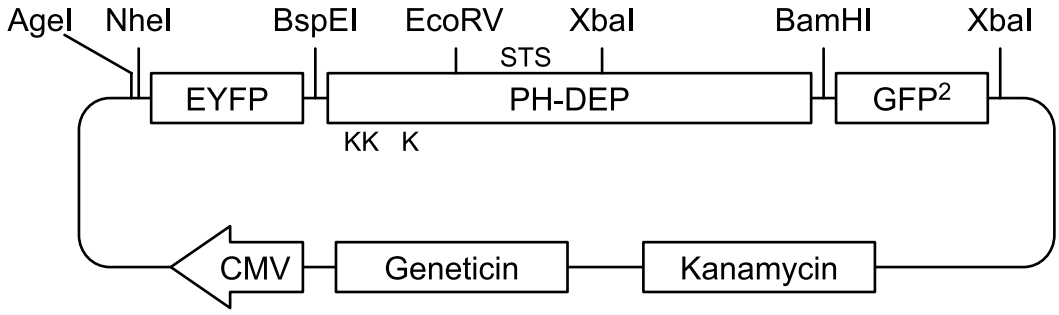

Figure 6.2: Restriction sites in the vector harboring the KCP-1 sequence.

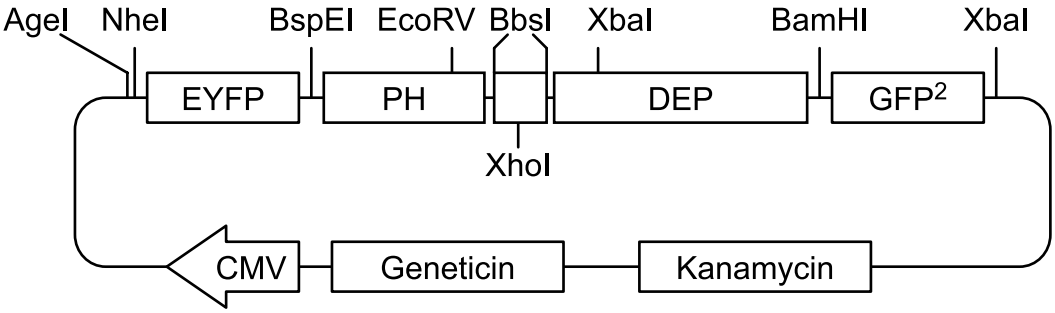

Figure 6.3: Schematic representation of the vector with UKP. The native phosphorylation site (between PH and DEP domain) was replaced with a dummy sequence. This was removed traceless and sequences of choice were inserted.

6.2.4 Mutations in the substrate loop

The substrate loop in the 239 aa pleckstrin fragment was exchanged to a dummy sequence with 5'- and 3'-BbsI restriction sites (Figure 6.3). These allowed for the excision of the dummy fragment and generated two unique overhangs, which were used for ligation with oligo dimers of choice.

pYG-UKP: The sequence was split into two parts for introduction of the dummy sequence. The 5'-DNA string that contained the PH domain was amplified from pleckstrin with primers introducing 5'-NcoI and 3'-XhoI sites. Adjacent to the XhoI-site was a BbsI site. The 3'-fragment was amplified using primers carrying a 5'-XhoI site followed by a BbsI site and having a 3'-BamHI site. These two fragments were ligated into an NcoI/BamHI opened pET-9d vector and were joined with the common XhoI site.

The sequence, termed "universal kinase probe" (UKP), was confirmed by DNA sequencing and then transferred into the FRET vector pYG. The resulting vector was called pYG-UKP (Figure 6.3).

New sequences: A mixture of sense and antisense oligos (each 5 µl of a 0,1 µM solution) was heated for oligo dimerization to 95°C for five minutes in a PCR thermocycler and slowly cooled to room temperature. The solution was diluted one to ten with water and the dimers were phosphorylated with T4-polynucleotide kinase (T4-PNK). ATP (1 µl, 0.2 mM), oligo dimer (1 µl of above's solution, 10 nM), 10x buffer (2 µl, 500 mM Tris-HCl, 100 mM $MgCl_2$, 50 mM DTT, 1 mM spermidine, 1 mM EDTA, pH 7.6), T4-PNK (1 µl, 10 units) and water (15 µl) was mixed, incubated for 40 minutes at 37°C, and then 20 minutes at 60°C to inactivate T4-PNK. A dilution of the mixture 1:25 with water (480 µl) gave best results for subsequent ligation and transformation. Other tested dilutions were 1:1000, 1:300, 1:100, 1:10, 1:3, 1:1.

This solution was used for ligation with BbsI opened UKP vectors. Oligos, vector, 10x buffer and T4 ligase (1 µl each) were mixed in water (6 µl) and incubated at room temperature for 40 minutes. The mixture was used for bacterial transformation.

A synopsis of used primers is given below.

Primers used in mutating S113, T114, and S117:

KCP-1/STS: RKSTRRSIRL
Sense 5'-TGCCAGGAAATCTACCAGGAGGTCCATTCGACTG-3′
Reverse 5′-CTGGCAGTCGAATGGACCTCCTGGTAGATTTCCT-3′
KCP-1/ATA: RKATRRAIRL
Sense 5'-TGCCAGGAAAGCCACCAGGAGGGCCATTCGACTG-3′
Reverse 5′-CTGGCAGTCGAATGGCCCTCCTGGTGGCTTTCCT-3′
KCP-1/ETE: RKETRREIRL
Sense 5'-TGCCAGGAAAGAGACCAGGAGGGAGATTCGACTG-3′
Reverse 5′-CTGGCAGTCGAATCTCCCTCCTGGTCTCTTTCCT-3′
KCP-1/ETA: RKETRRAIRL
Sense 5'-TGCCAGGAAAGAGACCAGGAGGGCCATTCGACTG-3′
Reverse 5′-CTGGCAGTCGAATGGCCCTCCTGGTCTCTTTCCT-3′
KCP-1/ATE: RKATRREIRL
Sense 5'-TGCCAGGAAAGCCACCAGGAGGGAGATTCGACTG-3′
Reverse 5′-CTGGCAGTCGAATCTCCCTCCTGGTGGCTTTCCT-3′
KCP-1/SAE: RKSARREIRL
Sense 5'-TGCCAGGAAATCTGCCAGGAGGGAGATTCGACTG-3′
Reverse 5′-CTGGCAGTCGAATCTCCCTCCTGGCAGATTTCCT-3′
KCP-1/SEA: RKSERRAIRL
Sense 5'-TGCCAGGAAATCTGAGAGGAGGGCCATTCGACTG-3′
Reverse 5′-CTGGCAGTCGAATGGCCCTCCTCTCAGATTTCCT-3′
KCP-1/AES: RKAERRSIRL
Sense 5'-TGCCAGGAAAGCCGAGAGGAGGAGCATTCGACTG-3′
Reverse 5′-CTGGCAGTCGAATGCTCCTCCTCTCGGCTTTCCT-3′
KCP-1/EAS: RKSERRAIRL
Sense 5'-TGCCAGGAAAGAGGCCAGGAGGAGCATTCGACTG-3′
Reverse 5′-CTGGCAGTCGAATGCTCCTCCTGGCCTCTTTCCT-3′
KCP-1/TAA: RKTARRAIRL
Sense 5'-TGCCAGGAAAACCGCCAGGAGGGCCATTCGACTG-3′
Reverse 5′-CTGGCAGTCGAATGGCCCTCCTGGCGGTTTTCCT-3′
KCP-1/ASA: RKASRRAIRL
Sense 5'-TGCCAGGAAAGCCAGCAGGAGGGCCATTCGACTG-3′
Reverse 5′-CTGGCAGTCGAATGGCCCTCCTGCTGGCTTTCCT-3′
KCP-1/SSS: RKSSRRSIRL
Sense 5'-TGCCAGGAAATCTAGCAGGAGGTCTATTCGACTG-3′
Reverse 5′-CTGGCAGTCGAATAGACCTCCTGCTAGATTTCCT-3′
KCP-1/TTT: RKTTRRTIRL
Sense 5'-TGCCAGGAAAACCACAAGGAGGACCATTCGACTG-3′
Reverse 5′-CTGGCAGTCGAATGGTCCTCCTTGTGGTTTTCCT-3′

Other pleckstrin fragments (aa 1-239) with mutations in S113, T114, and S117 were gifts from A. Gasch and were inserted into BbsI opened pYG vector. These fragments resulted in the constructs KCP-1/SAA, SEE, AAS, EES, STA, STE, SAS, SES, ATS, and ETS. The following DNA-oligos were used to generate probes with altered kinase sensitivities:

Autocamptide2: LRRQETVDAL
Sense 5'-TGCCCTGCGGCGCCAGGAGACCGTGGACGCCCTG-3′
Reverse 5'-CTGGCAGGGCGTCCACGGTCTCCTGGCGCCGCAG-3′
Crosstide: RPRTSSFAEL
Sense 5′-TGCCCGCCCACGGACGTCTAGCTTCGCCGAGCTG-3′
Reverse 5′-CTGGCAGCTCGGCGAAGCTAGACGTCCGTGGGCG-3′
Cross1: RARTSSRIRL
Sense 5′-TGCCCGCGCTAGAACGAGCTCTCGCATCAGACTG-3′
Reverse 5′-CTGGCAGTCTGATGCGAGAGCTCGTTCTAGCGCG-3′
Kemptide: RKSLRRASLG
Sense 5′-TGCCAGGAAATCTTTGCGCAGAGCTAGCCTGGGC-3′
Reverse 5′-CTGGGCCCAGGCTAGCTCTGCGCAAAGATTTCCT-3′
2xKemptide: RRASLRRASL
Sense 5'-TGCCCGCCGTGCAAGCTTGCGCAGAGCCAGCCTG-3′
Reverse 5′-CTGGCAGGCTGGCTCTGCGCAAGCTTGCACGGCG-3′
PKA1: RRRRSRRASL
Sense 5'-TGCCCGCAGGCGTAGAAGCCGCAGAGCCAGCCTG-3′
Reverse 5′-CTGGCAGGCTGGCTCTGCGGCTTCTACGCCTGCG-3′
PKAPKC: KRSTRRSVRL
Sense 5'-TGCCAAGCGCAGCACCCGCAGAAGCGTGCGCCTG-3′
Reverse 5′-CTGGCAGGCGCACGCTTCTGCGGGTGCTGCGCTT-3′
ACh: RRSSSRRIRL
Sense 5'-TGCCCGCAGAAGCTCTTCCCGCAGAATCCGCCTG-3′
Reverse 5′-CTGGCAGGCGGATTCTGCGGGAAGAGCTTCTGCG-3′
H2B: RKRSSRRIRL
Sense 5'-TGCCCGCAAGCGCTCTTCCCGCAGAATCCGCCTG-3′
Reverse 5′-CTGGCAGGCGGATTCTGCGGGAAGAGCGCTTGCG-3′
Kemp1: RKSLRRASRL
Sense 5'-TGCCCGCAAGAGCCTGCGCAGAGCCAGCCGCCTG-3′
Reverse 5′-CTGGCAGGCGGCTGGCTCTGCGCAGGCTCTTGCG-3′
Kemp2: RKSLRRAIRL
Sense 5'-TGCCCGCAAGAGCCTGCGCAGAGCCATCCGCCTG-3′
Reverse 5′-CTGGCAGGCGGATGGCTCTGCGCAGGCTCTTGCG-3′
Kemp3: RKSLRRASLL
Sense 5'-TGCCCGCAAGAGCCTGCGCAGAGCCAGCCTCCTG-3′
Reverse 5′-CTGGCAGGAGGCTGGCTCTGCGCAGGCTCTTGCG-3′
Kemp4: RKSLRRASFL
Sense 5'-TGCCCGCAAGAGCCTGCGCAGAGCCAGCTTCCTG-3′
Reverse 5′-CTGGCAGGAAGCTGGCTCTGCGCAGGCTCTTGCG-3′
Kemp5: RKSLRRASFF
Sense 5'-TGCCCGCAAGAGCCTGCGCAGAGCCAGCTTCTTT-3′
Reverse 5′-CTGGAAAGAAGCTGGCTCTGCGCAGGCTCTTGCG-3′

```
Kemp6:        RKSLRRASLF
     Sense    5'-TGCCCGCAAGAGCCTGCGCAGAGCCAGCCTGTTC-3′
     Reverse  5′-CTGGGAACAGGCTGGCTCTGCGCAGGCTCTTGCG-3′
Kemp7:        RKSLRRLSFF
     Sense    5'-TGCCCGCAAGAGCCTGCGCAGACTGAGCTTCTTT-3′
     Reverse  5′-CTGGAAAGAAGCTCAGTCTGCGCAGGCTCTTGCG-3′
Kemp8:        RKSLRRALFL
     Sense    5'-TGCCCGCAAGAGCCTGCGCAGAGCCCTGTTCCTG-3′
     Reverse  5′-CTGGCAGGAACAGGGCTCTGCGCAGGCTCTTGCG-3′
Kemp9:        RKALRRASLL
     Sense    5'-TGCCCGCAAGGCCCTGCGCAGAGCCAGCCTCCTG-3′
     Reverse  5′-CAGGAGGCTGGCTCTGCGCAGGGCCTTGCGGGCA-3′
Kemp10:       RKELRRASLL
     Sense    5'-TGCCCGCAAGGAGCTGCGCAGAGCCAGCCTCCTG-3′
     Reverse  5′-CAGGAGGCTGGCTCTGCGCAGCTCCTTGCGGGCA-3′
Kemp11:       RKSLRRAALL
     Sense    5'-TGCCCGCAAGAGCCTGCGCAGAGCCGCTCTCCTG-3′
     Reverse  5′-CAGGAGAGCGGCTCTGCGCAGGCTCTTGCGGGCA-3′
Kemp12:       RKALRRAALL
     Sense    5'-TGCCCGCAAGGCCCTGCGCAGAGCCGCTCTCCTG-3′
     Reverse  5′-CAGGAGAGCGGCTCTGCGCAGGGCCTTGCGGGCA-3′
```

6.2.5 Mutations in the PH domain

pET9d plasmids carrying full length pleckstrin mutants (K13N, K14N, or K22N) were gifts from G. Stier. The sequence had 5'-NcoI and 3'-BamHI restriction sites.

The fragments were digested with NcoI/BamHI and ligated into BbsI opened pYG vector. After amplification, the vector was cut with EcoRV/BamHI, excising the. 3'-part of the (N-terminal) PH domain and the rest of pleckstrin (see Figure 6.2). An EcoRV/BamHI fragment from KCP-1/SAA was inserted into these vectors, resulting in the double mutant vectors KCP-1/SAA/K13N, KCP-1/SAA/K14N, and KCP-1/SAA/K22N, in which both the PH domain and phosphorylation site were altered.

6.2.6 Recombinant KCP-1

Recombinant KCP-1 protein was engineered and produced by G. Stier. Briefly, cloned restriction fragments of EYFP and GFP² cassettes were co-ligated in frame with the NcoI/BamHI PH-DEP fragment in a pET-9d N-His vector. Positive clones were transformed in *E.coli* BL21(DE3) and protein was expressed at 25°C by 16 hrs induction. Cells were lysed by ultrasonication. Protein was purified on a Ni-chelate column under batch conditions following a standard protocol.[276] The imidazole eluate was buffer-exchanged on a gelfiltration column. The resulting protein solution was used for further experiments.

6.2.7 Generation of HeLa cell lines stably expressing KCP-1

HeLa cells were transfected over night with KCP-1 in 3 cm cell culture dishes. Then the transfection medium was exchanged to complete medium with 0.5 mg/ml geneticin (selective marker for KCP-1). Geneticin was added in the medium for the following steps. The cells were cultured for one week after which half a dish was seeded into a 20 cm cell culture dish. Cells were grown to patches of 2-5 mm diameter. Approximately 30 fluorescent cell colonies, putatively KCP-1 positive, were picked under a fluorescence microscope and separated into a 96-well plate. The cells were grown for 3 weeks at which time dense, fluorescent cultures were transferred into 3 cm dishes. When the cells reached 80% confluency, they were cultured in 40 cm^2 flasks. Part of each culture was seeded into Mattek chambers and tested for KCP-1 activity. This procedure gave two HeLa cell lines that were KCP-1 positive. The cell lines were propagated with 0.5 mg/ml geneticin in the medium.

6.2.8 Other fluorescent reporters and plasmids

pmRFP-C1: mRFP[143] was amplified by PCR (sense 5'-GCG CTA CCG GTC GCC ACC ATG GCC TCC TCC GAG-3'; reverse 5'-TAC GTA TCC GGA CTT GTA CAG GGC GCC-3') from pmRFP-N2. The fragment was digested with AgeI and BspEI and was ligated into a pEYFP-C1 vector opened with the same restriction enzymes.

PLCδ1PH-mRFP: PLCδ1PH was amplified by PCR (sense 5'-GCT GCA GCT AGC CGC CAC CAT GGA CTC GGG CCG GG-3'; reverse 5'-TGC AGC ACC GGT CCG CTG ATG TTG AGC TCC TTC AGG-3'), restricted with NheI/AgeI and ligated into pmRFP-C1 that was treated with the same enzymes. This procedure gave a plasmid encoding the PH domain upstream from mRFP. Since the 3' multiple cloning site in pmRFP-C1 was not removed, the protein construct PLCδ1PH-mRFP contained an additional downstream amino acid sequence (TDI KLD ITS HNE DYT IVE QYE RAE GRH STG ALY KSG LRS RAQ ASN SAV DGT AGP GST GSR). This construct was not functional in living cells.

mRFP-PLCδ1PH: mRFP was amplified from pmRFP-N2 by PCR (sense 5'-ATC CAC GGA TCC ATC GCC ACC ATG GCC TCC TCC GAG GAC-3'; reverse 5'-ATC GTA GGA TTC GGC TTG TAC AGG GCG CCG-3'). The fragment and pcDNA3.1(EGFP-PLCδ1PH)[183] were treated with BamHI/EcoRI and ligated.

C1a-mRFP: The C1a domain PKCγ was excised with NheI/AgeI from pC1a-EGFP[275] and was ligated into pmRFP-C1.

pEGFP-Pleckstrin: A strategy similar to that used for pYG was chosen for the cloning of pEGFP-Pleckstrin. In a first step, PCR amplified (sense 5'-CCG TTC TCC GGA GCC ATG GAG TCT TCC CAA AGC GGA TCA GAG AGG GC-3'; reverse 5'-GCG AGT CAG ATC TTA GGA TCC GGT CTT CAA TGG CCT TAT TGA TAT CCC G-3') dummy sequence was introduced into the commercial vector pEGFP-C1 which was opened with BspEI and BglII. BbsI excised the complete dummy sequence and generated 5'-NcoI and 3'-BamHI compatible overhangs, into which a pleckstrin sequence was ligated. The pleckstrin sequence was obtained after NcoI/BamHI digest of the vector pET9d-Pleckstrin(1-350).

6.3 DNA spotting

A mixture of 0.4M sucrose in OptiMEM (4µl) and Lipofectamine 2000 (3µl) was incubated for 15 minutes at room temperature. Then DNA (0.3-0.7 µg in 1.5 µl H_2O) was added. After additional 15 minutes incubation, 7 µl of an aqueous solution containing 0.2% (w/v) gelatine and 0.001% (w/v) fibronectin were added. This mixture was spotted onto welled glass slides (LabTek chambers) with 600 µm diameter-pin. A suspension of HeLa cells in OptiMEM was applied, so that attached cells were 60-80% confluent. The arrays could be used for microscopy after cell attachment, overnight transfection, and exchange of the medium to Hepes buffer.

The following conditions were varied:

Transfection reagent: Fugene6 and ExGene500 did not transfect cells. Effectene gave poorer results than Lipofectamine 2000.

Gelatine: 0.2% gelatine gave better results than 0.08%.

DNA: Best results were obtained with 0.5-1.0 µg DNA. 0.05 µg DNA did not transfect cells. DNA from Minipreps gave better results than DNA from one Maxiprep.

Pin size: Spotting with a thick pin gave higher transfection efficiencies than a small pin.

Incubation: Preincubation of Lipofectamine 2000 without DNA for 15 minutes was important.

6.4 In vitro experiments

6.4.1 Fluorimeter

KCP-1 (1µg) in 50 µl buffer was used in *in vitro* experiments. The reactions were followed on a fluorimeter using 10 µl cuvettes. Excitation wavelength was 405 nm. Emission spectra (490-540 nm; 1 nm step size; 1 sec integration time) were recorded every 90 seconds. The construct was digested after complete reaction by adding 2 µl of trypsin (0.5 % in PBS). Ratios were calculated from the average fluorescence values of 490-510 nm and 520-540 nm. The different kinases required the following buffers:

PKM: pH 7.4; 20 mM Hepes, 10 mM $MgSO_4$, 0.1 mM EGTA, 1 mM DTT, 0.2 µg/µl BSA, 200 µM ATP (when appropriate) and protease inhibitor cocktail ("Complete EDTA free"); 20 ng PKM.

PKA: Manufacturer's buffer contained 50 mM Tris, 10 mM $MgCl_2$ and was adjusted to pH 7.5. BSA (0.2 µg/µl), ATP (200 µM), DTT (1 mM), and protease inhibitor cocktail was added; 500 ng PKA.

CaMKII: Manufacturer's buffer contained 50 mM Tris, 10 mM $MgCl_2$, 2mM DTT, 0.1 mM EGTA.. BSA (0.2 µg/µl), ATP (200 µM), DTT (1 mM), and protease inhibitors cocktail was added; CaMKII was pre-activated according to manufacturer's recommendations in buffer with $CaCl_2$, calmoduline and ATP; 100 ng CaMKII.

6.4.2 In vitro phosphorylation of KCP-1 with PKC isoforms and other kinases

Phosphorylation reactions with radioactive compounds were performed by A. Gasch according to PKC isozyme manufacturer's instructions at 30°C.

Briefly, KCP-1 was mixed with reaction buffer, kinase and lipid vesicles (for PKC isozymes). The reaction was started by adding ATP and γ-^{32}P-ATP. Samples were taken after 10 min and 30 min. The reactions were stopped by heat-inactivation of the kinase (65°C; 10 min). For each experiment histone H3 phosphorylation control and KCP-1 phosphorylation were performed. Kinases included PKCδ, PKCε, PKCη, PKCθ, PKCζ, CaMKII and the catalytic subunits of PKA and PKC (PKM).

Reaction products were separated by sodium dodecylsulfate polyacrylamide gel electrophoresis (SDS-PAGE) and visualized on X-ray films.

6.5 Microscopy

6.5.1 General

Cell medium was exchanged to Hepes buffer or CO_2-independent medium two hours before the experiments. Cells were stored at 37°C. Most cell experiments were performed at room temperature (above 25°C). For temperature equilibration, cell dishes were removed from the incubation 10 minutes prior mounting onto the microscope.

Drugs were prepared as 1000x stock solutions. Compounds were dissolved in DMSO or water according to manufacturer's recommendations. Prior to addition, stock solutions were diluted in 100 µl imaging medium. This solution was administered during a time series, between frames.

6.5.2 Confocal microscopy

Confocal images were recorded on Leica SP2 and Zeiss LSM Meta confocal microscopes equipped with 64x oil objectives. These microscopes were used for single and multiple probe imaging. For both microscopes, the detection ranges for emitted fluorescence could be selected freely. The detection ranges for GFP^2 and EYFP imaging were set to 490 nm to 510 nm and 520 nm to 540 nm, respectively. ECFP was imaged between 450 nm and 480 nm, mRFP between 560 nm and 630 nm, and fura red between 630 nm and 750 nm.

KCP-1, ECFP, and fura red were excited with a 405 nm diode laser. mRFP fluorescence was excited with a green He/Ne laser line (543 nm).

Image fields with several transfected, equally bright cells were selected for imaging. Cells with very high or very low fluorescence yielded no meaningful results and were rejected. Laser and PMT powers were adjusted for every experiment. PMT powers for the GFP^2 and EYFP detection channels were set to the same value; offsets of the PMTs were set to "0". This allowed for simple linear unmixing with constant parameters. Bleed through for GFP^2 and EYFP into EYFP and GFP^2 detection channels were determined to be 0.8 and 0.15, respectively. Images were acquired with four lines averaging. Usually, frames were recorded every 15 seconds.

6.5.3 Wide field microscopy

Wide field microscopy was performed on a Zeiss Axiovert microscope equipped with a xenon lamp, automatic stage, and fast emission and excitation filter wheels. Images were recorded with a charge coupled device (CCD) camera and the system was controlled by Metamorph software. KCP-1 was excited through a DAPI filter (405/20), excitation and emission light were separated by a 425dclp beam splitter, and fluorescence was detected after 500/20 and 535/30 (or 560/40) filters for GFP^2 and EYFP, respectively.

The excitation light was dimmed with a 90% neutral gray filter to minimize photobleaching of the fluorophores. Camera sensitivity was increase by 4X4 binning. Exposure times were adjusted for each experiment, but were generally set between 200 and 500 ms.

6.5.4 DNA arrays and 96 well plates

The Metamorph software's "multiparameter" and "plate reader" applets were used to automate imaging. The implemented autofocus routine did not provide satisfactory results and was not employed.

When, cell dishes were mounted on the microscope, it was crucial that the optical axis was perpendicular to the bottom of the dish to avoid manual focusing for single imaging sites.

The imaging sites of DNA arrays were set manually while the positions of 96 well plates were predefined in the software. GFP^2 and EYFP images were recorded, then cells were incubated with either 200 nM TPA or 10µM drugs for ten minutes and a second image set was acquired. In case of drug treatment for a compound screen an additional round of TPA treatment and image acquisition followed.

Drugs included:

a1: DMSO, a2: Chloramphenicol, a4: H13, a6: Sertindol; a8: G14-4,

b1: 4α-TPA, b2: ADI264, b4: Levomepromazin, b6: Serotonin*HCl, b8: ADI118,

c1: TPA, c2: Miconazole nitrate, c4:Methoxsalen, c6: PB229, c8G67,

d1: Gö6983, d2: G-MAZ-217, d4: Doxepin, d6: A10, d8: Pimozide.

6.6 Image processing

6.6.1 KCP-1 and its variants

Two image stacks representing the donor and acceptor channels were loaded into ImageJ. Regions of interest (ROI) were drawn and stored with the "Multi Measure" plugin. The option "Multi" provided a table with each column representing the time course for one ROI. The tables for donor and acceptor channels were copied into Origin spread sheets. A macro (see Appendix) was used to subtract background (as defined in the first ROI), and to calculat ratios of acceptor to donor fluorescence ($\text{Ratio} = \frac{\text{EYFP} - \text{a} \times \text{GFP}^2}{\text{GFP}^2 - \text{b} \times \text{EYFP}}$, where the variables a and b are the bleed through coefficients of the two fluorophores for linear unmixing). Linear unmixing was applied only for the FRET pair GFP^2/EYFP with images recorded on a Leica SP2 system. The coefficients were $a = 0.8$ and $b = 0.15$.

The resulting ratios could be automatically normalized to the average of the baseline values (prior to addition of drugs).

6.6.2 DNA arrays and 96 well plates

Image stacks for GFP^2 and EYFP emission were loaded into ImageJ. Every slice represented one imaged site. Both stacks were median-filtered to level extreme pixel values. A background image, calculated as median image, was subtracted from the corresponding stack. In one stack, the slice with the highest pixel value was chosen and a threshold was set to select cells and some single pixel background noise. With ImageJ's "Analyze Particles" routine, a stack representing cell-masks for each slice was created. Background noise was rejected by setting a minimum area for the masks (typically 50 to 80 pixels). The pixel values in the mask stack were set to "1" and "Not a Number" ("NaN") for foreground and background pixels, respectively. Ratio images were calculated by dividing the "EYFP" through the "GFP^2" stack. The resulting ratio-image stack was multiplied with the mask stack, resulting in a stack, in which only pixels representing cells had real values and background pixels were null ("NaN"). The whole image was selected as a ROI and median values for each slide were calculated by using the "Plot Z-stack" command. Pixels having "NaN" as value did not contribute to calculated medians.

When this procedure was performed for images from cells before and after

drug treatment, two ratio values were obtained for each imaged site. These two values defined a point in a scatter plot. Images that represented cells, which had a positive or negative ratio change, corresponded in points in the upper left or lower right area of the diagram, respectively. No ratio change was represented in points along a straight line in the middle of the diagram.

To simplify the data analysis in the diagram, the coordinate system of the scatter plot could be rotated. For rotation, Cartesian x/y-coordinates were transferred to polar coordinates [$r = \sqrt{x^2 + y^2}$, θ = atan(x/y)] and an angle (ω) was subtracted from the angular coordinate. Retransformation yielded Cartesian coordinates [$x' = r \cdot \cos(\theta-\omega)$, $y' = r \cdot \sin(\theta-\omega) + c$], in a rotated coordinate system.

An arbitrary number c was added to the new y-values. This number was chosen so that spots indicating positive, no, or negative FRET changes were located above, on, or below the abscissa.

7 References

[1] F. A. Lipmann, P. A. Levene, *J. Biol. Chem.* **1932**, *98*, 109-114.
[2] L. N. Johnson, M. OReilly, *Curr. Opin. Struct. Biol.* **1996**, *6*, 762-769.
[3] F. H. Westheimer, *Science* **1987**, *235*, 1173-1178.
[4] S. Stabel, P. J. Parker, *Pharmacol. Ther.* **1991**, *51*, 71-95.
[5] A. C. Newton, *J. Biol. Chem.* **1995**, *270*, 28495-28498.
[6] S. Jaken, *Curr. Opin. Cell Biol.* **1996**, *8*, 168-173.
[7] H. Mellor, P. J. Parker, *Biochem. J.* **1998**, *332*, 281-292.
[8] A. C. Newton, *Chem. Rev.* **2001**, *101*, 2353-2364.
[9] A. C. Newton, *Protein Kinase C Protocols, Vol. 233*, Humana Press Inc., Totowa, New Jersey, **2003**.
[10] Y. Takai, A. Kishimoto, M. Inoue, Y. Nishizuka, *J. Biol. Chem.* **1977**, *252*, 7603-7609.
[11] M. Inoue, A. Kishimoto, Y. Takai, Y. Nishizuka, *J. Biol. Chem.* **1977**, *252*, 7610-7616.
[12] A. Kishimoto, Y. Takai, Y. Nishizuka, *J. Biol. Chem.* **1977**, *252*, 7449-7452.
[13] Y. Nishizuka, *J. Biochem. (Tokyo).* **2003**, *133*, 155-158.
[14] A. Toker, *Front. Biosci.* **1998**, *3*, D1134-D1147.
[15] C. Ventura, M. Maioli, *Crit. Rev. Eukaryot. Gene Expr.* **2001**, *11*, 243-267.
[16] E. Livneh, D. D. Fishman, *Eur. J. Biochem.* **1997**, *248*, 1-9.
[17] J. D. Black, *Front. Biosci.* **2000**, *5*, 406-423.
[18] C. Keenan, D. Kelleher, *Cell. Signal.* **1998**, *10*, 225-232.
[19] S. L. Tan, P. J. Parker, *Biochem. J.* **2003**, *376*, 545-552.
[20] A. Pascale, S. Govoni, F. Battaini, *Mol. Neurobiol.* **1998**, *16*, 49-62.
[21] I. Gutcher, P. R. Webb, N. G. Anderson, *Cell. Mol. Life Sci.* **2003**, *60*, 1061-1070.
[22] A. P. Fields, W. C. Gustafson, in *Protein Kinase C Protocols, Vol. 233* (Ed.: A. C. Newton), Humana Press Inc., Totowa, New Jersey, **2003**, pp. 519-537.
[23] I. Idris, S. Gray, R. Donnelly, *Diabetologia* **2001**, *44*, 659-673.
[24] C. D. Stubbs, S. J. Slater, *Alcohol. Clin. Exp. Res.* **1999**, *23*, 1552-1560.
[25] F. Battaini, *Pharmacol. Res.* **2001**, *44*, 353-361.
[26] I. B. Weinstein, *Environ. Health Perspect.* **1991**, *93*, 175-179.
[27] P. G. Goekjian, M. R. Jirousek, *Expert Opin Inv Drug* **2001**, *10*, 2117-2140.
[28] C. A. O'Brian, N. E. Ward, J. R. Stewart, F. Chu, *Cancer Metastasis Rev.* **2001**, *20*, 95-100.
[29] H. C. Swannie, S. B. Kaye, *Curr. Oncol. Rep.* **2002**, *4*, 37-46.
[30] P. S. Lorenzo, P. A. Dennis, *Drug Resist. Updat.* **2003**, *6*, 329-339.
[31] H. J. Mackay, C. J. Twelves, *Endocr. Relat. Cancer* **2003**, *10*, 389-396.
[32] C. A. Carter, C. J. M. Kane, *Curr. Med. Chem.* **2004**, *11*, 2883-2902.
[33] J. Hofmann, *Curr. Cancer Drug Targets* **2004**, *4*, 125-146.
[34] J. Koivunen, V. Aaltonen, J. Peltonen, *Cancer Lett.* **2005**, *17*, 17.
[35] Y. Nishizuka, *Science* **1984**, *225*, 1365-1370.
[36] Y. Asaoka, S. Nakamura, K. Yoshida, Y. Nishizuka, *Trends Biochem. Sci.* **1992**, *17*, 414-417.
[37] Y. Asaoka, K. Yoshida, M. Oka, T. Shinomura, K. Koide, K. Ogita, U. Kikkawa, Y. Nishizuka, *J. Nutr. Sci. Vitaminol. (Tokyo).* **1992**, *Spec*, 7-12.
[38] Y. Nishizuka, *Neurosci. Res.* **1992**, *15*, 3-5.
[39] E. Oancea, T. Meyer, *Cell* **1998**, *95*, 307-318.
[40] Y. Nishizuka, *Science* **1992**, *258*, 607-614.
[41] J. H. Exton, *J. Biol. Chem.* **1990**, *265*, 1-4.
[42] Y. Nishizuka, *FASEB J.* **1995**, *9*, 484-496.

[43] S. A. Sproull, S. C. Morash, D. M. Byers, F. B. S. Palmer, H. W. Cook, *Neurochem. Res.* **1995**, *20*, 1397-1407.
[44] M. N. Hodgkin, T. R. Pettitt, A. Martin, R. H. Michell, A. J. Pemberton, M. J. O. Wakelam, *Trends Biochem. Sci.* **1998**, *23*, 200-204.
[45] M. Castagna, Y. Takai, K. Kaibuchi, K. Sano, U. Kikkawa, Y. Nishizuka, *J. Biol. Chem.* **1982**, *257*, 7847-7851.
[46] P. M. Blumberg, *Cancer Res.* **1988**, *48*, 1-8.
[47] S. P. Davies, H. Reddy, M. Caivano, P. Cohen, *Biochem. J.* **2000**, *351*, 95-105.
[48] P. J. Parker, S. J. Parkinson, *Biochem. Soc. Trans.* **2001**, *29*, 860-863.
[49] M. Gschwendt, S. Dieterich, J. Rennecke, W. Kittstein, H. J. Mueller, F. J. Johannes, *FEBS Lett.* **1996**, *392*, 77-80.
[50] L. Stempka, A. Girod, H. J. Muller, G. Rincke, F. Marks, M. Gschwendt, D. Bossemeyer, *J. Biol. Chem.* **1997**, *272*, 6805-6811.
[51] L. Coussens, P. J. Parker, L. Rhee, T. L. Yangfeng, E. Chen, M. D. Waterfield, U. Francke, A. Ullrich, *Science* **1986**, *233*, 859-866.
[52] Y. Ono, T. Kurokawa, T. Fujii, K. Kawahara, K. Igarashi, U. Kikkawa, K. Ogita, Y. Nishizuka, *FEBS Lett.* **1986**, *206*, 347-352.
[53] J. E. Johnson, J. Giorgione, A. C. Newton, *Biochemistry* **2000**, *39*, 11360-11369.
[54] J. J. Sando, in *Protein Kinase C Protocols, Vol. 233* (Ed.: A. C. Newton), Humana Press Inc., Totowa, New Jersey, **2003**, pp. 45-62.
[55] U. Hommel, M. Zurini, M. Luyten, *Nat. Struct. Biol.* **1994**, *1*, 383-387.
[56] G. G. Zhang, M. G. Kazanietz, P. M. Blumberg, J. H. Hurley, *Cell* **1995**, *81*, 917-924.
[57] J. H. Hurley, A. C. Newton, P. J. Parker, P. M. Blumberg, Y. Nishizuka, *Protein Sci.* **1997**, *6*, 477-480.
[58] J. Hritz, J. Ulicny, A. Laaksonen, D. Jancura, P. Miskovsky, *J. Med. Chem.* **2004**, *47*, 6547-6555.
[59] R. B. Sutton, B. A. Davletov, A. M. Berghuis, T. C. Sudhof, S. R. Sprang, *Cell* **1995**, *80*, 929-938.
[60] R. B. Sutton, S. R. Sprang, *Structure* **1998**, *6*, 1395-1405.
[61] N. Verdaguer, S. Corbalan-Garcia, W. F. Ochoa, I. Fita, J. C. Gomez-Fernandez, *EMBO J.* **1999**, *18*, 6329-6338.
[62] E. A. Nalefski, A. C. Newton, *Biochemistry* **2001**, *40*, 13216-13229.
[63] W. F. Ochoa, J. Garcia-Garcia, I. Fita, S. Corbalan-Garcia, N. Verdaguer, J. C. Gomez-Fernandez, *J. Mol. Biol.* **2001**, *311*, 837-849.
[64] C. H. Benes, N. Wu, A. E. H. Elia, T. Dharia, L. C. Cantley, S. P. Soltoff, *Cell* **2005**, *121*, 271-280.
[65] C. House, B. E. Kemp, *Science* **1987**, *238*, 1726-1728.
[66] J. W. Orr, L. M. Keranen, A. C. Newton, *J. Biol. Chem.* **1992**, *267*, 15263-15266.
[67] J. W. Orr, A. C. Newton, *J. Biol. Chem.* **1994**, *269*, 8383-8387.
[68] L. M. Keranen, E. M. Dutil, A. C. Newton, *Curr. Biol.* **1995**, *5*, 1394-1403.
[69] S. E. Tsutakawa, K. F. Medzihradszky, A. J. Flint, A. L. Burlingame, D. E. Koshland, *J. Biol. Chem.* **1995**, *270*, 26807-26812.
[70] R. Czerwinski, A. Aulabaugh, R. M. Greco, S. Olland, K. Malakian, S. Wolfrom, L. Lin, R. Kriz, M. Stahl, Y. Huang, L. Liu, D. Chaudhary, *Biochemistry* **2005**, *44*, 9563 -9573.

[71] M. M. Chou, W. M. Hou, J. Johnson, L. K. Graham, M. H. Lee, C. S. Chen, A. C. Newton, B. S. Schaffhausen, A. Toker, *Curr. Biol.* **1998**, *8*, 1069-1077.
[72] E. M. Dutil, A. Toker, A. C. Newton, *Curr. Biol.* **1998**, *8*, 1366-1375.
[73] J. A. Le Good, W. H. Ziegler, D. B. Parekh, D. R. Alessi, P. Cohen, P. J. Parker, *Science* **1998**, *281*, 2042-2045.
[74] A. Toker, A. C. Newton, *Cell* **2000**, *103*, 185-188.
[75] F. Bornancin, P. J. Parker, *Curr. Biol.* **1996**, *6*, 1114-1123.
[76] A. S. Edwards, M. C. Faux, J. D. Scott, A. C. Newton, *J. Biol. Chem.* **1999**, *274*, 6461-6468.
[77] M. B. Yaffe, K. Rittinger, S. Volinia, P. R. Caron, A. Aitken, H. Leffers, S. J. Gamblin, S. J. Smerdon, L. C. Cantley, *Cell* **1997**, *91*, 961-971.
[78] A. S. Edwards, A. C. Newton, *J. Biol. Chem.* **1997**, *272*, 18382-18390.
[79] S. Gysin, R. Imber, *Eur. J. Biochem.* **1997**, *249*, 156-160.
[80] W. H. Ziegler, D. B. Parekh, J. A. Le Good, R. D. H. Whelan, J. J. Kelly, M. Frech, B. A. Hemmings, P. J. Parker, *Curr. Biol.* **1999**, *9*, 522-529.
[81] R. M. Biondi, P. C. F. Cheung, A. Casamayor, M. Deak, R. A. Currie, D. R. Alessi, *EMBO J.* **2000**, *19*, 979-988.
[82] D. Mochly-Rosen, *Science* **1995**, *268*, 247-251.
[83] D. Mochly-Rosen, H. Khaner, J. Lopez, *Proc. Natl. Acad. Sci. U. S. A.* **1991**, *88*, 3997-4000.
[84] D. Mochly-Rosen, H. Khaner, J. Lopez, B. L. Smith, *J. Biol. Chem.* **1991**, *266*, 14866-14868.
[85] C. Chapline, J. Cottom, H. Tobin, J. Hulmes, J. Crabb, S. Jaken, *J. Biol. Chem.* **1998**, *273*, 19482-19489.
[86] D. Ron, J. H. Luo, D. Mochly-Rosen, *J. Biol. Chem.* **1995**, *270*, 24180-24187.
[87] D. Schechtman, D. Mochly-Rosen, *Methods Enzymol.* **2002**, *345*, 470-489.
[88] J. J. Sando, J. K. Beals, in *Protein Kinase C Protocols, Vol. 233* (Ed.: A. C. Newton), Humana Press Inc., Totowa, New Jersey, **2003**, pp. 63-76.
[89] N. E. Lewin, P. M. Blumberg, in *Protein Kinase C Protocols, Vol. 233* (Ed.: A. C. Newton), Humana Press Inc., Totowa, New Jersey, **2003**, pp. 129-156.
[90] D. Ron, M. G. Kazanietz, *FASEB J.* **1999**, *13*, 1658-1676.
[91] M. G. Kazanietz, *Mol. Pharmacol.* **2002**, *61*, 759-767.
[92] C. F. Yang, M. G. Kazanietz, *Trends Pharmacol. Sci.* **2003**, *24*, 602-608.
[93] J. J. Sando, J. K. Beals, I. M. Hussaini, in *Protein Kinase C Protocols, Vol. 233* (Ed.: A. C. Newton), Humana Press Inc., Totowa, New Jersey, **2003**, pp. 77-85.
[94] T. Ng, A. Squire, G. Hansra, F. Bornancin, C. Prevostel, A. Hanby, W. Harris, D. Barnes, S. Schmidt, H. Mellor, P. I. H. Bastiaens, P. J. Parker, *Science* **1999**, *283*, 2085-2089.
[95] N. Saito, in *Protein Kinase C Protocols, Vol. 233* (Ed.: A. C. Newton), Humana Press Inc., Totowa, New Jersey, **2003**, pp. 93-104.
[96] M. Tyers, R. A. Rachubinski, M. I. Stewart, A. M. Varrichio, R. G. L. Shorr, R. J. Haslam, C. B. Harley, *Nature* **1988**, *333*, 470-473.
[97] R. J. Haslam, J. A. Lynham, *Biochem. Biophys. Res. Commun.* **1977**, *77*, 714-722.
[98] T. Imaoka, J. A. Lynham, R. J. Haslam, *J. Biol. Chem.* **1983**, *258*, 1404-1414.
[99] M. Tyers, R. J. Haslam, R. A. Rachubinski, C. B. Harley, *J. Cell. Biochem.* **1989**, *40*, 133-145.
[100] R. J. Haslam, J. A. Lynham, J. E. B. Fox, *Biochem. J.* **1979**, *178*, 397-406.
[101] R. M. Lyons, N. Stanford, P. W. Majerus, *J. Clin. Invest.* **1975**, *56*, 924-936.

[102] R. J. Haslam, H. B. Koide, B. A. Hemmings, *Nature* **1993**, *363*, 309-310.
[103] M. A. Lemmon, K. M. Ferguson, *Biochem. J.* **2000**, *350*, 1-18.
[104] C. P. Ponting, P. Bork, *Trends Biochem. Sci.* **1996**, *21*, 245-246.
[105] C. S. Abrams, W. Zhao, E. Belmonte, L. F. Brass, *J. Biol. Chem.* **1995**, *270*, 23317-23321.
[106] K. L. Craig, C. B. Harley, *Biochem. J.* **1996**, *314*, 937-942.
[107] J. H. Brumell, K. L. Craig, D. Ferguson, M. Tyers, S. Grinstein, *J. Immunol.* **1997**, *158*, 4862-4871.
[108] K. Sano, Y. Takai, J. Yamanishi, Y. Nishizuka, *J. Biol. Chem.* **1983**, *258*, 2010-2013.
[109] D. C. Sloan, P. Wang, X. K. Bao, R. J. Haslam, *Biochem. Biophys. Res. Commun.* **2002**, *293*, 640-646.
[110] V. Auethavekiat, C. S. Abrams, P. W. Majerus, *J. Biol. Chem.* **1997**, *272*, 1786-1790.
[111] A. Al-Aoukaty, B. Rolstad, A. A. Maghazachi, *J. Immunol.* **1999**, *162*, 3249-3255.
[112] M. H. Hu, E. M. Bauman, R. L. Roll, N. Yeilding, C. S. Abrams, *J. Biol. Chem.* **1999**, *274*, 21515-21518.
[113] T. Inazu, A. Kuroiwa, Y. Matsuda, K. Miyamoto, *Mol. Biol. Rep.* **2005**, *32*, 35-40.
[114] T. Inazu, K. Yamada, K. Miyamoto, *Biochem. Biophys. Res. Commun.* **1999**, *265*, 87-93.
[115] R. Y. Tsien, *Annu. Rev. Biochem.* **1998**, *67*, 509-544.
[116] M. Zimmer, *Chem. Rev.* **2002**, *102*, 759-781.
[117] F. H. Johnson, O. Shimomura, Y. Saiga, L. C. Gershman, G. T. Reynolds, J. R. Waters, *J. Cell Comp. Physiol.* **1962**, *60*, 85-103.
[118] O. Shimomura, F. H. Johnson, Y. Saiga, *J Cell Comp. Physiol.* **1962**, *59*, 223-239.
[119] O. Shimomura, *J. Microsc.* **2005**, *217*, 3-15.
[120] M. Chalfie, Y. Tu, G. Euskirchen, W. W. Ward, D. C. Prasher, *Science* **1994**, *263*, 802-805.
[121] J. A. Schmid, H. Neumeier, *ChemBioChem* **2005**, *6*, 1149-1156.
[122] A. Miyawaki, *Dev. Cell* **2003**, *4*, 295-305.
[123] O. Griesbeck, *Curr. Opin. Neurobiol.* **2004**, *14*, 636-641.
[124] C. W. Cody, D. C. Prasher, W. M. Westler, F. G. Prendergast, W. W. Ward, *Biochemistry* **1993**, *32*, 1212-1218.
[125] R. Heim, D. C. Prasher, R. Y. Tsien, *Proc. Natl. Acad. Sci. U. S. A.* **1994**, *91*, 12501-12504.
[126] A. B. Cubitt, R. Heim, S. R. Adams, A. E. Boyd, L. A. Gross, R. Y. Tsien, *Trends Biochem. Sci.* **1995**, *20*, 448-455.
[127] B. G. Reid, G. C. Flynn, *Biochemistry* **1997**, *36*, 6786-6791.
[128] M. Ormö, A. B. Cubitt, K. Kallio, L. A. Gross, R. Y. Tsien, S. J. Remington, *Science* **1996**, *273*, 1392-1395.
[129] F. Yang, L. G. Moss, G. N. Phillips, *Nat. Biotechnol.* **1996**, *14*, 1246-1251.
[130] S. H. Bokman, W. W. Ward, *Biochem. Biophys. Res. Commun.* **1981**, *101*, 1372-1380.
[131] W. W. Ward, S. H. Bokman, *Biochemistry* **1982**, *21*, 4535-4540.
[132] G. S. Baird, D. A. Zacharias, R. Y. Tsien, *Proc. Natl. Acad. Sci. U. S. A.* **1999**, *96*, 11241-11246.

[133] T. T. Yang, P. Sinai, G. Green, P. A. Kitts, Y. T. Chen, L. Lybarger, R. Chervenak, G. H. Patterson, D. W. Piston, S. R. Kain, *J. Biol. Chem.* **1998**, *273*, 8212-8216.
[134] N. G. Gurskaya, A. F. Fradkov, A. Terskikh, M. V. Matz, Y. A. Labas, V. I. Martynov, Y. G. Yanushevich, K. A. Lukyanov, S. A. Lukyanov, *FEBS Lett.* **2001**, *507*, 16-20.
[135] N. G. Gurskaya, A. F. Fradkov, N. I. Pounkova, D. B. Staroverov, M. E. Bulina, Y. G. Yanushevich, Y. A. Labas, S. Lukyanov, K. A. Lukyanov, *Biochem. J.* **2003**, *373*, 403-408.
[136] V. I. Martynov, B. I. Maksimov, N. Y. Martynova, A. A. Pakhomov, N. G. Gurskaya, S. A. Lukyanov, *J. Biol. Chem.* **2003**, *278*, 46288-46292.
[137] N. C. Shaner, R. E. Campbell, P. A. Steinbach, B. N. G. Giepmans, A. E. Palmer, R. Y. Tsien, *Nat. Biotechnol.* **2004**, *22*, 1567-1572.
[138] M. A. Rizzo, G. H. Springer, B. Granada, D. W. Piston, *Nat. Biotechnol.* **2004**, *22*, 445-449.
[139] V. V. Verkhusha, K. A. Lukyanov, *Nat. Biotechnol.* **2004**, *22*, 289-296.
[140] L. Wang, W. C. Jackson, P. A. Steinbach, R. Y. Tsien, *Proc. Natl. Acad. Sci. U. S. A.* **2004**, *101*, 16745-16749.
[141] A. Miyawaki, T. Nagai, H. Mizuno, *Adv. Biochem. Eng. Biotechnol.* **2005**, *95*, 1-15.
[142] S. J. Remington, R. M. Wachter, D. K. Yarbrough, B. Branchaud, D. C. Anderson, K. Kallio, K. A. Lukyanov, *Biochemistry* **2005**, *44*, 202-212.
[143] R. E. Campbell, O. Tour, A. E. Palmer, P. A. Steinbach, G. S. Baird, D. A. Zacharias, R. Y. Tsien, *Proc. Natl. Acad. Sci. U. S. A.* **2002**, *99*, 7877-7882.
[144] M. Kozak, *Nucleic Acids Res.* **1987**, *15*, 8125-8148.
[145] R. Heim, A. B. Cubitt, R. Y. Tsien, *Nature* **1995**, *373*, 663-664.
[146] B. P. Cormack, R. H. Valdivia, S. Falkow, *Gene* **1996**, *173*, 33-38.
[147] G. J. Palm, A. Zdanov, G. A. Gaitanaris, R. Stauber, G. N. Pavlakis, A. Wlodawer, *Nat. Struct. Biol.* **1997**, *4*, 361-365.
[148] A. A. Heikal, S. T. Hess, G. S. Baird, R. Y. Tsien, W. W. Webb, *Proc. Natl. Acad. Sci. U. S. A.* **2000**, *97*, 11996-12001.
[149] O. Griesbeck, G. S. Baird, R. E. Campbell, D. A. Zacharias, R. Y. Tsien, *J. Biol. Chem.* **2001**, *276*, 29188-29194.
[150] D. A. Zacharias, J. D. Violin, A. C. Newton, R. Y. Tsien, *Science* **2002**, *296*, 913-916.
[151] D. M. Chudakov, V. V. Verkhusha, D. B. Staroverov, E. A. Souslova, S. Lukyanov, K. A. Lukyanov, *Nat. Biotechnol.* **2004**, *22*, 1435-1439.
[152] V. V. Verkhusha, A. Sorkin, *Chem. Biol.* **2005**, *12*, 279-285.
[153] G. H. Patterson, J. Lippincott-Schwartz, *Science* **2002**, *297*, 1873-1877.
[154] R. Ando, H. Mizuno, A. Miyawaki, *Science* **2004**, *306*, 1370-1373.
[155] R. Ando, H. Hama, M. Yamamoto-Hino, H. Mizuno, A. Miyawaki, *Proc. Natl. Acad. Sci. U. S. A.* **2002**, *99*, 12651-12656.
[156] D. M. Chudakov, V. V. Belousov, A. G. Zaraisky, V. V. Novoselov, D. B. Staroverov, D. B. Zorov, S. Lukyanov, K. A. Lukyanov, *Nat. Biotechnol.* **2003**, *21*, 191-194.
[157] K. Lukyanov, unpublished results.
[158] T. Förster, *Ann. Phys.* **1948**, *2*, 55-75.
[159] E. A. Jares-Erijman, T. M. Jovin, *Nat. Biotechnol.* **2003**, *21*, 1387 - 1395.
[160] F. D. Lewis, L. Zhang, X. Zuo, *J. Am. Chem. Soc.* **2005**, *127*, 10002-10003.

[161] F. S. Wouters, P. J. Verveer, P. I. H. Bastiaens, *Trends Cell Biol.* **2001**, *11*, 203-211.
[162] J. Zhang, R. E. Campbell, A. Y. Ting, R. Y. Tsien, *Nat. Rev. Mol. Cell Biol.* **2002**, *3*, 906-918.
[163] R. Y. Tsien, *Annu. Rev. Neurosci.* **1989**, *12*, 227-253.
[164] G. Grynkiewicz, M. Poenie, R. Y. Tsien, *J. Biol. Chem.* **1985**, *260*, 3440-3450.
[165] M. D. Shults, B. Imperiali, *J. Am. Chem. Soc.* **2003**, *125*, 14248-14249.
[166] M. D. Shults, K. A. Janes, D. A. Lauffenburger, B. Imperiali, *Nat. Methods* **2005**, *2*, 277-283.
[167] J. Llopis, J. M. McCaffery, A. Miyawaki, M. G. Farquhar, R. Y. Tsien, *Proc. Natl. Acad. Sci. U. S. A.* **1998**, *95*, 6803-6808.
[168] G. Miesenbock, D. A. De Angelis, J. E. Rothman, *Nature* **1998**, *394*, 192-195.
[169] T. B. Dansen, K. W. A. Wirtz, R. J. A. Wanders, E. H. W. Pap, *Nat. Cell Biol.* **2000**, *2*, 51-53.
[170] S. Jayaraman, P. Haggie, R. M. Wachter, S. J. Remington, A. S. Verkman, *J. Biol. Chem.* **2000**, *275*, 6047-6050.
[171] N. Doi, H. Yanagawa, *FEBS Lett.* **1999**, *453*, 305-307.
[172] J. Nakai, M. Ohkura, K. Imoto, *Nat. Biotechnol.* **2001**, *19*, 137-141.
[173] Y. Kawai, M. Sato, Y. Umezawa, *Anal. Chem.* **2004**, *76*, 6144-6149.
[174] T. Meyer, E. Oancea, in *Methods Enzymol., Vol. 327*, **2000**, pp. 500-513.
[175] M. N. Teruel, T. Meyer, *Cell* **2000**, *103*, 181-184.
[176] J. H. Hurley, T. Meyer, *Curr. Opin. Cell Biol.* **2001**, *13*, 146-152.
[177] G. Halet, *Biol. Cell* **2005**, *97*, 501-518.
[178] T. P. Stauffer, S. Ahn, T. Meyer, *Curr. Biol.* **1998**, *8*, 343-346.
[179] K. Hirose, S. Kadowaki, M. Tanabe, H. Takeshima, M. Iino, *Science* **1999**, *284*, 1527-1530.
[180] T. Balla, T. Bondeva, P. Varnai, *Trends Pharmacol. Sci.* **2000**, *21*, 238-241.
[181] R. W. Holz, M. D. Hlubek, S. D. Sorensen, S. K. Fisher, T. Balla, S. Ozaki, G. D. Prestwich, E. L. Stuenkel, M. A. Bittner, *J. Cell Biol.* **2000**, *275*, 17878-17885.
[182] M. S. Nash, K. W. Young, G. B. Willars, R. A. J. Challiss, S. R. Nahorski, *Biochem. J.* **2001**, *356*, 137-142.
[183] J. van der Wal, R. Habets, P. Varnai, T. Balla, K. Jalink, *J. Biol. Chem.* **2001**, *276*, 15337-15344.
[184] T. Balla, P. Varnai, *Sci. STKE* **2002**, pl3.
[185] J. P. DiNitto, T. C. Cronin, D. G. Lambright, *Sci. STKE* **2003**, re16.
[186] E. Oancea, M. N. Teruel, A. F. G. Quest, T. Meyer, *J. Cell Biol.* **1998**, *140*, 485-498.
[187] M. N. Teruel, T. Meyer, *Science* **2002**, *295*, 1910-1912.
[188] K. Almholt, P. O. G. Arkhammar, O. Thastrup, S. Tullin, *Mol. Biol. Cell* **1997**, *8*, 72-72.
[189] N. Sakai, K. Sasaki, N. Ikegaki, Y. Shirai, Y. Ono, N. Saito, *J. Cell Biol.* **1997**, *139*, 1465-1476.
[190] K. Almholt, P. O. G. Arkhammar, O. Thastrup, S. Tullin, *Biochem. J.* **1999**, *337*, 211-218.
[191] B. A. Pollok, R. Heim, *Trends Cell Biol.* **1999**, *9*, 57-60.
[192] P. I. H. Bastiaens, R. Pepperkok, *Trends Biochem. Sci.* **2000**, *25*, 631-637.
[193] A. Miyawaki, R. Y. Tsien, *Methods Enzymol.* **2000**, *327*, 472-500.
[194] S. A. Grant, J. T. Xu, E. J. Bergeron, J. Mroz, *Biosens. Bioelectron.* **2001**, *16*, 231-237.

[195] P. Verveer, A. G. Harpur, P. I. H. Bastiaens, in *Protein-protein interactions. A molecular cloning manual* (Ed.: E. Golemis), Cold Spring Harbor Laboratory Press, **2002**, pp. 181-213.
[196] J. E. Baader, A. G. Beck-Sickinger, *Methods Mol. Biol.* **2004**, *259*, 335-352.
[197] A. Schleifenbaum, I. Yudushkin, C. Schultz, P. I. H. Bastiaens, **2005**, unpublished results.
[198] P. I. H. Bastiaens, in *EP20010113815 20010606; EP20010115483 20010606*, EMBL, **2002**.
[199] G. Zlokarnik, P. A. Negulescu, T. E. Knapp, L. Mere, N. Burres, L. X. Feng, M. Whitney, K. Roemer, R. Y. Tsien, *Science* **1998**, *279*, 84-88.
[200] B. Xing, A. Khanamiryan, J. H. Rao, *J. Am. Chem. Soc.* **2005**, *127*, 4158-4159.
[201] O. Wichmann, C. Schultz, *Chem. Commun.* **2001**, 2500-2501.
[202] A. W. Nguyen, P. S. Daugherty, *Nat. Biotechnol.* **2005**, *23*, 355-360.
[203] A. Miyawaki, J. Llopis, R. Heim, J. M. McCaffery, J. A. Adams, M. Ikura, R. Y. Tsien, *Nature* **1997**, *388*, 882-887.
[204] A. Miyawaki, O. Griesbeck, R. Heim, R. Y. Tsien, *Proc. Natl. Acad. Sci. U. S. A.* **1999**, *96*, 2135-2140.
[205] A. Miyawaki, *Curr. Opin. Neurobiol.* **2003**, *13*, 591-596.
[206] A. E. Palmer, C. Jin, J. C. Reed, R. Y. Tsien, *Proc. Natl. Acad. Sci. U. S. A.* **2004**, *101*, 17404-17409.
[207] V. O. Nikolaev, M. Bunemann, L. Hein, A. Hannawacker, M. J. Lohse, *J. Biol. Chem.* **2004**, *279*, 37215-37218.
[208] C. W. Lin, C. Y. Jao, A. Y. Ting, *J. Am. Chem. Soc.* **2004**, *126*, 5982-5983.
[209] Y. Nagai, M. Miyazaki, R. Aoki, T. Zama, S. Inouye, K. Hirose, M. Iino, M. Hagiwara, *Nat. Biotechnol.* **2000**, *18*, 313-316.
[210] A. Y. Ting, K. H. Kain, R. L. Klemke, R. Y. Tsien, *Proc. Natl. Acad. Sci. U. S. A.* **2001**, *98*, 15003-15008.
[211] J. Zhang, Y. L. Ma, S. S. Taylor, R. Y. Tsien, *Proc. Natl. Acad. Sci. U. S. A.* **2001**, *98*, 14997-15002.
[212] M. Sato, T. Ozawa, K. Inukai, T. Asano, Y. Umezawa, *Nat. Biotechnol.* **2002**, *20*, 287-294.
[213] C. W. Lin, A. Y. Ting, *Angew. Chem., Int. Ed. Engl.* **2004**, *43*, 2940-2943.
[214] J. D. Violin, J. Zhang, R. Y. Tsien, A. C. Newton, *J. Cell Biol.* **2003**, *161*, 899-909.
[215] B. Simon, M. Sattler, unpublished results.
[216] T. Zimmermann, J. Rietdorf, A. Girod, V. Georget, R. Pepperkok, *FEBS Lett.* **2002**, *531*, 245-249.
[217] G. Zhang, V. Gurtu, S. R. Kain, *Biochem. Biophys. Res. Commun.* **1996**, *227*, 707-711.
[218] J. Brumbaugh, A. Schleifenbaum, A. Gasch, M. Sattler, C. Schultz, *J. Am. Chem. Soc.* **2005**, *submitted*.
[219] A. Gasch, M. Sattler, unpublished results.
[220] A. Sacchetti, V. Cappetti, P. Marra, R. Dell'Arciprete, T. El Sewedy, C. Crescenzi, S. Alberti, *J. Cell. Biochem.* **2001**, 117-128.
[221] K. B. Seamon, W. Padgett, J. W. Daly, *Proc. Natl. Acad. Sci. U. S. A.* **1981**, *78*, 3363-3367.
[222] O. Thastrup, P. J. Cullen, B. K. Drobak, M. R. Hanley, A. P. Dawson, *Proc. Natl. Acad. Sci. U. S. A.* **1990**, *87*, 2466-2470.

[223] J. H. Zhang, T. D. Y. Chung, K. R. Oldenburg, *J. Biomol. Screen.* **1999**, *4*, 67-73.
[224] G. S. Sittampalam, P. W. Iversen, J. A. Boadt, S. D. Kahl, S. Bright, J. M. Zock, W. P. Janzen, M. D. Lister, *J. Biomol. Screen.* **1997**, *2*, 159-169.
[225] H. Tsurui, H. Nishimura, S. Hattori, S. Hirose, K. Okumura, T. Shirai, *J. Histochem. Cytochem.* **2000**, *48*, 653-662.
[226] T. Zimmermann, *Adv. Biochem. Eng. Biotechnol.* **2005**, *95*, 245-265.
[227] ImageJ, W. Rasband, NIH, http://rsb.info.nih.gov/ij/.
[228] Origin v6.1, OriginLab Corporation, Northampton, MA, USA.
[229] M. E. Dickinson, G. Bearman, S. Tille, R. Lansford, S. E. Fraser, *BioTechniques* **2001**, *31*, 1272-1278.
[230] Y. Hiraoka, T. Shimi, T. Haraguchi, *Cell Struct. Funct.* **2002**, *27*, 367-374.
[231] B. Simon, M. Sattler, unpublished results.
[232] M. Torvinen, D. Marcellino, M. Canals, L. F. Agnati, C. Lluis, R. Franco, K. Fuxe, *Mol. Pharmacol.* **2005**, *67*, 400-407.
[233] A. Gasch, M. Sattler, unpublished results.
[234] L. A. Pinna, M. Ruzzene, *Biochim. Biophys. Acta - Mol. Cell Res.* **1996**, *1314*, 191-225.
[235] N. R. Leslie, R. M. Biondi, D. R. Alessi, *Chem. Rev.* **2001**, *101*, 2365-2380.
[236] R. M. Biondi, A. R. Nebreda, *Biochem. J.* **2003**, *372*, 1-13.
[237] P. I. Hanson, M. S. Kapiloff, L. L. Lou, M. G. Rosenfeld, H. Schulman, *Neuron* **1989**, *3*, 59-70.
[238] B. E. Kemp, D. J. Graves, E. Benjamini, E. G. Krebs, *J. Biol. Chem.* **1977**, *252*, 4888-4894.
[239] D. A. E. Cross, D. R. Alessi, P. Cohen, M. Andjelkovich, B. A. Hemmings, *Nature* **1995**, *378*, 785-789.
[240] K. Nishiyama, K. Sakai, Y. Tanaka, T. Kobayashi, S. Nakamura, Y. Sakanoue, E. Hashimoto, H. Yamamura, *Biochem. Int.* **1988**, *17*, 51-58.
[241] T. C. Chambers, J. Pohl, D. B. Glass, J. F. Kuo, *Biochem. J.* **1994**, *299*, 309-315.
[242] B. S. Skalhegg, K. Tasken, *Front. Biosci.* **2000**, *5*, D678-D693.
[243] S. S. Taylor, J. A. Buechler, W. Yonemoto, *Annu. Rev. Biochem.* **1990**, *59*, 971-1005.
[244] P. Schaap, M. Vanmentscohen, R. D. M. Soede, R. Brandt, R. A. Firtel, W. Dostmann, H. G. Genieser, B. Jastorff, P. J. M. Vanhaaster, *J. Biol. Chem.* **1993**, *268*, 6323-6331.
[245] J. Kruppa, S. Keely, F. Schwede, C. Schultz, K. E. Barrett, B. Jastorff, *Bioorg. Med. Chem. Lett.* **1997**, *7*, 945-948.
[246] J. E. Harlan, H. S. Yoon, P. J. Hajduk, S. W. Fesik, *Biochemistry* **1995**, *34*, 9859-9864.
[247] J. Ziauddin, D. M. Sabatini, *Nature* **2001**, *411*, 107-110.
[248] E. Ruoslahti, *Annu. Rev. Biochem.* **1988**, *57*, 375-413.
[249] E. Hecker, *Cancer Res.* **1968**, *28*, 2338-2349.
[250] P. Cohen, *Nat. Rev. Drug Discov.* **2002**, *1*, 309-315.
[251] G. X. Shen, *Curr. Drug. Targets. Cardiovasc. Haematol. Disord.* **2003**, *3*, 301-307.
[252] H. Y. Sun, K. E. Low, S. Woo, R. L. Noble, R. J. Graham, S. S. Connaughton, M. A. Gee, L. G. Lee, *Anal. Chem.* **2005**, *77*, 2043-2049.
[253] A. M. Parissenti, H. Riedel, in *Protein Kinase C Protocols, Vol. 233* (Ed.: A. C. Newton), Humana Press Inc., Totowa, New Jersey, **2003**, pp. 491-516.

[254] Metamorph, V6.2r4, Universal Imaging Corp., 2004.
[255] SiLib, SiChem GmbH, Bremen.
[256] C. Schultz, A. Schleifenbaum, J. Goedhart, T. W. J. Gadella, *ChemBioChem* **2005**, *6*, 1323-1330.
[257] Y. Nishizuka, *Trends Biochem. Sci.* **1992**, *17*, 367-367.
[258] T. Zimmermann, J. Rietdorf, R. Pepperkok, *FEBS Lett.* **2003**, *546*, 87-92.
[259] G. Reiser, B. Hamprecht, *Pflugers Arch.* **1985**, *405*, 260-264.
[260] P. A. Iredale, K. F. Martin, S. J. Hill, D. A. Kendall, *Eur. J. Pharmacol., Mol. Pharmacol. Sect.* **1992**, *226*, 163-168.
[261] J. S. Coggan, S. H. Thompson, *Am. J. Physiol.* **1995**, *269*, C841-848.
[262] C. C. Fink, B. Slepchenko, I. I. Moraru, J. Watras, J. C. Schaff, L. M. Loew, *Biophys. J.* **2000**, *79*, 163-183.
[263] G. Benitez-King, M. E. Hernandez, R. Tovar, G. Ramirez, *Neurochem. Int.* **2001**, *39*, 95-102.
[264] S. M. Elbashir, J. Harborth, W. Lendeckel, A. Yalcin, K. Weber, T. Tuschl, *Nature* **2001**, *411*, 494-498.
[265] D. M. Dykxhoorn, C. D. Novina, P. A. Sharp, *Nat. Rev. Mol. Cell Biol.* **2003**, *4*, 457-467.
[266] H. Erfle, J. C. Simpson, P. I. H. Bastiaens, R. Pepperkok, *BioTechniques* **2004**, *37*, 454-458.
[267] B. Simon, M. Sattler, unpublished results
[268] D. I. Svergun, L. A. Feigin, B. M. Schedrin, *Acta Crystallogr., Sect. A: Found. Crystallogr.* **1982**, *38*, 827-835.
[269] A. D. Ma, L. F. Brass, C. S. Abrams, *J. Cell Biol.* **1997**, *136*, 1071-1079.
[270] J. Brumbaugh, A. Schleifenbaum, C. Schultz, unpublished results.
[271] L. M. DiPilato, X. Cheng, J. Zhang, *Proc. Natl. Acad. Sci. U. S. A.* **2004**, *101*, 16513-16518.
[272] S. Pyne, N. J. Pyne, *Biochem. J.* **1995**, *311*, 637-642.
[273] G. R. Sambrano, G. Chandy, S. Choi, D. Decamp, R. Hsueh, K. M. Lin, D. Mock, N. O'Rourke, T. Roach, H. J. Shu, B. Sinkovits, M. Verghese, H. Bourne, *Nature* **2002**, *420*, 708-710.
[274] T. Meyer, M. N. Teruel, *Trends Cell Biol.* **2003**, *13*, 101-106.
[275] E. Oancea, M. N. Teruel, A. F. G. Quest, T. Meyer, *J. Cell Biol.* **1998**, *140*, 485-498.
[276] J. Sambrook, E. F. Frisch, T. Maniatis, *Molecular Cloning: A Laboratory Manual*, Cold Spring Harbour Laboratory Press, Inc., New York, **1989**.
[277] D. Hanahan, *J. Mol. Biol.* **1983**, *166*, 557-580.

8 Appendix

8.1 Plugin and macro scripts

8.1.1 ImageJ

Visitron related plugins and macros

The visitron microscope was controlled by Metamorph software. The software could image multiple sites during a time course experiment. When these image stacks were saved, a running number identified single time points and imaging sites. However, these numbers were not formatted and had no leading “0”. Therefore, when stacks imported into (early versions of) ImageJ were not loaded in the correct time-and site-order, but according to the alphabet (t1, t10, t11 … t2, t20, t21 …; s1, s10, s11 … s2, s20, s21 …).

Plugin: Visitron_Rename_T

Script

```
 1: import ij.*;
 2: import ij.process.*;
 3: import ij.gui.*;
 4: import java.awt.*;
 5: import ij.plugin.*;
 6: import ij.io.*;
 7: import java.io.*;
 8: import java.util.*;
 9: public class VisitronRename_T_ implements PlugIn {
10:         private int digits = 3;
11:         private String dirl, namel;
12:         public void run(String arg) {
14:             OpenDialog od = new OpenDialog("Select a folder by selecting
                                    any file...", arg);
15:             dirl = od.getDirectory();
16:             namel=od.getFileName();
17:             if (namel==null) return;
18:             dialog();
19:         }
20:         void dialog () {
21:             GenericDialog gd = new GenericDialog("Settings",
                                    IJ.getInstance());
22:             gd.addNumericField("Number of digits:", digits,0);
23:             gd.addStringField("Recognition site:","_t");
24:             gd.addStringField("Suffix:","TIF");
25:             gd.showDialog();
26:             if (gd.wasCanceled()) return;
```

```
27:                 digits=(int)gd.getNextNumber();
28:                 String recsite=gd.getNextString();
29:                 String suffix = gd.getNextString();
30:                 int recsitelength = recsite.length();
31:                 File fl = new File(dirl);
32:                 File fileliste [] = fl.listFiles();
33:                 int ii=0, t=0;
34:                 String oldname, rightpart;
35:                 long start = System.currentTimeMillis();
36:                 IJ.showStatus("Working on "+fileliste.length+" files.");
37:                 for (ii=0; ii<fileliste.length; ii++){
38:                         oldname = fileliste[ii].getName();
39:                         IJ.showProgress(ii,fileliste.length);
40:                         if (oldname.substring(oldname.length()-
                                    suffix.length()).equals(suffix)) {
41:                                 t = oldname.lastIndexOf(recsite);
42:                                 rightpart = oldname.substring(t+recsitelength);
43:                                 while (rightpart.length() < digits+1+suffix.length())
                                            rightpart = "0" + rightpart;
44:                                 fileliste[ii].renameTo(new File(dirl,
                                            oldname.substring(0, t+recsitelength) +
                                                        rightpart));
45:                         }
46:                 }
47:                 IJ.showStatus("Job done in "+IJ.d2s((System.currentTimeMillis()-
                                    start)/1000.0, 2)+" seconds");
48:         }
49: }
```

Function

All files in a selected folder were renamed with leading “0” for the time identifier “_t”. The total number of digits could be selected.

Plugin: Visitron_Rename_S

Script

```
 1: import ij.*;
 2: import ij.process.*;
 3: import ij.gui.*;
 4: import java.awt.*;
 5: import ij.plugin.*;
 6: import ij.io.*;
 7: import java.io.*;
 8: import java.util.*;
 9: public class VisitronRenames_S_ implements PlugIn {
10:         private int digits = 3;
11:         private String dirl, namel;
```

```
12:         public void run(String arg) {
13:             OpenDialog od = new OpenDialog("Select a folder by selecting
                        any file...", arg);
14:             dirl = od.getDirectory();
15:             namel=od.getFileName();
16:             if (namel==null) return;
17:             dialog();
18:         }
19:         void dialog () {
20:             GenericDialog gd = new GenericDialog("Settings",
                        IJ.getInstance());
21:             gd.addNumericField("Number of digits:", digits,0);
22:             gd.addStringField("Recognition site:","_s");
23:             gd.addStringField("Suffix:","TIF");
24:             gd.showDialog();
25:             if (gd.wasCanceled()) return;
26:             digits=(int)gd.getNextNumber();
27:             String recsite=gd.getNextString();
28:             String suffix = gd.getNextString();
29:             int recsitelength = recsite.length();
30:             File fl = new File(dirl);
31:             File fileliste [] = fl.listFiles();
32:             int ii=0, t=0;
33:             String oldname, rightpart;
34:             long start = System.currentTimeMillis();
35:             IJ.showStatus("Working on "+fileliste.length+" files.");
36:             for (ii=0; ii<fileliste.length; ii++){
37:                 oldname = fileliste[ii].getName();
38:                 IJ.showProgress(ii,fileliste.length);
39:                 if (oldname.substring(oldname.length()-
                            suffix.length()).equals(suffix)) {
40:                     t = oldname.lastIndexOf(recsite);
41:                     rightpart = oldname.substring(t+recsitelength);
42:                     while (rightpart.length() < digits+4+suffix.length())
                            rightpart = "0" + rightpart;
43:                     fileliste[ii].renameTo(new File(dirl,
                            oldname.substring(0, t+recsitelength) +
                                    rightpart));
44:                 }
45:
46:             }
47:             IJ.showStatus("Job done in "+IJ.d2s((System.currentTimeMillis()-
                        start)/1000.0, 2)+" seconds");
48:         }
49: }
```

Function

All files in a selected folder were renamed with leading “0” for the imaging site identifier “_s”. The total number of digits could be selected.

Macro: Screenhelper

Script

```
slicenamestack=getString("Name of the Slicename containing stack","Stack");
ratiostackname=getString("Name of the ratio stack","Result");
setBatchMode(true);
selectWindow(slicenamestack);
slicenames=newArray(nSlices+1);
for(i=1;i<=nSlices();i++){
        setSlice(i);
        inf=split(getImageInfo(),'\n');
        slicenames[i]=substring(inf[8],indexOf(inf[8],'(')+1,lastIndexOf(inf[8],'_'));
}
selectWindow("Result");
run("Select All");
sc=-1;
for(i=1;i<=nSlices();i++){
        setSlice(i);
        getStatistics(area, mean);
        oldname=slicenames[i-1];
        newname=slicenames[i];
        if (oldname!=newname) sc=-1;
        sc++;
        setResult(slicenames[i],sc,mean);
}
updateResults()
selectWindow("Results");
setBatchMode(false);
```

Function

The macro allowed for simultaneous processing of data from multiple imaging sites. Data from entire experiments (several time points and imaging sites), represented as ratio-value image stack, were sorted into a worksheet (columns: imaging sites; rows: time points). Since a calculated ratio-stack did not have frame-names, a reference stack for frame-identification was required (typically one of the genuine image stacks).

Leica SP2 related Plugin

Software Leica SP2 confocal microscopes saved detection channels in single images. Different channels had identifiers like “ch00” and “ch01”. To simplify data import into ImageJ, a plugin was written that automatically loads images from different channels into several stacks.

Script

```
 1: import ij.*;
 2: import ij.process.*;
 3: import ij.gui.*;
 4: import java.awt.*;
 5: import ij.plugin.*;
 6: import ij.io.*;
 7: import java.io.*;
 8: import java.util.*;
 9: public class SEQopener_ implements PlugIn {
10:         private int Chn = 2, notiff=2, stim=0, nim=0;
11:         private boolean saveseq = false, closeseq=false;
12:         private String namel, dirl, names, dirs, arg;
13:         private boolean [] Channels;
14:         public void run(String arg) {
15:                 OpenDialog od = new OpenDialog("Read Image Sequence...",
                                        arg);
16:                 dirl = od.getDirectory();
17:                 namel = od.getFileName();
18:                 if (namel==null) return;
19:                 loadthestuff();
20:         }
21:     void loadthestuff () {
22:         GenericDialog gd = new GenericDialog("Read Image Sequence",
                                        IJ.getInstance());
23:         gd.addNumericField("Number of different channels in folder:", Chn, 0);
24:         gd.addNumericField("Number of non-tiff files at
                                        beginning:",notiff,0);
25:         gd.addNumericField("Starting image:",stim, 0);
26:         gd.addNumericField("Number of images (0=remaining pix):", nim,0);
27:         gd.addCheckbox("Save sequences?", saveseq);
28:         gd.addCheckbox("Close sequence?", closeseq);
29:         gd.showDialog();
30:         if (gd.wasCanceled()) return;
31:         Chn=(int)gd.getNextNumber();
32:         notiff=(int)gd.getNextNumber();
33:         stim=(int)gd.getNextNumber();
34:         nim=(int)gd.getNextNumber();
35:         saveseq = gd.getNextBoolean();
36:         closeseq = gd.getNextBoolean();
37:         if (saveseq) {
38:                 OpenDialog od1 = new OpenDialog("Save Files to...", arg);
39:                 dirs = od1.getDirectory();
40:                 names = od1.getFileName();
41:                 if (names==null) return;
42:         }
43:         Channels = new boolean[Chn];
44:         int jj=0;
```

```
45:         GenericDialog gd1 = new GenericDialog("Which Channels",
                                        IJ.getInstance());
46:         for (jj=0; jj<Chn;jj++){
47:                 Channels[jj]=true;
48:                 gd1.addCheckbox("Channel Ch0"+jj,Channels[jj]);
49:         }
50:         gd1.showDialog();
51:         if (gd1.wasCanceled()) return;
52:         int ii=0;
53:         int firstimg=0;
54:         for(ii=0;ii<Chn;ii++){
55:                 Channels[ii]=gd1.getNextBoolean();
56:                 if (Channels[ii]) {
57:                         firstimg=Chn*stim+ii+notiff+1;
58:                         IJ.run("Image Sequence...", "open='"+dirl+namel+"'
                                        number="+nim+" starting="+firstimg+"
                                                increment="+Chn);
59:                         IJ.run("Rename...", "title=ch0"+ii);
60:                         if (saveseq) IJ.run("Image Sequence... ", "format=Tiff
                                        name='"+names+"_ch0"+ii+"_' start=0
                                                digits=4 save='"+dirs+names+
                                                        "_ch0"+ii+".tif'");
61:                         if (closeseq) IJ.run("Close");
62:                 }
63:         }
64:     }
65: }
```

Function

After selecting a folder with images, the number of different channels had to be entered. In a next step, the channels to be imported were selected.

8.1.2 Felix

The fluorimeter was controlled by the software Felix v1.41. A macro was written to record a time series of spectra for two samples in parallel.

Script

```
1: Version1.41
2: File Root Name: C:\AS00.FLX
3: User Name: Andreas
4: Reset Acq. Sequence Counter
5: Set Acquisition Mode: Emission Scan
6: Sample Mode
7: Set EX Wavelength Index:1 Value:405
8: Set EM Scan Start  Index:1 Value:490
9: Set EM Scan End    Index:1 Value:540
```

```
10:  Set EM Scan Start  Index:2 Value:490
11:  Set EM Scan End    Index:2 Value:540
12:  Set Step Size Value: 1 nm
13:  Set Integration Time Value: 1 sec
14:  Reset Clock
15:  Start Clock
16:  Start Loop
17:          Start Loop
18:                  Prep/Start Acquisition
19:                  Go To Sample: Value: 3
20:                  Time Out: Value: 81
21:          Number of loops: Value: 10
22:          Save Data File
23:  Number of loops: Value: 200
```

Function

Data were saved with file names entered in line 2. Samples were removed from excitation light while no data were recorded. Data was saved in a new file (AS01.FLX, AS 02.FLX …) after every tenth time point. Resulting files represented each time point as an octet of columns: fluorescence data of two samples and two detectors, and for every column on additional column with corresponding emission wavelengths; rows represented wavelengths and fluorescence values.

8.1.3 Origin

Macros for ratio calculations

For these scripts, an Origin project was required with one graph window (“Graph1”) and three worksheets (“gfp”, “yfp”, and “ratio”). The worksheet “ratio” contained five control buttons with the scripts.

Button 1: Calculate ratio with background subtraction

Script

```
1:  getnumber
2:          (Contribution of gfp) k1
3:          (Contribution of yfp) k2
4:          (Normalize) norm:2s
5:          (on how many values) xxx
6:          (Unmixing parameter; gfp2/yfp:0.8/0.15);
7:  for (ii=3; ii<100;ii++) {
8:          if (%(yfp,ii)[1]<0) break;
9:          %(ratio,ii)=(((%(yfp,ii)-%(yfp,2))-(%(gfp,ii)-%(gfp,2))*k1)/((%(gfp,ii)-
                        %(gfp,2))-(%(yfp,ii)-%(yfp,2))*k2));
```

```
10:         if (norm) {
11:                 js=0;
12:                 for (jj=1; jj<xxx+1;jj++) {
13:                         js+=%(ratio,ii)[jj];
14:                 }
15:                 js/=xxx;
16:                 %(ratio,ii)=%(ratio,ii)/js;
17:         }
18: }
```

Function

This script calculated ratio values (“yfp”/”gfp”) with background subtraction. Background values were taken from the second column of the worksheets “yfp” and “gfp”. k1 and k2 were the bleed through coefficients for linear unmixing. These values were set 0, when unmixing was not required. Values were normalized to the first *xxx* values of a data set.

Button 2: Calculate ratio without background subtraction

Script

```
 1: getnumber
 2:         (Contribution of gfp) k1
 3:         (Contribution of yfp) k2
 4:         (Normalize) norm:2s
 5:         (on how many values) nov
 6:         (Unmixing parameter; gfp2/yfp:0.8/0.15);
 7: for (ii=3; ii<100;ii++) {
 8:         if (%(yfp,ii)[1]<0) break;
 9:         %(ratio,ii)=(((%(yfp,ii))-(%(gfp,ii))*k1)/((%(gfp,ii))-(%(yfp,ii))*k2));
10:         if (norm) {
11:                 js=0;
12:                 for (jj=1; jj<nov+1;jj++) {
13:                         js+=%(ratio,ii)[jj];
14:                 }
15:                 js/=nov;
16:                 %(ratio,ii)=%(ratio,ii)/js;
17:         }
18: }
```

Function

Similar function as *Button 1*, but background subtraction was omitted.

Button 3: Set time

Script

```
getnumber
        (Delay in seconds) delay
        (Addition after frame) addition
        (How many frames) framecount
        (Rescale X-Axis) rescale:2
        (Delay between frames);
for(ii=1;ii<framecount+1;ii++) {
        ratio_A[ii]=ii*(delay/60)-(addition*delay/60);
}
if (rescale) {
        Graph1!Layer1.X.from = round((delay/60)-(addition*delay/60),0);
        Graph1!Layer1.X.to = round((framecount*(delay/60)-
                                (addition*delay/60))+0.5,0);
}
```

Function

Calculated the x-values and reset the minimal and maximal values of the x-axis. “Delay in seconds” was the interval between recorded frames and the value “Addition after frame” was used to set t = 0 for the appropriate frame.

Button 4: Clear worksheets

Script

```
ClearWorksheet gfp;
ClearWorksheet yfp;
ClearWorksheet ratio;
```

Function

Clears all worksheets.

Button 5: Calculate Z-value

Script

```
getnumber
        (Start Background) sb
        (Start Signal) ss
        (Length) sl
        (Calculate Z);
ratio_B[1]=0;
ratio_B[2]=0;
```

```
 8:  for (jj=3; jj<100;jj++) {
 9:          if (%(ratio,jj)[1]<0) break;
10:          aa2=0;
11:          bb2=0;
12:          aas=0;
13:          bbs=0;
14:          for(ii=0;ii<sl;ii++){
15:                  aa2+=(%(ratio,jj)[ii+sb]*%(ratio,jj)[ii+sb]);
16:                  bb2+=(%(ratio,jj)[ii+ss]*%(ratio,jj)[ii+ss]);
17:                  aas+=%(ratio,jj)[ii+sb];
18:                  bbs+=%(ratio,jj)[ii+ss];
19:          }
20:          aastdev=sqrt((sl*aa2-aas*aas)/(sl*sl));
21:          bbstdev=sqrt((sl*bb2-bbs*bbs)/(sl*sl));
22:          ratio_B[jj]=1-3*(aastdev+bbstdev)*sl/abs(aas-bbs);
23:  }
```

Function

Calculated Z-values of data sets. “Start Background” and “Start Signal” were the frame (or row) numbers of the first data point for a baseline or signal. “Length” determined the number of data points used for mean and average calculation.

Macro for evaluation of fluorimeter experiments

The Origin project contained one worksheet “Start” with two buttons (“Make All” and “New Ratios”). Fluorimeter data were imported into one worksheet, which was named “FLDATA”; row depicted wavelength and respective fluorescence values, columns contained data for the single measurements. The fluorimeter data had to have the following format: two samples were measured with two detectors, and for each time point fluorescence was recorded from 490 nm to 540 nm.

Button 1: Make All

Script

```
 1:  getnumber
 2:          (Start GFP2) k1
 3:          (Start EYFP) k2
 4:          (Range Size) k3
 5:          (Settings for Ratio);
 6:  wlsetoff=488;                    //488 wenn 2. Col mit 490 anfaengt
 7:  create S1D1t_b -c 51;
 8:  edit S1D1t_b;
 9:  create S1D2t_b -c 51;
10:  edit S1D2t_b;
```

```
11:  create S2D1t_b -c 51;
12:  edit S2D1t_b;
13:  create S2D2t_b -c 51;
14:  edit S2D2t_b;
15:  maxcol=%(FLDATA,@#)/8;
16:  for (ii=1; ii<maxcol;ii++){
17:          S1D1t!wks.addCol();
18:          S1D2t!wks.addCol();
19:          S2D1t!wks.addCol();
20:          S2D2t!wks.addCol();
21:  }
22:  for (ii=0; ii<maxcol+1;ii++){
23:          %(S1D1t,ii+2)=%(FLDATA,ii*8+2);
24:          %(S1D2t,ii+2)=%(FLDATA,ii*8+4);
25:          %(S2D1t,ii+2)=%(FLDATA,ii*8+6);
26:          %(S2D2t,ii+2)=%(FLDATA,ii*8+8);
27:  }
28:  S1D1t_a=FLDATA_a;
29:  S1D2t_a=FLDATA_a;
30:  S2D1t_a=FLDATA_a;
31:  S2D2t_a=FLDATA_a;
32:  create S1D1_b -c S1D1t!wks.nCols;
33:  edit S1D1_b;
34:  create S1D2_b -c S1D1t!wks.nCols;
35:  edit S1D2_b;
36:  create S2D1_b -c S1D1t!wks.nCols;
37:  edit S2D1_b;
38:  create S2D2_b -c S1D1t!wks.nCols;
39:  edit S2D2_b;
40:  for (ii=2;ii<S1D1t!wks.maxRows+1;ii++){
41:          S1D1!wks.addCol();
42:          S1D2!wks.addCol();
43:          S2D1!wks.addCol();
44:          S2D2!wks.addCol();
45:  }
46:  for (ii=1;ii<S1D1t!wks.maxRows+1;ii++)
47:          for(jj=1;jj<S1D1t!wks.nCols;jj++){
48:                  %(S1D1,ii+1,jj)=%(S1D1t,jj,ii);
49:                  %(S1D2,ii+1,jj)=%(S1D2t,jj,ii);
50:                  %(S2D1,ii+1,jj)=%(S2D1t,jj,ii);
51:                  %(S2D2,ii+1,jj)=%(S2D2t,jj,ii);
52:          }
53:  create S1D1Ratio_b -c S1D1!wks.maxRows;
54:  edit S1D1Ratio_b;
55:  create S1D2Ratio_b -c S1D2!wks.maxRows;
56:  edit S1D2Ratio_b;
57:  create S2D1Ratio_b -c S2D1!wks.maxRows;
58:  edit S2D1Ratio_b;
59:  create S2D2Ratio_b -c S2D2!wks.maxRows;
60:  edit S2D2Ratio_b;
```

```
61:  for (ii=1;ii<3;ii++){
62:          S1D1Ratio!wks.addCol();
63:          S1D2Ratio!wks.addCol();
64:          S2D1Ratio!wks.addCol();
65:          S2D2Ratio!wks.addCol();
66:  }
67:  startcol=k1-wlsetoff; //32=520 nm; 42=530 nm;53=540nm
68:  avnum=k3;
69:  %(S1D1Ratio,2)=%(S1D1,startcol);
70:  %(S1D2Ratio,2)=%(S1D2,startcol);
71:  %(S2D1Ratio,2)=%(S2D1,startcol);
72:  %(S2D2Ratio,2)=%(S2D2,startcol);
73:  for (ii=startcol;ii<(startcol+avnum+1);ii++){
74:     %(S1D1Ratio,2)=(%(S1D1Ratio,2)*(ii-startcol)+%(S1D1,ii))/(ii-startcol+1);
75:     %(S1D2Ratio,2)=(%(S1D2Ratio,2)*(ii-startcol)+%(S1D2,ii))/(ii-startcol+1);
76:     %(S2D1Ratio,2)=(%(S2D1Ratio,2)*(ii-startcol)+%(S2D1,ii))/(ii-startcol+1);
77:     %(S2D2Ratio,2)=(%(S2D2Ratio,2)*(ii-startcol)+%(S2D2,ii))/(ii-startcol+1);
78:  }
79:  startcol=k2-wlsetoff;                    //32=520 nm; 42=530 nm;53=540nm
80:  avnum=k3;
81:  %(S1D1Ratio,3)=%(S1D1,startcol);
82:  %(S1D2Ratio,3)=%(S1D2,startcol);
83:  %(S2D1Ratio,3)=%(S2D1,startcol);
84:  %(S2D2Ratio,3)=%(S2D2,startcol);
85:  for (ii=startcol;ii<(startcol+avnum+1);ii++){
86:     %(S1D1Ratio,3)=(%(S1D1Ratio,3)*(ii-startcol)+%(S1D1,ii))/(ii-startcol+1);
87:     %(S1D2Ratio,3)=(%(S1D2Ratio,3)*(ii-startcol)+%(S1D2,ii))/(ii-startcol+1);
88:     %(S2D1Ratio,3)=(%(S2D1Ratio,3)*(ii-startcol)+%(S2D1,ii))/(ii-startcol+1);
89:     %(S2D2Ratio,3)=(%(S2D2Ratio,3)*(ii-startcol)+%(S2D2,ii))/(ii-startcol+1);
90:  }
91:  %(S1D1Ratio,4)=%(S1D1Ratio,3)/%(S1D1Ratio,2);
92:  %(S1D2Ratio,4)=%(S1D2Ratio,3)/%(S1D2Ratio,2);
93:  %(S2D1Ratio,4)=%(S2D1Ratio,3)/%(S2D1Ratio,2);
94:  %(S2D2Ratio,4)=%(S2D2Ratio,3)/%(S2D2Ratio,2);
```

Function

An input box requested values to define ranges from which mean values and ratios are calculated. The script divided FLDATA in single worksheets (for every sample [S1 and S2] and detector [D1 and D2]). Worksheets were transposed so that columns represented wavelength and fluorescence values and rows the time points. According to initial values from the input box, mean and ratio values were calculated. It must be noted that this macro is very slow and may easily need 20 min to finish.

Button 2: New Ratios

Script

```
getnumber
        (Start GFP2) k1
        (Start EYFP) k2
        (Range Size GFP2) k3
        (Range Size EYFP) k4
        (Settings for Ratio);
wlsetoff=490-2;
startcol=k1-wlsetoff; //32=520 nm; 42=530 nm;53=540nm
avnum=k3;
%(S1D1Ratio,2)=%(S1D1,startcol);
%(S1D2Ratio,2)=%(S1D2,startcol);
%(S2D1Ratio,2)=%(S2D1,startcol);
%(S2D2Ratio,2)=%(S2D2,startcol);
for (ii=startcol;ii<(startcol+avnum+1);ii++){
    %(S1D1Ratio,2)=(%(S1D1Ratio,2)*(ii-startcol)+%(S1D1,ii))/(ii-startcol+1);
    %(S1D2Ratio,2)=(%(S1D2Ratio,2)*(ii-startcol)+%(S1D2,ii))/(ii-startcol+1);
    %(S2D1Ratio,2)=(%(S2D1Ratio,2)*(ii-startcol)+%(S2D1,ii))/(ii-startcol+1);
    %(S2D2Ratio,2)=(%(S2D2Ratio,2)*(ii-startcol)+%(S2D2,ii))/(ii-startcol+1);
}
startcol=k2-wlsetoff; //32=520 nm; 42=530 nm;53=540nm
avnum=k4;
%(S1D1Ratio,3)=%(S1D1,startcol);
%(S1D2Ratio,3)=%(S1D2,startcol);
%(S2D1Ratio,3)=%(S2D1,startcol);
%(S2D2Ratio,3)=%(S2D2,startcol);
for (ii=startcol;ii<(startcol+avnum+1);ii++){
    %(S1D1Ratio,3)=(%(S1D1Ratio,3)*(ii-startcol)+%(S1D1,ii))/(ii-startcol+1);
    %(S1D2Ratio,3)=(%(S1D2Ratio,3)*(ii-startcol)+%(S1D2,ii))/(ii-startcol+1);
    %(S2D1Ratio,3)=(%(S2D1Ratio,3)*(ii-startcol)+%(S2D1,ii))/(ii-startcol+1);
    %(S2D2Ratio,3)=(%(S2D2Ratio,3)*(ii-startcol)+%(S2D2,ii))/(ii-startcol+1);
}
%(S1D1Ratio,4)=%(S1D1Ratio,3)/%(S1D1Ratio,2);
%(S1D2Ratio,4)=%(S1D2Ratio,3)/%(S1D2Ratio,2);
%(S2D1Ratio,4)=%(S2D1Ratio,3)/%(S2D1Ratio,2);
%(S2D2Ratio,4)=%(S2D2Ratio,3)/%(S2D2Ratio,2);
```

Function

This script recalculated ratios according to user input.

8.2 Publications

A fluorescent protein kinase C activity reporter based on pleckstrin

C. Schultz, A. Schleifenbaum, G. Stier, M. Sattler

40th ASCB Meeting, San Francisco, USA.

Imaging protein kinase C activity in live cells with the FRET reporter KCP-1

A. Schleifenbaum, C. Schultz

Cambridge Healthtech Institute (CHI) Meeting, San Diego, USA.

Improvements and applications of the protein kinase C reporter KCP-1

A. Schleifenbaum, A. Gasch, G. Stier, M. Sattler, C. Schultz

41th ASCB Meeting, Washington DC, USA.

Small molecule vs genetically encoded FRET sensors: pros and cons

C. Schultz, O. Wichmann, A. Schleifenbaum, J. J. Brumbaugh

229th ACS National Meeting, San Diego, USA.

Genetically encoded FRET probe for PKC activity based on pleckstrin

A. Schleifenbaum, G. Stier, A. Gasch, M. Sattler, C. Schultz

Journal of the American Chemical Society **2004**, *126(38)*, 11786-11787.

Multiparameter imaging for the analysis of intracellular signaling

C. Schultz, A. Schleifenbaum, J. Goedhart, T. W. J. Gadella Jr.

ChemBioChem **2005**, *6*, 1323-1330.

A dual parameter FRET probe for measuring PKC and PKA activity in living cells

J. J. Brumbaugh, A. Schleifenbaum, A. Gasch, M. Sattler, and C. Schultz

Journal of the American Chemical Society, submitted.

Acknowledgements

I am grateful to Carsten Schultz who gave me the opportunity to work at the interface between chemistry and biology and for his constant support and spirit. I also thank the members of my TAC committee, Iain Mattaj, Michael Sattler, and Nils Metzler-Nolte (also for the opportunity to complete my PhD at the University of Heidelberg).

My PhD-work could not have succeeded without the help of several people. I highly appreciate the help of Gunter 'Cloning Machine' Stier, who revealed deep secrets of molecular biology, Alex Gasch who performed radioactivity-experiments, Jens Rietdorf, Stefan Terjung, and Timo Zimmermann, who gave great microscopy-support, and Holger Erfle, who introduced me to DNA spotting. An diesem Punkt kann ich auch endlich dem THC-Team (vor allem Brigitte, Christl und Gabi) der Uni Köln danken, die mich geduldig in das Arbeiten mit Bakterien, Zellen, Vektoren und ähnlichem einführten.

I am thankful to Marc Gentzel, Thilo Werner, and Manfred Raida for mass-spectroscopy used for projects, which, however, are not described in this thesis. For another great collaboration, whose fruits did not enter this thesis, I thank Ivan Yudushkin.

A big "THANK YOU" goes to the Schultz-group for a relaxed and pleasant working atmosphere. In particular, I will miss the esprit and sense of humor of Oliver Wichmann and Sirus "die Zentrale der Macht" Zarbakhsh – these guys were just fun. A special thank also goes to Justin Brumbaugh, with whom I know the further project will be in good hands. It is also he, who converted German English to real English in this thesis. I thank Heike Stichnoth for taking care of cell culture and providing cells even at the last instant.

The vacation of my PhD time was only possible with the help of some Russian friends: Marina Chekulaeva, Stepan Belyakin, and Ivan Yudushkin helped Cerstin and me survive (unexpectedly) a trip from Moscow to Beijing.

Josef und Robert danke ich einfach so.

Für zahlreiche wunderbare Diskussionen, Abende, Grillen, Bier, Shrimp und andere Köstlichkeiten im schönsten Balkonien Heidelbergs danke ich Martina und Oliver.

Zum Schluss danke ich noch meiner Familie, die mir das Fundament gab, auf dem ich nun stehe und in die Welt blicken kann.

… und natürlich geht mein ganzer Dank an Cerstin, für unsere Zweisamkeit in Heidelberg.